Studies of non-identical meson-meson correlations at low relative velocities in relativistic heavy-ion collisions registered in the STAR experiment

Adam Kisiel

rozprawa doktorska pod kierunkiem dr hab. Jana Pluty

10th August 2004

Contents

List of Figures

List of Tables

Pracę tę dedykuję moim Rodzicom oraz Ani.
Powstała dzięki waszemu wsparciu i pomocy.

Acknowledgements

I wish to thank my supervisor professor Jan Pluta for his immense help, support and guidance. His example was an inspiration. Thanks to Him, I was able to take advantage of the opportunities I never thought possible.

A special thanks goes to Dr Fabrice Retiere. I was lucky to be able to work with Him, and take advantage of his invaluable experience and expertise at all stages of creating this thesis.

I would also like to thank professor Richard Lednicky. His ideas and insight helped me reach a new level of understanding of my work. Without his help this thesis would not have been created.

I wish to thank professors Mike Lisa, Nu Xu, Sergey Panitkin and Barbara Erazmus. They provided essential encouragement, insight and critique when necessary.

I would also like to thank professor Tim Hallman and the STAR Group from Brookhaven National Laboratory, professor Hans Georg Ritter and the Nuclear Collisions Group at the Lawrence Berkeley National Laboratory as well as professor Barbara Erasmus and the STAR group from SUBATECH at Nantes for their support and hospitality during my numerous stays at their laboratories.

I would also like to acknowledge the help of several people, especially Drs Laurent Conin, Kai Schweda and Aihong Tang for providing data and code which were very helpful in completing this work.

I would also thank the whole STAR Collaboration and especially the HBT Working Group for providing an excellent working environment and giving me the opportunity to take part in the greatest adventure of my life.

Last but not least I would like to thank all the members of the Heavy-Ion Reactions Group at Warsaw University of Technology, especially dr Tomasz Pawlak, as well as Piotr, Michał, Zbyszek, Hania and Maciek.

This work has been supported by the Polish Committee for Scientific Research in years 2003/2004 as a research project, grant no. 2 P03B 123 25.

Chapter 1

Introduction

The goal of physics has always been to study and understand the world that we live in. Through the work of many scientists this understanding was developed and the boundaries of knowledge have been pushed further and further. Building on the experience and achievements of past generations was the crucial ingredient of the process. In this process four basic forces in the Universe were identified: the gravitation, electromagnetic force, weak interaction and strong interaction, with the range of the forces ranging from infinity for gravity to the size of the nucleon for the strong force. From the very fact that the strong force has such a small scale comes the difficulty in studying it. It has been done only very recently, the field is about a hundred years old.

Today the strong force is known in its basic form and is described by the theory of Quantum Chromo-dynamics. However the properties of strongly interacting matter are still unknown - they now form the boundary of human knowledge. Heavy-ion collisions aim to study this strongly interacting matter. We expect that in the process of colliding heavy-ions, consisting of large number of strongly-interacting nucleons, and accelerated to velocities almost at the speed of light we will be able create matter that exhibits qualities not normally seen in Earth conditions. It may correspond to the state of matter created at the very beginning of the Universe, shedding light on how the known nuclear matter was created. Such discovery would significantly enhance our knowledge of the world around us and lead us to new discoveries and challenges.

Meson-meson correlations are one of the experimental techniques used in studying heavy-ion collisions. They provide a rare possibility to measure space scales of the order of the size of the nucleon - 10^{-15} m and times of the order of 10^{-23} s. They also enable studying of the evolution and dynamics of the system created in heavy-ion collisions, providing unique insight into the collectivity exhibited by the created matter. As the correlations of particles are the only technique that gives the access to space-time part of the phase-space of the collision they constitute a necessary ingredient in our search for understanding the states of matter not previously seen by man.

In this work, the non-identical meson-meson correlations were studied by measuring pion-kaon correlation functions in the STAR experiment. It is a part of a scientific program of the RHIC community, aiming at the confirmation of the discovery and determining the properties of a new state of matter - a Quark Gluon Plasma (QGP), which is possibly formed in the heavy-ion collisions in this accelerator.

In chapter 2 the introduction to the physics of heavy-ion collisions was given. The current state of search for the QGP was presented. The importance of flow, more specifically transverse and elliptic flow was shown. Particle correlations were introduced as one of the signatures of the existence of the QGP, as well as a tool to study the collectivity of matter. The theoretical models, which will be later used to analyze and interpret the data are also described.

In chapter 3 the detailed description of the close-velocity particle correlations technique was given. Results of identical particle correlations was shown and their implications given. The technique of non-identical particle correlations was introduced, and the formalism for the description of final-state interactions was given. The idea of measuring emission asymmetries between non-identical particles was presented.

In chapter 4 the STAR experiment, part of the RHIC accelerator complex is described. The detectors most important in this analysis, the STAR TPC and the trigger detectors were described in detail and the characteristics of the detectors affecting the non-identical particle measurement were shown. The data analysis procedure was briefly described and the FileCatalog software package and its role in the STAR data analysis effort was presented.

In chapter 5, the non-identical particle analysis technique in the STAR experiment environment was introduced. The experimental cuts and corrections were described in detail and their effect on the experimental correlation functions was defined. The data sample used was also characterized.

In chapter 6 the pion-kaon correlation functions from the STAR experiment were shown, both at $\sqrt{s_{NN}} = 130\,GeV$ and $200\,GeV$. The asymmetry measurement in the form of "double-ratios" was also presented. The obtained functions were then fitted with the help of CorrFit software. The fit results and the detailed description of the source models used were also given in this chapter. The data presented are the main experimental result of this work.

In chapter 7 the results of pion-kaon correlations are discussed and the main conclusions drawn. The non-zero asymmetry between pions and kaons is observed for the first time in heavy-ion collisions. It is compared to the predictions of the theoretical models. The shift in average space points is explained as the result of the existence of transverse radial flow in heavy-ion collisions and is the independent confirmation of the existence of space-momentum correlations, which are the essence of the radial flow hypothesis. The importance of average time shift, arising from the decay of hadronic resonances is studied. The conclusion can be drawn, that the combination of time and space emission asymmetries exist, which add up to form the observed asymmetry.

In the Appendices, the detailed technical description of the tools developed by the author and used in this work is given. The STAR particle correlations software is described, in particular the theoretical classes used to construct the theoretical non-identical particle correlation functions. The CorrFit software, which is essential in extracting quantitative information from non-identical particle correlations is described. The FileCatalog module, important for managing STAR dataset, part of the service of the author to the STAR community is described in detail. The numerical implementation of the "blast-wave" analytical model, and its use as a particle generator is also shown.

Chapter 2

Physics of heavy-ion collisions

Relativistic heavy-ion collisions are a relatively new field, which enables the study of matter at high densities and temperatures. It is believed that they produce conditions that only existed in the first microseconds after the Big Bang, the moment the Universe was created. These studies may produce discoveries useful in many fields of physics, including particle physics, astrophysics and nuclear physics.

2.1 QCD, deconfinement and Quark-Gluon Plasma

The system of colliding nuclei is rich with particles interacting on a scale of a size of a nucleon - $fm = 10^{-15}m$. At these scales the dominant force is a strong interaction between nucleons, as well as between quarks, which the nucleons consist of. The underlying theory of the strong interaction is Quantum Chromodynamics or QCD. The mediator of the strong interaction is called a gluon. A free quark has not yet been seen in nature. Instead a large number of strong-interacting particles were observed. In order to explain the observed symmetries and the fact that these particles could be categorized into groups showing with similar quantum numbers Gell-Mann and Zweig have postulated that hadrons (strongly interacting particles) are actually built from smaller constituents called quarks. Furthermore they can be grouped into the ones built from two quarks - called mesons, and the ones built from three quarks - called barions. It is now known that there are six quark *flavors*: u, d, s, c, t, b called *up*, *down*, *strange*, *charm*, *top* (or *true*) and *bottom* (or *beauty*). Some of the observed particles - namely Δ^{++}, Δ^{-} and Ω^{-} appeared to consist of three quarks of identical flavor (uuu, ddd and sss respectively), which was in conflict with the Pauli principle. Therefore the existence of new quantum number, called *color*, was postulated. Three values of color were possible (usually called *red*, *green* and *blue*) as well as their anti-colors. Only color-neutral (or white) particles could exist, mesons are assumed to be a *color-anticolor* pair, while barions are *red-green-blue* triplets. As a consequence the strong force quanta - the gluons, are color-charged; there are $2^3 = 8$ types of gluons. This means that QCD is a *gauge theory* based on the SU(3) color symmetry group.

The fact that quarks only exist in pairs or triplets, called the *confinement*, still wait for a quantitative explanation. The QCD predicts a running coupling constant, dependent of the momentum transfer Q^2:

$$g^2\left(Q^2\right) = \frac{16\pi^2}{\left(11 - \frac{2}{3}N_f\right)\ln\left(Q^2/\Lambda^2\right)}, \tag{2.1}$$

where $\Lambda = 150$ MeV is the QCD scale parameter and N_f is the number of flavors. This provides a simple picture explaining the quark confinement. As two quarks are pulled apart, the distance grows, the momentum transfer decreases and the coupling constant and the strong interaction grows. The situation resembles stretching of a string. At some point the energy stored in the string is so large, that it becomes energetically favorable to create the quark-antiquark pair. At some point such a pair (or several pairs) is formed, the quarks from the pair recombine with the original ones, the string breaks and the confinement is preserved.

Another consequence of the running coupling constant is that at large momentum transfer, or short distances the quarks and gluons become asymptotically free. It is assumed that if a system sufficiently dense and hot is created, barions and mesons will melt forming a so-called Quark-Gluon Plasma (QGP), where quarks and gluons will become the relevant degrees of freedom.

Because of the running coupling constant, which can have values larger than 1.0, the QCD calculations present a challenge. One possibility to perform them are the numerical calculations on a discretized space-time lattice, or Lattice QCD. The results of such calculation are shown on Fig. 2.1. The quantity plotted, energy density ϵ divided by T^4 is a measure of the number of degrees of freedom in the system. As the temperature increases past the critical value T_C one observes significant increase in the number of degrees of freedom signaling the formation of the QGP.

Lattice QCD calculations are constantly improved, enlarging our knowledge about the behavior of strongly interacting matter. One of the questions they can answer are the values of parameters: the temperature T_C as a function of barion potential μ_B, where the phase transition will occur. The schema shown on Fig 2.2 illustrates the current state of knowledge. Calculations show that a state of matter where quarks and gluons are free is expected to exist at large temperatures. At small temperatures and large barion densities a different state - a color

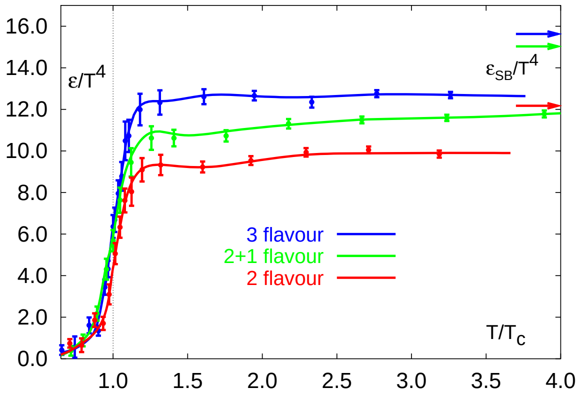

Figure 2.1: Energy density as a function of temperature from Lattice QCD calculations[1].

superconductor, may exist. The phase transition between QGP and hadronic matter is thought to be of 1st order at non-vanishing μ_B. However as $\mu_B \rightarrow 0$ quark masses become significant and a sharp phase transition transforms into a rapid but smooth cross-over. It is believed that in AuAu collisions at RHIC the created matter has high enough temperature to be in the QGP region, then cools down and converts into hadrons, undergoing a smooth transition. The exact position of the critical end-point is not known, but it is thought to be far from the line of evolution of the RHIC collision system. This hypothesis can be tested, as large event-by-event fluctuations are expected in the system that traverses the phase diagram close to the critical endpoint.

2.2 Relativistic Heavy-Ion Collisions

Relativistic heavy-ion collisions are the only way to produce and study large volumes of nuclear matter at high energy density. A schema of such collision at RHIC is shown on Fig. 2.3. It consists of several stages going from the earliest(bottom) to the latest(top): a) two Lorentz-contracted Au nuclei, moving towards each other, b) initial stage of the collision where matter is highly excited, non-thermalized and quickly approaching thermalization, c) possible QGP phase, d) possible mixed phase (recent data from RHIC show that this stage is either non-existing or very short), e) hadron gas stage, f) particles free-streaming to the detector. There are three characteristic time-scales associated with these stages: initial formation time τ_0, marking the end of the first stage of the collision, when the matter is though to be thermalized. It is assumed to be on the order of 1 fm/c; chemical freeze-out τ_{ch} where inelastic collision

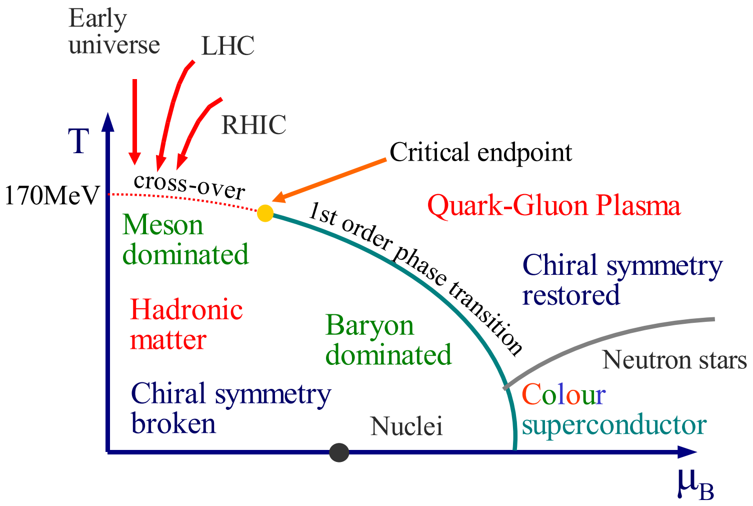

Figure 2.2: Phase-space diagram resulting from Lattice QCD calculations.

rate becomes smaller than elastic collision rate - a time when chemical composition of matter is fixed; τ_{kin}- kinetic freeze-out, when system becomes so diluted that even elastic collision stop - the momenta of the particles are fixed. The chemical and kinetic freeze-out are usually associated with their characteristic temperatures: T_{ch} and T_{kin} respectively. If a transition to QGP occurs, T_{ch} obviously cannot be grater than T_C, which is estimated to be around 170 MeV from Lattice QCD calculations.

The most compelling motivation for studying heavy-ion collisions is the search for QGP. Several experimental observable were proposed as QGP signatures. Some of them have been measured already at SPS in CERN:

- A threshold to produce a strange quark measured in the elementary collisions is equal to the mass of the lowest meson containing a strange quark - a kaon - which is on the order of 500 MeV. If a true QGP is created, than $s\bar{s}$ pair can be created through gluon fusion and a threshold for such a process is equal to the mass of two strange quarks, which is on the order of 300 MeV. Therefore a significant *enhancement of strangeness production* in AA collision when compared to pp or pA collisions is expected. Such an enhancement is indeed observed in SPS experiments WA97, NA57 and NA49[3, 4, 5].

- In QGP quark flavor can be screened in a way similar to electric charge Debye screening known from QED. Therefore if a bound state of rare (heavy) quarks, e.g. a $c\bar{c}$ pair - a J/Ψ particle, is created it will quickly dissolve. In this case creation of a singly-charmed particle, a D meson,

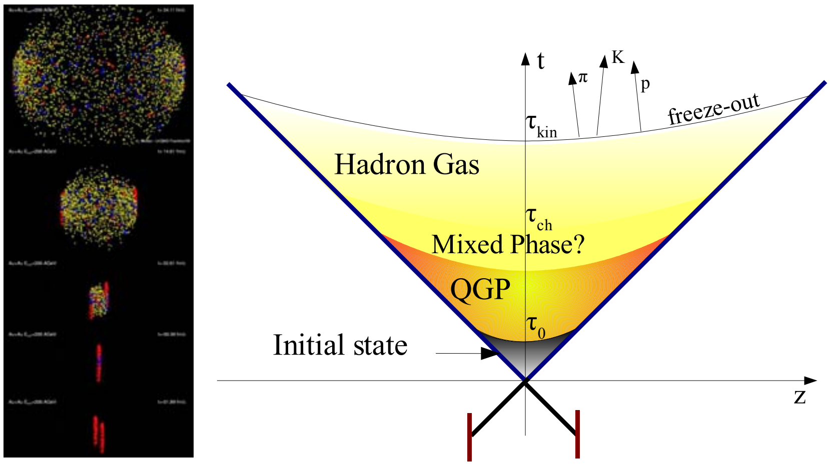

Figure 2.3: Left panel: stages of a heavy-ion collision simulated in UrQMD model[2]. Right panel: schematic view of a heavy-ion collision evolution

will be statistically preferred. Therefore one can look for the onset of the suppression of J/Ψ production as a function of collision energy as a signature of a phase transition. Such a suppression was indeed observed by the NA50 experiment at CERN[6]. However models exist[7, 8] that claim to explain the observed suppression by the effects not connected to QGP. Some studies also show that J/Ψ particle would melt only at temperatures significantly higher than T_C[9].

- Leptons are a convenient probe of a system created in heavy-ion collision as they do not interact strongly, and their mean free path is larger than the size of the system. Therefore they can probe the early hot and dense stage of the system. If a hot, thermalized QGP is created it is expected to produce a number of thermalized leptons. Therefore lepton spectrum can be measured and one can look for the excess of lepton production with respect to all known, non-QGP lepton sources. Such an analysis was performed by the CERES collaboration at SPS[10].

- Lattice QCD calculations show that energy density required to create a QGP is on the order of 1 GeV/fm^3. Energy density ϵ obtained in the heavy-ion collisions can be estimated by a simple Bjorken formula[11]:

$$\epsilon = \frac{1}{A\tau_0}\frac{dE_T}{dy}, \tag{2.2}$$

where τ_0 is the initial formation time, $A = \pi R_A^2 = 3.94A^{2/3}$ and produced transverse energy E_T per unit rapidity is measured in the experiment. A formation time is assumed to be on the order of 1 fm/c. At SPS the formula gives $\epsilon = 3.5 GeV/fm^3$ for central Pb+Pb collisions at center of mass energy per nucleon $\sqrt{s_{NN}} = 17GeV$[12], while at RHIC collisions at $\sqrt{s_{NN}} = 130GeV$ it gives $\epsilon = 4.6$ GeV/fm^3[13]. Both in SPS and RHIC central collisions the energy density is therefore sufficient for QGP creation.

Since the beginning of RHIC operation a new colliding system of Au ions at the highest energy achieved so far ($\sqrt{s_{NN}} = 200GeV$) is available for study. In addition to the QGP signatures mentioned above, several new observables were proposed as evidence for the creation of a new state of matter:

- QGP models predict that a parton traversing the excited system will suffer significant energy loss by induced gluon radiation. Several observables suggest that a strong parton energy loss is indeed observed: strong suppression of the inclusive hadron production in AuAu collisions with respect to pp collisions at the same energy scaled by the number of binary collisions (also known as R_{AA}) and with respect to hadron production in peripheral AuAu collisions scaled accordingly (known as R_{cp})[72, 73, 74], strong suppression of the back-to-back high-p_t jet-like correlation[75, 76] and large values of elliptic anisotropy, v_2, at high-p_t[77].

Furthermore a QGP is, by its nature, created in a large, thermalized system, which is expected to behave like a fluid and should develop collective characteristics. Their description and measurement is described in the next section.

2.3 Collective phenomena in Heavy-Ion collisions

It has been recently suggested[14, 15], that in view of current experimental observations from RHIC, matter created in AuAu collisions is not a loosely bound mixture of quarks and gluons, which can be described by perturbative QCD. On the contrary: it is a new state of matter - a *strongly coupled* Quark-Gluon Plasma, which behaves as an ideal fluid. One of the main observables leading to such conclusion is the collective behavior of matter at small transverse momenta - so called “radial flow” and “elliptic flow”.

2.3.1 Elliptic flow

In a non-central collision of two Au nuclei the initial overlap region has an almond shape, with it’s shorter axis in the *reaction plane* (in the coordinate

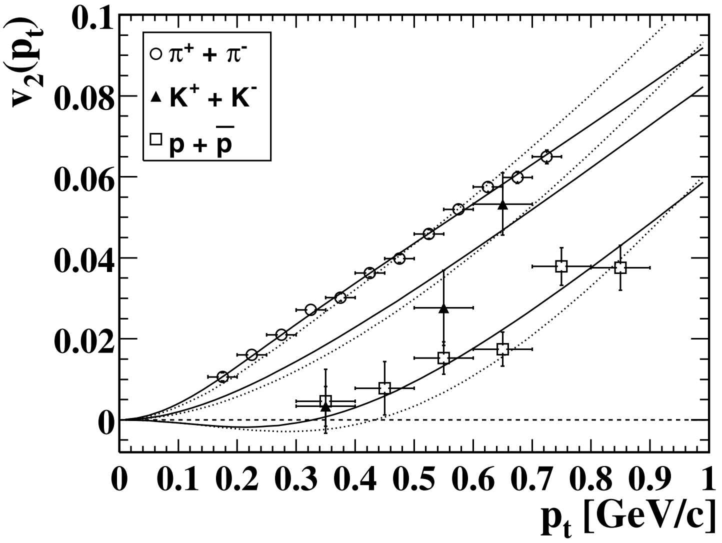

Figure 2.4: Differential elliptic flow for pions, kaons and protons+antiprotons for minimum-bias AuAu events at 130 *AGeV* measured by STAR. The lines show the fit with Blast-wave model.[18]

system traditionally used in heavy-ion community it is the x-z plane, where z is the direction of the beam, and the x is in the transverse plane, along the line connecting centers of colliding nuclei). Naturally pressure gradients are much larger in-plane then out-of-plane, producing larger acceleration and transverse velocities in-plane than out-of-plane. Such differences can be measured by studying the distribution of particles with respect to the reaction plane orientation:

$$\frac{dN}{dyp_T dp_T d\phi} = \frac{dN}{dyp_T dp_T}\frac{1}{2\pi}\left(1 + 2v_1\cos(\phi) + 2v_2\cos(2\phi) + 2v_4\cos(4\phi) + \ldots\right), \tag{2.3}$$

where ϕ is the angle between particle transverse momentum and the reaction plane. In Eq. 2.3 v_2 is the measure of elliptic anisotropy. It has two important characteristics: it is self-quenching, because as particles move faster in-plane, the systems expands faster in this direction, naturally reducing the difference in pressure gradients. Also v_2 needs to build up at the very early stage of the collision, as later the system becomes to dilute to exhibit such collective behavior. Therefore the observation of elliptic flow means that the created system was in fact a strongly interacting matter.

v_2 measurements have been made already at CERN SPS[16]. At RHIC v_2 has been measured with great accuracy as a function of event centrality, particle transverse momentum and particle species[17, 18]. It became clear, that for the first time hydrodynamics successfully describes the collision dynamics, as the measured v_2 reached a hydrodynamic limit, which is illustrated in Fig. 2.4. The lines show the fit of the hydrodynamics-inspired Blast-wave parameterization. The dotted line show results for the calculation with only a momentum anisotropy, while solid lines show fit with both spatial and momentum anisotropy included. As expected, there is a mass ordering of v_2 as a function of p_T with pions having the largest and protons the smallest anisotropy. This plot shows that strong collectivity is observed at RHIC.

RHIC collaborations proceeded to study v_2 with even greater precision. Of particular interest were the measurements of v_2 of strange particles[19]. At the same time it was observed that v_2 diverges from the hydrodynamical expectation at $p_T \sim 2$ GeV, and flattens at a non-zero value at larger p_T up to of at least 7 GeV. Such behavior was expected, as the lower end of the spectrum is the bulk, collectively developing matter, and at the higher end it is thought to be governed by jet physics described by pQCD (see previous section). Only recently however the importance of the intermediate-p_T region (roughly 2-4 GeV) was realized. A striking feature was observed in the nuclear modification factor R_{CP} at this range - shown in Fig. 2.5. It appeared that mesons scale differently than the barions, regardless of their mass.

A similar measurement with v_2 is shown in Fig. 2.6. When measured v_2 was scaled by the number of quarks in a given particle, all measurements appeared to be consistent in an intermediate range of p_T, including singly strange Λ and doubly-strange Ξ particles. This strongly suggested that not only is collectivity present at RHIC, it is also a collectivity present *in a partonic phase*, where the relevant degrees of freedom are, among others, quarks. Particles would later be formed by a coalescence of quarks, and they would pick up elliptic flow v_2 at $2v_2^q$ for mesons and $3v_2^q$ for barions (where v_2^q is the elliptic flow of quarks).

The partonic collectivity observed at RHIC would be one of the most convincing evidence for the existence of QGP, however these measurements have emerged only recently and are still considered preliminary.

2.3.2 Transverse radial flow at mid-rapidity

Elliptic flow discussed in the previous chapter is produced by pressure gradients, which must also produce a more simple collective behavior of matter - a movement inside-out, called radial flow. Particles are pushed to higher momenta and they move away from the center of the collision. A source not showing collective behavior - such as pp collision at RHIC, produces particle spectra that can be

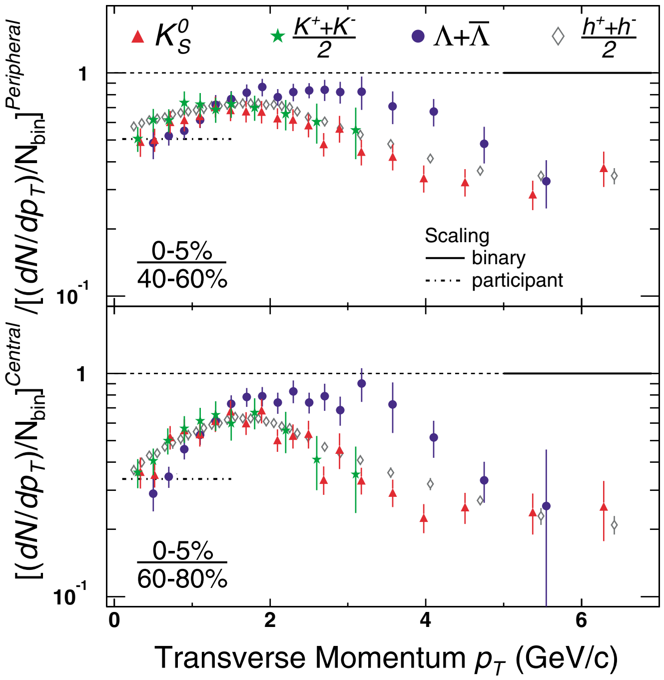

Figure 2.5: The ratio R_{CP} for K_S^0, $K^\pm$ and $\Lambda + \bar{\Lambda}$ at midrapidity for two classes of centrality measured by STAR at $\sqrt{s_{NN}} = 200GeV$[20].

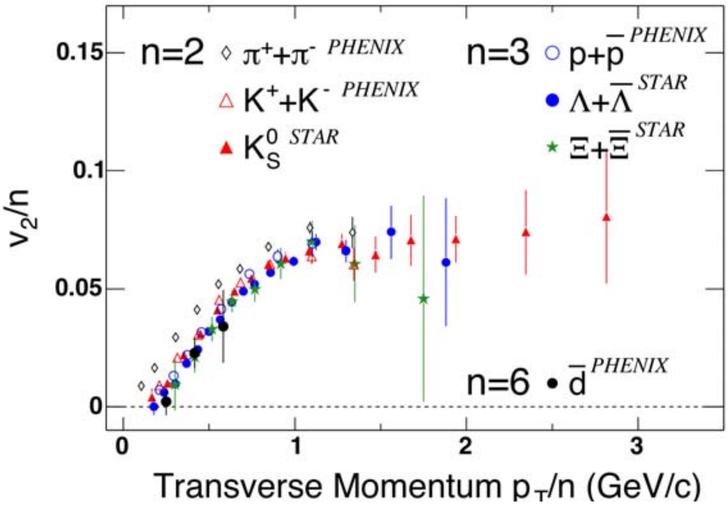

Figure 2.6: v_2 measured at RHIC as a function of particle's quark content[21].

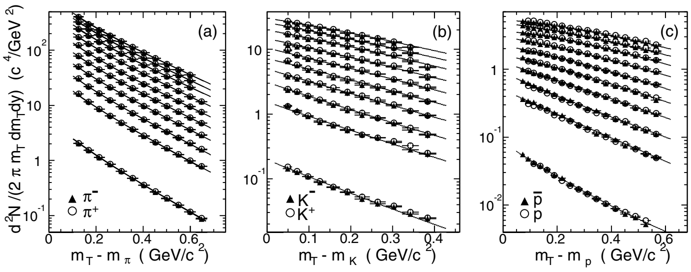

Figure 2.7: Invariant yield as a function of transverse mass m_T for $\pi^{\pm}$, $K^{\pm}$, p and $\bar{p}$ at mid-rapidity for pp (bottom) and Au+Au events from 70-80% (second bottom) to 0-5% (top) centrality[22].

fitted by a power-law:

$$\frac{1}{2\pi p_T}\frac{dN}{dp_T d\eta} = C\left(1+\frac{p_T}{p_0}\right)^{-n}. \tag{2.4}$$

Radial flow shifts particles to higher p_T, which would produce a spectra, which would have a smaller slope parameter. Such behavior is indeed observed in data shown on Fig. 2.7. Spectra for AuAu collisions are significantly less steep than pp collisions, and the difference grows with centrality - as it is expected. The fits are made with the blast-wave parameterization, which is described in section 2.4.2. The shift to higher momenta means that the mean transverse momentum $\langle p_T \rangle$ of the particles also increases.

In radial flow matter moves collectively, so the flow velocity is the same for all particle species. This means that particles with higher mass will be boosted more, and at sufficiently high momenta, the proton spectrum will cross kaon and pion spectra.

Radial flow can also be viewed as a correlation between the space-time freeze-out point where the particle is emitted and it's momentum - more specifically the spatial emission angle ϕ_S will be correlated with the momentum emission angle ϕ_P, or in other words the particle momentum is most likely to point outwards from the center of the collision. This effect, and the fact that for heavier particles flow will determine their momentum, as they are less smeared by thermal motion, is the main cause of the emission asymmetries, that will be studied later in this work.

2.4 Heavy Ion Collision models

2.4.1 RQMD

The Relativistic Quantum-Molecular Dynamic model (RQMD)[23] has been used extensively in modeling heavy-ion collisions at SPS. This model has been written explicitly to study collective interactions in the preequilibrium quark matter and hadronic resonance gas stage in the framework of the transport theoretical approach. The base for the interactions are string fusion into color ropes and hadronic rescattering.

The goal of the model is to develop a complete transport theoretical scenario of nucleus-nucleus interactions, from the initial state of two nuclei before overlap to the final state after the strong interactions have ceased (freeze-out). The code is a semi-classical microscopic approach which combines classical propagation with stochastic interactions. Strings and resonances can be excited in elementary collisions. Their fragmentation and decay leads to production of particles. Overlapping strings form "ropes", chromoelectric flux-tubes. In low energy collisions (around 1 $AGeV$) RQMD reduces to solving transport equations for a system of nucleons, other hadrons and eventually resonances interacting in binary collisions in mean fields. At large beam energies (> 10 $AGeV$) the description of a projectile hadron interacting in a medium as a sequence of separated hadron or resonance collisions breaks down. A multiple collision series can be formulated on a sub-hadronic (quark) level. Following the paths of the ingoing constituent quarks, a Glauber-type multiple collision series is generated in RQMD. The secondaries which emerge from the fragmenting strings, ropes and resonances may interact with each other and the original ingoing hadrons (rescattering and mean-field interaction).

In this work we use the RQMD model in the study of a generated final-state of the collision. Of particular interest is the collective behavior of matter, which may be generated both at the initial, prehadronic or quark matter stage as well as at the hadronic stage. It is expected that independent string fragmentation, which means no collectivity at all, breaks down at central nucleus-nucleus collisions because the string density gets too large. Interactions between multiple overlapping strings is modeled as color rope formation in RQMD. Ropes can be viewed as a model of locally deconfinded quark matter. The evolution of the rope is governed by non-perturbative dynamics.

The resonance are introduced in RQMD as quasi-particles under a limiting condition ($\Gamma/M \ll 1$). If the system is sufficiently dense their interaction may become important. They are of particular relevance in the study of non-identical particle correlations. On one hand the collective behavior of matter is also developed in the hadronic stage. More importantly, because of resonance finite life-time, their decay products will be produced later than direct particles, that is at the moment of the resonance decay. The asymmetry analysis (see section 3.2.3), which is the main topic of this work, is directly sensitive to such time differences. Full resonance treatment implemented in RQMD, makes the studies with this model the best method to estimate the relative importance of time and space contributions to the emission asymmetries.

2.4.2 Understanding freeze-out - blast-wave parameterization

All hadrons in heavy-ion collisions, including mesons, have their momenta finally determined at the moment of their last scattering. Close relative velocity two-particle correlations are sensitive to this final space-momentum distribution, also called the "freeze-out" distribution. However a consistent description of all low-p_T variables has not yet been achieved in most physical models which aim to describe the evolution of the collision. Hadronic cascade models like RQMD predict too large source sizes, measured by HBT techniques (see section 3.1) and too small momentum elliptic anisotropy v_2[24]. As described in the previous section, the hydrodynamic models successfully describe the momentum part of the freeze-out distributions - particle p_T spectra and elliptic anisotropy v_2. However no hydrodynamic model was able to consistently describe complete momentum and space-time freeze-out distribution[25], which is often called the "RHIC HBT puzzle" (see section 3.1).

In order to further the understanding the freeze-out in heavy-ion collisions a "blast-wave" parameterization was developed[26, 27], basing on the functional form derived from hydrodynamic models. The physical parameters of the configuration are treated as free parameters of the fit. The aim is to describe all the observables in the soft sector with the combination of as few parameters as possible. The "blast-wave" parameterization was chosen as a model useful in the study of meson-meson correlations, because it deals directly with transverse collective behavior of the bulk of the matter created in heavy-ion collisions - both the radial and elliptic flow.

In this work, the most recent and most advanced form of "blast-wave" from Lisa and Retiere was used[27]. The mathematics concept of the model is described below.

The source is parameterized as a cylinder, infinite in the longitudinal direction and longitudinally boost-invariant. The cylinder is, in the most general form, composed of elliptical shells, suitable for modeling collisions with finite impact parameter. The sharpness of the boundary of the system can be changed, and can be set e.g. to a box shape, or a gaussian-like smooth edge. The formula includes non-trivial space-momentum correlations, which manifest themselves as e.g. radial and elliptical flow.

The "blast-wave" has eight independent parameters: T, ρ_0, ρ_a, R_y, R_x, a_s, τ_0 and $\Delta\tau$. Their meaning is given below. The transverse shape is controlled by the radii:

$$\Omega\left(r,\phi_s\right)=\Omega\left(\tilde{r}\right)=\frac{1}{1+e^{(\tilde{r}-1)/\alpha_s}}, \tag{2.5}$$

where $\tilde{r}$ is the normalized elliptical radius:

$$\tilde{r}\left(r,\phi_s\right)=\sqrt{\frac{\left(r\cos\phi_s\right)^2}{R_x^2}+\frac{\left(r\sin\phi_s\right)^2}{R_y^2}}. \tag{2.6}$$

As can be seen, parameter α_s controls the sharpness of the source edge, while R_x and R_y give the size of the source. An elliptical source is produced when $R_x \neq R_y$. The source can be viewed as divided into elements; each of them, located at (x, y, z) is emitting particles with fixed temperature T (the same for all elements). The particles are additionally boosted by a transverse rapidity $\rho\left(x,y\right)$ (a flow vector field). The azimuthal direction ϕ_b of the boost is normal to the surface of the corresponding elliptical sub-shell. Following hydrodynamical calculations the boost strength depends linearly on the freeze-out radius $\tilde{r}$. The flow strength also is azimuthally anisotropic, as suggested by the v_2 measurements, giving the final formula for the flow field:

$$\rho\left(r,\phi_s\right)=\tilde{r}\left(\rho_0+\rho_a\cos\left(2\phi_b\right)\right). \tag{2.7}$$

The ρ_a parameter and a ratio R_x/R_y are both sources of elliptical anisotropy. From the assumption of longitudinal boost-invariance it follows that the freeze-out occurs with the distribution in longitudinal proper time $\tau=\sqrt{t^2-z^2}$. The proposed distribution:

$$\frac{dN}{d\tau}\sim\exp\left(\frac{-\left(\tau-\tau_0\right)^2}{2\Delta\tau}\right), \tag{2.8}$$

shows that the τ parameter corresponds to average emission time, while $\Delta\tau$ controls the duration of the emission.

The dependencies 2.5, 2.6, 2.7, 2.8 are combined in the generalized form of the emission function taken from[28]:

$$S\left(x,K\right)=m_T\cosh\left(\eta-Y\right)e^{-K\cdot u/T}\Omega\left(r,\phi_s\right)e^{\frac{-\left(\tau-\tau_0\right)^2}{2\Delta\tau}}. \tag{2.9}$$

The Boltzmann factor is a consequence of the assumption of the thermal equilibrium within a source element moving with four-velocity $u_\mu(x)$. From boost-invariance follows the longitudinal flow velocity $v_L = z/t$, which gives:

$$\begin{aligned} u_\mu(x) &= (\cosh\eta\cosh\rho(r,\phi_s), \sinh\rho(r,\phi_s)\cos\phi_b, & (2.10) \\ & \quad \sinh\rho(r,\phi_s)\sin\phi_b, \sinh\eta\cosh\rho(r,\phi_s)) & (2.11) \end{aligned}$$

and

$$K_\mu = (m_T\cosh Y, K_T\cos\phi_p, m_T\sin\phi_p, m_T\sinh Y), \tag{2.12}$$

where K_T is the transverse momentum, m_T - transverse mass, Y - rapidity and ϕ_p - momentum azimuthal angle of the emitted particle. The equations 2.9, 2.10 and 2.12 can be rewritten as the final emission function:

$$S(x,K) = m_T\cosh(\eta - Y)\, e^{\alpha\cos(\phi_b-\phi_p)} e^{-\beta\cosh(\eta-Y)}\Omega(r,\phi_s)\, e^{\frac{-(\tau-\tau_0)^2}{2\Delta\tau}}, \tag{2.13}$$

where we define:

$$\alpha \equiv \frac{K_T}{T}\sinh\rho(r,\phi_s) \tag{2.14}$$

$$\beta \equiv \frac{m_T}{T}\cosh\rho(r,\phi_s). \tag{2.15}$$

In order to obtain the results which can be compared to the data, the described model has been implemented as the Monte-Carlo generator of particles, which is described in detail in Appendix D. The emission function $S(x,K)$ is then treated as an unnormalized probability density function. The results of the "blast-wave" parameterization fit, the predictions for the emission asymmetries as well as their comparison to the data and its implications are described in Chapter 7.

Chapter 3

Two-particle correlations at low relative velocity

Two-particle interferometry is used to measure the smallest sizes possible - the ones of a single nucleon. Through particle correlations, their momentum distributions can be used to deduce the space-time extent of the emitting system. It is one of the few methods available, which measures sizes of the order of 10^{-15} m.

3.1 Identical particle correlations

Historically the first measurement which can be connected to particle correlations was made in astronomy. R. Hanbury-Brown and R.Q. Twiss in their work[29] have proposed a method to measure angular size of stars by studying correlations of intensity of electromagnetic waves reaching the Earth[30]. The idea of the technique is shown on Fig. 3.1. The measured quantity is the intensity of signals in two telescopes x_3 and x_4 as a function of the distance $d = |x_3 - x_4|$. Using the intensity interferometry method, which is introduced in more detail in the next chapter, we can obtain the momentum characteristic of the source. Then, using the relation:

$$\vec{q} \approx \omega_0 \vec{\theta} \tag{3.1}$$

one can infer from the momentum difference $\vec{q} = \vec{p_1} - \vec{p_2}$ the angular size of the star $\vec{\theta} = \vec{R}/L$. ω_0 is the average wavelength of the electromagnetic radiation detected. Although the HBT measurement can be explained in quantum language, Hanbury-Brown and Twiss explained their observation in classical terms.

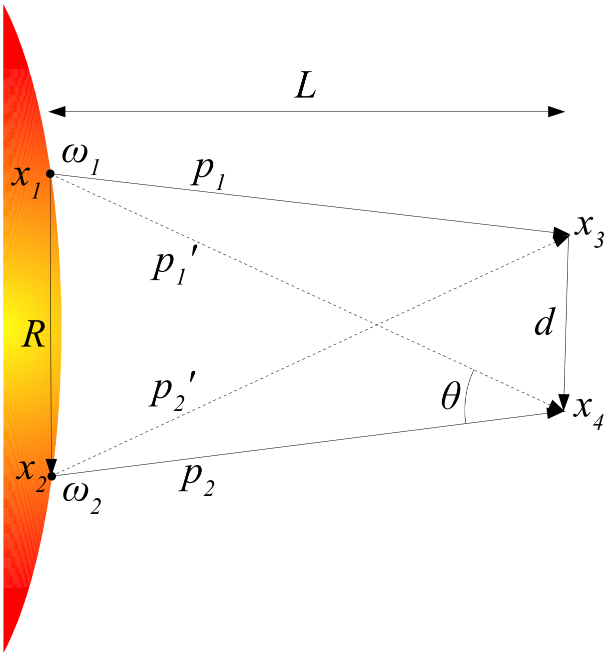

Figure 3.1: Illustration of the HBT technique in astronomy

Intensity interferometry in heavy ion physics employs similar mathematical formalism as the astronomy HBT measurement. It uses the momenta of the particles in the detector to measure the space-time extent of the emitting source. More specifically through the measurement of the correlation between two particles as as function of their relative momenta $\vec{q} = \vec{p_1} - \vec{p_2}$ one can infer the average relative separation between sources, which is illustrated on Fig. 3.2 as $\mathbf{x} = |\mathbf{x}_A - \mathbf{x}_B|$. HBT methods in astronomy and two-particle interferometry in nucleus-nucleus collisions use correlations in one part of the phase-space to obtain information about the complementary part of the phase-space which is not measurable otherwise.

3.1.1 Two-particle intensity interferometry in heavy-ion reactions

Two particles p_1 and p_2 are emitted from two regions $\mathbf{x}_A$ and $\mathbf{x}_B$. Usually it is assumed that the sizes of these regions of coherent emission are small $r_A, r_B \ll |\mathbf{x}_A - \mathbf{x}_B|$, which is called the *smoothness condition*:

$$\begin{aligned} \mathbf{x}_1 \approx \mathbf{x}_1' &\approx \mathbf{x}_A \\ \mathbf{x}_2 \approx \mathbf{x}_2' &\approx \mathbf{x}_B \end{aligned} \tag{3.2}$$

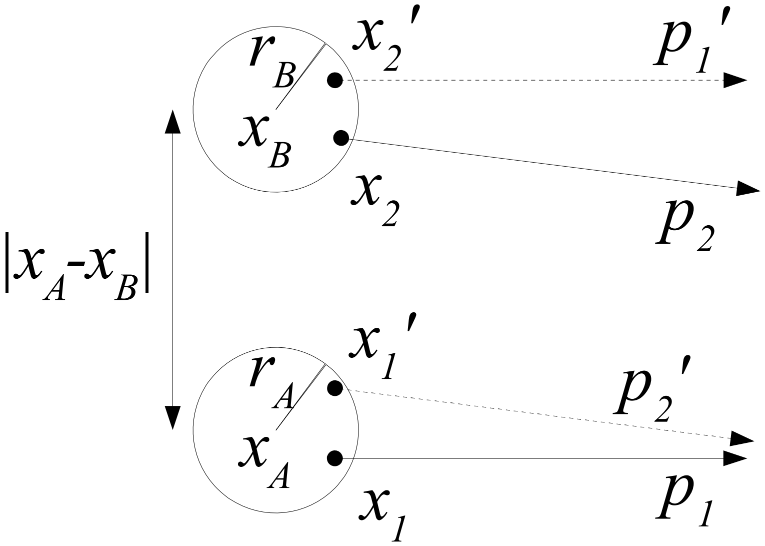

Figure 3.2: Intensity interferometry in heavy-ion collisions

$$\mathbf{x} = \mathbf{x}_A - \mathbf{x}_B \quad \approx \quad \mathbf{x}_1 - \mathbf{x}_2. \tag{3.3}$$

The emitted particles can then be treated as two incoherent waves. Particle p_1 is emitted from $\mathbf{x}_A$ and particle p_2 is emitted from $\mathbf{x}_B$. However if the particles are identical, and therefore indistinguishable, one also has to consider the scenario, where particle p_1 came from $\mathbf{x}_B$ and particle p_2 came from $\mathbf{x}_A$. In such case, the wave-function of the pair has to contain both components:

$$\frac{1}{\sqrt{2}}\left[\exp\left(-ip_1x_A - ip_2x_B\right) \pm \exp\left(-ip_2x_A - ip_1x_B\right)\right]. \tag{3.4}$$

It is a phenomenon well known from quantum mechanics: the wave-function needs to be (anti-)symmetrized for the system of many bosons(fermions).

Such correlation was first seen by Goldhaber et al.[31], which noted the excess of the probability of detecting a pair of identical pions ($\pi^+\pi^+$, $\pi^-\pi^-$) at small opening angle with respect to similar probability for non-identical pions $\pi^+\pi^-$. They have also correctly interpreted it as a Bose-Einstein correlation. Later Kopylov and Podgoretsky have developed an interferometry method[32, 33], orthogonal to astronomy HBT[34], which allowed for studying the space-time extent (of the order of 10^{-15} m) of the source emitting elementary particles. This method is introduced below[35, 36, 37].

We consider the distribution of the momenta of pairs of particles:

$$\sigma\left(p_1,p_2\right) \sim \sum_{\alpha} \left|T\left(p_1,p_2;\alpha\right)\right|^2, \tag{3.5}$$

where σ is the cross-section for the emission of two particles with momenta p_1 and p_2, T is the amplitude of such process and the sum runs over all possible states α of the system. It is also necessary to introduce the proper (anti-)symmetrization for bosons(fermions). For particles with spin 0:

$$\sigma\left(p_1,p_2\right) \sim \sum_{\alpha} \left|\frac{1}{\sqrt{2}}\left[T\left(p_1,p_2;\alpha\right)+T\left(p_2,p_1;\alpha\right)\right]\right|^2. \tag{3.6}$$

When two independent single-particle sources are considered, the emission function factorizes:

$$T(p_1,p_2;\underbrace{x_A,x_B,..}_{\alpha}) = t_A\left(p_1;x_A,..\right)t_B\left(p_2;x_B,..\right). \tag{3.7}$$

If the particles are free-streaming, they can be viewed as plane waves:

$$t_A\left(p_1;x_A\right) = \int d^4x_1 e^{ip_1x_1}\widetilde{u}_A\left(x_1-x_A;..\right) \equiv e^{ip_1x_A}\underbrace{\int d^4\xi e^{ip_1\xi}\widetilde{u}_A\left(\xi;..\right)}_{u_A(p_1;..)} \tag{3.8}$$

where u_A amplitude depends on the internal structure of the source. The momentum distribution function can then be written as:

$$\begin{aligned}\sigma\left(p_1,p_2\right) \quad \sim \quad & \sum_{A,B,..}\int d^4x_A d^4x_B \left\{\left|u_{A(p_1;..)}u_{B(p_2;..)}\right|^2\right. \\ & \left. +Re\left[e^{iqx}u_{A(p_1;..)}u_{B(p_2;..)}u^*_{A(p_2;..)}u^*_{B(p_1;..)}\right]\right\}, \end{aligned} \tag{3.9}$$

where q and x were defined in the previous section, and $p=\frac{1}{2}\left(p_1+p_2\right)\equiv\frac{1}{2}P$. In the case of universal sources $u_A=u_B$, the formula can be simplified, but at small separation of the sources they cannot be considered independent. Therefore further calculation require one more assumption, so called "smoothness assumption", which says that the change of the parameters of the source is small in the area influenced by the correlation effect:

$$|q|<1/r_0 \ll |p| \quad \rightarrow \quad u_A\left(p\pm q/2;..\right)\approx u_A\left(p;..\right) \iff \left|\Delta x_{source}\right| \ll \left|x_A-x_B\right|, \tag{3.10}$$

where r_0 is the average squared radius of the emission region. The following result is then obtained:

$$\sigma \sim 1+\langle\cos qx\rangle. \tag{3.11}$$

Using quantum mechanics notation it can be also written as:

$$\begin{aligned}\sigma_{12} &\sim \left\langle \left| \langle p_1 |\, x_A \rangle \langle p_2 |\, x_B \rangle + \langle p_2 |\, x_A \rangle \langle p_1 |\, x_B \rangle \right|^2 \right\rangle \\ &\sim \left\langle \left| e^{ip_1 x_A} e^{ip_2 x_B} + e^{ip_2 x_A} e^{ip_1 x_B} \right|^2 \right\rangle = 1 + \langle \cos qx \rangle \,. \qquad (3.12)\end{aligned}$$

As can be seen, the correlation effect for identical bosons has a form $\langle \cos qx \rangle$. It arises from the symmetrization of the wave-function in Eq. (3.6). It can be explained by the following argument. Let's assume situation 1): particle 1 is emitted from source A and particle 2 is emitted from source B. Such situation is possible regardless on the relative distance of source A and source B. However if both source are in the same emitting system it is possible that they are so close that an additional situation 2) is possible: particle 1 is emitted from source B and particle 2 is emitted from source A. If the particles are identical and therefore indistinguishable situation 1) cannot be distinguished from 2). So one can take the distribution E of the relative momenta of pairs of particles, where both particles are emitted from the same system. Both cases 1) and 2) are then possible. One can also take corresponding distribution D where two particles are emitted from different systems (e.g. from different heavy-ion collisions). Only situation 1) is then possible. If one performs the division E/D, one will obtain the factor 1 from dividing out situations 1) and an additional correlation term $\langle \cos qx \rangle$ coming from the situation 2) in distribution E. Quantum-mechanically it means that for sufficiently small relative momenta q the wave-packets of both particles overlap and start to interfere. One crucial difference between astronomy HBT technique and nucleus-nucleus intensity interferometry is apparent: in the former the particles interfere *in the detector*, while in the latter they interfere *in the emitting source*.

3.1.2 Correlation function for particles with small relative momenta

3.1.2.1 Theoretical approach

Single-particle and two-particle distributions can be expressed in terms of the creation $\widehat{a}_p^+$ and annihilation $\widehat{a}_p$ operators for particles of the momentum $\vec{p}$ [39]:

$$P_1\left(\overrightarrow{p}\right) = E\frac{dN}{d^3p} = E\left\langle \widehat{a}_p^+ \widehat{a}_p \right\rangle \qquad (3.13)$$

$$P_2\left(\overrightarrow{p}_a, \overrightarrow{p}_b\right) = E_a E_b \frac{dN}{d^3p_a d^3p_b} = E_a E_b \left\langle \widehat{a}_{p_a}^+ \widehat{a}_{p_b}^+ \widehat{a}_{p_b} \widehat{a}_{p_a} \right\rangle . \qquad (3.14)$$

They are normalized to $\langle N \rangle$ and $\langle N(N-1) \rangle$, that is to the average number of particles (pairs) observed in a single collision. Two-particle correlation function:

$$C\left(\overrightarrow{p}_a, \overrightarrow{p}_b\right) = \frac{P_2\left(\overrightarrow{p}_a, \overrightarrow{p}_b\right)}{P_1\left(\overrightarrow{p}_a\right) P_1\left(\overrightarrow{p}_b\right)} \tag{3.15}$$

can also be written as:

$$C\left(\overrightarrow{p}_a, \overrightarrow{p}_b\right) = 1 \pm \frac{\left|\left\langle \widehat{a}^+_{p_a} \widehat{a}_{p_b} \right\rangle\right|^2}{\left\langle \widehat{a}^+_{p_a} \widehat{a}_{p_a} \right\rangle \left\langle \widehat{a}^+_{p_b} \widehat{a}_{p_b} \right\rangle} \tag{3.16}$$

if the independent particle emission (factorization of the two-particle emission function) is assumed. The emission of particles can also be written using the "emission function" formalism. The emission function $S(x, K)$ is introduced. It can be understood as the generalized density function of the source, or as a probability density, which determines what is the probability of emission of the particle with momentum K from space-time point x. The following relation then holds:

$$E_p \frac{dN}{d^3p} = \int d^4x S(x, p) \tag{3.17}$$

and the correlation function becomes:

$$C\left(\overrightarrow{q}, \overrightarrow{K}\right) = 1 + \frac{\left|\int d^4x S(x, K) e^{iqx}\right|^2}{\int d^4x S\left(x, K + \frac{1}{2}q\right) \int d^4x S\left(x, K - \frac{1}{2}q\right)}, \tag{3.18}$$

where average momentum of the pair $\overrightarrow{K} = (\overrightarrow{p}_a + \overrightarrow{p}_b)/2$ is introduced. If one also approximates the product of single particle distributions in the denominator by the square of the single-particle distribution at average pair momentum $\vec{K}$, one obtains:

$$C\left(\overrightarrow{q}, \overrightarrow{K}\right) = 1 + \left|\frac{\int d^4x e^{iqx} S(x, K)}{\int d^4x S(x, K)}\right|^2 \equiv 1 + \left|\left\langle e^{iqx} \right\rangle\right|^2. \tag{3.19}$$

Therefore both single-particle spectra and correlation functions can be expressed as simple integrals of the emission function. Any further considerations of the particle correlations require that a specific form of this function is proposed.

3.1.2.2 Experimental approach

When studied in the experiment, the correlation function is defined as a ratio of the probability to register two particles simultaneously (in the same event) with respect to the product of registering such particles independently (in different events). The former is the conditional probability of registering particle with momentum p_2 when a particle with momentum p_1 is observed. The latter is the product of two single-particle probabilities. When the two are divided:

$$C\left(p_1, p_2\right) = \frac{P\left(p_1, p_2\right)}{P\left(p_1\right) P\left(p_2\right)}, \tag{3.20}$$

the single particle probabilities are divided out and only the conditional one (the correlation) remains. The formula 3.20 can be also formulated in the cross-section formalism:

$$C\left(p_1, p_2\right) \propto \frac{d^6\sigma}{d^3p_1 d^3p_2} \bigg/ \left(\frac{d^3\sigma}{d^3p_1}\frac{d^3\sigma}{d^3p_2}\right). \tag{3.21}$$

Usually the correlation function is analyzed as a function of pair relative momentum $\vec{q}$, as the natural reference frame for the two-particle interaction consideration is the frame, where the pair center-of-mass rests, or the pair rest frame (PRF). In the theoretical formulation the division 3.21 is, in principle, possible even when only a single event is considered. So far such attempts of "event-by-event" analysis in heavy-ion collisions have been unsuccessful. Usually one has to average over large number of events. However, since each system created in such collisions is, in principle, different, special care needs to be taken to analyze only events with similar characteristics (e.g. similar centrality).

3.1.2.3 Correlation function parameterizations

As stated in section 3.1.2.1, an emission function needs to be proposed in order to develop the technique further. Often the source is assumed to be a 3-dimensional sphere with Gaussian density profile in space-time coordinates:

$$S\left(\mathbf{r}\right) \sim \exp\left(-\overrightarrow{r}_A^2/2r_0^2 - t_A^2/2\tau_0^2\right), \tag{3.22}$$

where r_0 is the size of the source in space (more specifically a Root Mean Square of the distribution) , and τ_0 is the corresponding size in time. It is important to note, that such function describes a static source, as it does not depend on particle momentum $\vec{K}$. The integration in Eq. (3.19) can then be carried out, yielding the following form of the correlation function (for bosons with spin 0):

$$C\left(\overrightarrow{q}\right) \sim 1 + \exp\left(-\vec{r_0}^2\vec{q}^2 - \tau_0^2 q_0^2\right). \tag{3.23}$$

The $\vec{q}$ variable can be decomposed into three components, called the Bertsh-Pratt parameters[40], first introduced by Podgoretsky[41], shown schematically on Fig. 3.3. The $\vec{q}$ vector is decomposed into the longitudinal component q_L parallel to the beam-axis (the z-axis), the outwards component q_O parallel to the transverse momentum of the pair $\vec{K_T}$ and the sidewards component q_S per-

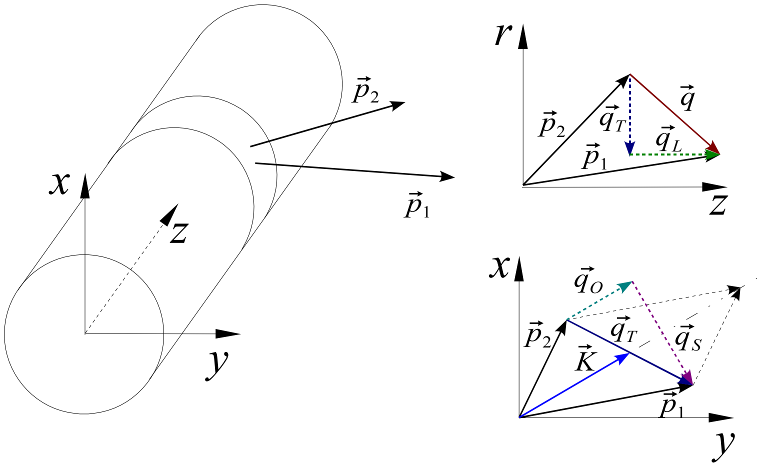

Figure 3.3: Bertsh-Pratt decomposition of the vector of the momentum difference $\vec{q}$

pendicular to the other two. Since there are only three independent components of $\vec{q}$ (the energy difference q_0 is completely determined by the particle momenta, since masses of the particles are the same) the time extent of the source cannot be independently determined. Putting 3.22 into 3.19 one gets the following, 3-dimensional correlation function:

$$C\left(q_L, q_S, q_O\right) = 1 + \lambda \exp\left(-q_L^2 r_{long}^2 - q_S^2 r_{side}^2 - q_O^2 r_{out}^2\right). \tag{3.24}$$

Simplifying the picture further one can analyze the correlation function as a function of only one variable - the value of the relative momentum $|\vec{q}|$ in the pair rest frame:

$$C\left(q, \lambda\right) = 1 + \lambda \exp\left(-r_0^2 q^2\right), \tag{3.25}$$

where λ parameter determines the relative strength of the correlation and is within $(0.0, 1.0)$. Values of λ lower than 1.0 are observed experimentally and are attributed to several reasons: the inclusion of misidentified particles in the sample (particle purity), the inclusion of non-correlated pairs (where one or both particles come from e.g. long-lived resonance) and detector inefficiencies.

The parameterized correlation functions (3.24) or (3.25) can be fitted to the experimental ones, providing the size of the emitting source - average Gaussian radius of the source r_0 in the case of 1-dimensional correlation function, or 3 radii r_{out}, r_{side} and r_{long} in the case of 3-dimensional correlation function. It is important to note that the r_{out} is the size along the direction of pair momentum and r_{side} is the size along the direction perpendicular to it and to the z axis. It must be emphasized, that the *out*, *side* and *long* directions are local for each pair, and the resulting averaged sizes r cannot be transformed into laboratory frame without further assumptions.

In the case of the experimental correlation functions for real particles it is possible that particles interact by Coulomb or strong forces. Such interaction will, in principle, influence the correlation function, and it needs to be taken into account when performing the fitting. Since these interactions are the basis of non-identical particle interaction, they will be described in detail in the next section.

The procedure described above assumes a static source emitting particles, while we know this is not the case in RHIC heavy-ion collisions. Even before that the importance of the dynamics of the source was noticed for the correlations between particles emitted by resonance decay[55, 56, 57], or the particles emitted from jets[58]. In heavy-ion collisions a true source dynamics is developed: transverse radial and elliptic flow exists there. To address this issue, the concept of the "lengths of homogeneity"[52, 53, 54] was introduced. It is defined simply as:

$$\frac{\left|f\left(p, x_0+\bar{\lambda}\right)-f\left(p, x_0\right)\right|}{f\left(p, x_0\right)}=1, \tag{3.26}$$

where $\bar{\lambda}$ is the homogeneity length. It can be interpreted as the distance at which the relative change of the source Wigner function f becomes large. It was shown, that the observed interferometry radii will not correspond to the size of the whole source, but will instead measure the average homogeneity length of the system. It can be intuitively explained based on the hydrodynamic models, where particles are emitted from source elements. Each of these particles is boosted with the flow velocity u_μ according to the point of origin. Since solutions of hydrodynamics are smooth, nearby source elements emit particles with similar velocities. These particles can combine into pairs of small relative momenta, and therefore can be correlated. If two particles are emitted far ($> \bar{\lambda}$) away from each other, the flow field u_μ in their point of emission might be very different and it will be impossible for them to have sufficiently small relative momenta in order to be in the region of the interference effect.

If one assumes boost-invariant longitudinal flow, which is a common feature in hydrodynamic solutions, one can extract the evolution timescale $\tau_{f.o.}$ (the time from the beginning of the collision to freeze-out), assuming zero initial separation in longitudinal direction[59]:

$$R_L\left(k_T\right)=\left\langle\tau_{f.o.}^2\right\rangle^{1/2} \sqrt{\frac{T_k}{m_T}}, \tag{3.27}$$

where T_k is the temperature of the kinetic freeze-out. The formula is valid in the Longitudinally Co-Moving frame (LCMS), where the longitudinal velocity

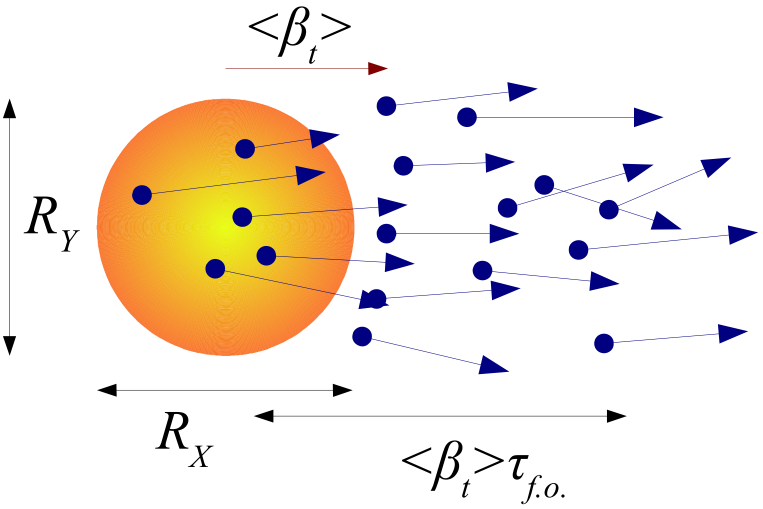

Figure 3.4: Emission duration and it's effect on *out* and *side* radii.

of the pair vanishes.

Following a different argument, one can extract another collision timescale - the duration of freeze-out $\Delta\tau_{f.o.}$. The basic idea is presented on Fig. 3.4. Particles emitted will be, by definition, moving, on the average, in the *out* direction. Therefore the resulting radii will be:

$$\begin{aligned} R_O &= \sqrt{R_X^2 + \beta_t^2 \Delta\tau^2} \\ R_S &= R_Y, \end{aligned} \tag{3.28}$$

where β_t is the particle velocity and $\Delta\tau$ is the emission duration. In the simplest case of a static source $R_X = R_Y$ and the ratio R_O/R_S can be used to estimate the duration of freeze-out.

3.1.2.4 STAR results on identical particles correlations and the “RHIC HBT puzzle”

The momentum Bose-Einstein correlations, which are sometimes called “HBT” correlations, have been measured in high-energy heavy-ion collisions at various energies, starting from Brookhaven National Laboratory AGS[42], through CERN SPS[43, 44, 45, 46, 47] up to BNL RHIC[48, 49]. The STAR experiment has also performed such analysis. The results shown in [49] were later updated[50] to the ones shown in Fig. 3.5. They proved to be a significant challenge to the dynamical models trying to describe the space-momentum evolution of the heavy-ion collision.

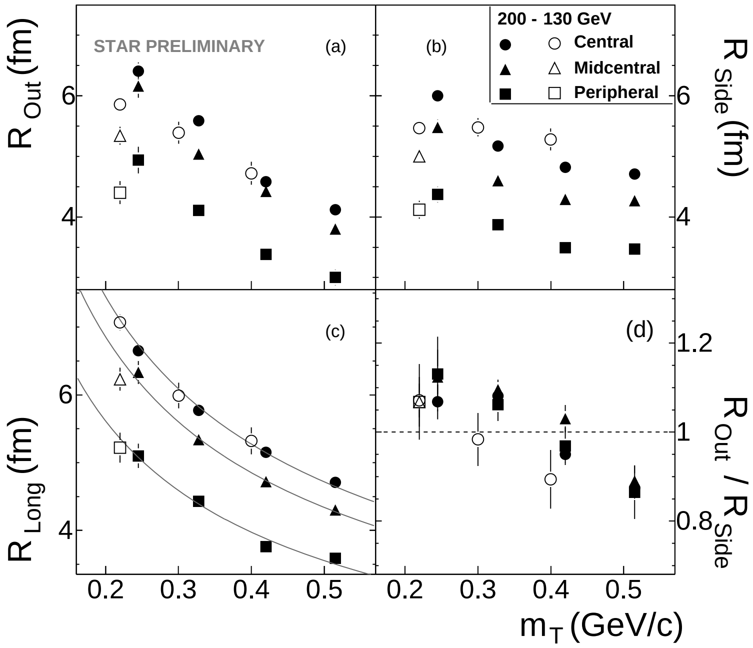

Figure 3.5: Centrality dependence of the m_T dependence of the $\pi^-\pi^-$ interferometry radii for $\sqrt{S_{NN}}$ = 130 GeV (open symbols) and 200 GeV (closed symbols). Results for 200 GeV are preliminary with statistical errors only. Fit in c) is explained in the text.

The most apparent feature of the obtained source sizes is that they were not significantly different than the ones observed at lower energies. In the most naive scenario a matter created in heavy-ion collision would undergo a first-order phase transition, spending significant amount of time in the mixed phase, allowing the system to expand. This would result in large (on the order of tens of fm) source sizes and large system lifetime. Such characteristics were not observed.

If one employs the formula 3.27, assuming freeze-out temperature $T_K = 110$ MeV, and tries to fit the data (as seen on panel c) of Fig. 3.5), one obtains system lifetimes on the order of $8 - 9$ fm/c. This is again in contrast with expectations from hydrodynamic models, which predict that system would need at least $10 fm/c$ to reach the densities at which mean-free path becomes larger than the size of the system[51], which is the effective equivalent of freeze-out. If a more plausible, combined model is used, connecting the early stage of the collision described by hydrodynamics with the later hadron stage simulated by RMQD[51], the evolution duration becomes even larger.

Finally, the ratio R_O/R_S can be used as a measure of the duration of freeze-out (see Eq. 3.28). The initial results from RHIC indicated that this ratio may be less than 1.0, later it turned out it is at 1.0 or slightly above. This again proved to be difficult for the hydro models to explain, as it would mean instantenous emission of particles. In Fig. 3.6 the predictions of hydrodynamic model for the interferometry radii are presented[25]. What is most striking, the same model which predicted, to very good accuracy, the momentum part of the freeze-out distribution, that is the spectra and elliptic flow v_2, fails at describing the space-time part. This and the two other above-mentioned failures of the hydro models were collectively called the "RHIC HBT puzzle". It is interesting to note however, that the "Blast-wave" parameterization (see section 2.4.2), which is based on hydro models is able to reproduce the observed interferometry radii[27], although with parameters, that do not correspond to a physical solution of hydrodynamic equations.

3.2 Non-identical particle correlations

The basis of the original HBT measurement in astronomy are the correlations of photons, which do not interact with each other strongly or by Coulomb forces. In meson-meson close velocity correlations the situation is different: mesons interact through strong force and through Coulomb force, if both of them are charged. Together they are called "final state interactions" (FSI), as they occur after the particles suffer their last collisions, that is after freeze-out, when the particles are in their "final" configuration. In identical particle

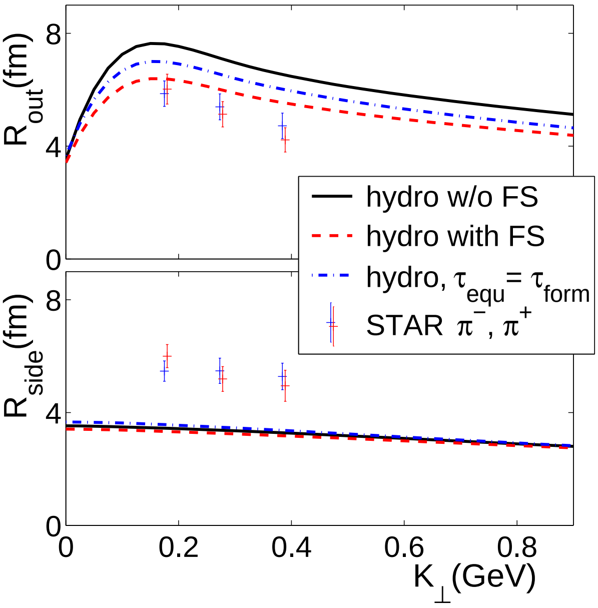

Figure 3.6: Interferometry radii R_O, R_S for central Au+Au collisions at $\sqrt{s_{NN}} = 130\ GeV$ at STAR compared with hydrodynamic predictions from the same simulations which provide an excellent fit to the spectra and elliptic flow (solid lines)[25]. For details of other lines see[25].

correlation analysis, FSI was treated as an effect disturbing the "real", that is the Bose-Einstein/Fermi-Dirac correlation. In case of $\pi\pi$ correlations, where strong interaction is small, the FSI can be approximated by Coulomb and can be corrected for. The most advanced approximate method of such correction has been proposed by Bowler [60] and Sinyukov et al. [61]. However as the mass of particles grows, the importance of Coulomb FSI grows, and e.g. for proton-proton system it dominates over the Fermi-Dirac effect.

A new way of treating FSI has been proposed by Lednicky et al.[62]. They noted that, similar to the effect of quantum statistics, the effect of FSI also influences a correlation between particles, which can be analyzed to obtain the information about the source. Such approach opens a new possibility to study correlation of non-identical particles, providing a qualitatively new piece of information - the emission asymmetries[62, 63, 64, 65]. First preliminary results of such analysis were shown by the NA49 [69] and E877 [70] collaborations.

3.2.1 Symbols and conventions used

In this section the basic symbols, which will be later used consistently in various parts of the text, are introduced. Also the conventions which adopted in the non-identical particle analysis are specified.

Each particle is described by its four-momentum $\mathbf{p_i} = \{E_i, \vec{p_i}\}$ and space-time position $\mathbf{x_i} = \{t_i, \vec{r_i}\}$ in the reference frame of the emitting source (CMS). When two particles are combined into a pair a new reference frame can be introduced, a frame where the center-of-mass of the pair rests. This frame is called Pair Rest Frame or PRF. Values in PRF are consistently marked with an asterisk $*$.

Pair-wise quantities can be calculated when a pair is formed. Most important are the total momentum of the pair $\mathbf{P} = \mathbf{p_1} + \mathbf{p_2} = 2\mathbf{p}$ and the relative momentum of the pair $\mathbf{q} = \mathbf{p_1} - \mathbf{p_2}$. For non-identical particles the generalized momentum difference is defined: $\tilde{\mathbf{q}} = \mathbf{q} - \mathbf{P}\left(\mathbf{qP}\right)/\mathbf{P}^2$. In PRF the one has $\tilde{\mathbf{q}} = \left\{0, 2\vec{k^*}\right\}$, where $\vec{k^*}$ is the momentum of the first particle in PRF. In CMS one also has the spatial coordinate $\mathbf{X} = \left[\left(\mathbf{p_1 P}\right)\mathbf{x_1} + \left(\mathbf{p_2 P}\right)\mathbf{x_2}\right]/\mathbf{P}^2$. Also new directions can be introduced, similar to the *out*, *side*, *long* decomposition of the Bertsch and Pratt shown on Fig. 3.3. The *long* direction is the direction of the beam axis, or z. In the transverse plane the *out* (or x) direction is the one of the momentum of the pair $\vec{P}$, while *side* (or y) is perpendicular to *out* and *long*.

Pair separation can also be calculated as $\vec{r} = \vec{r_1} - \vec{r_2}$. Time difference is $\Delta t = t_1 - t_2$. Both of these variables can also be calculated in the PRF and are then denoted by $\vec{r^*}$ and t^*. It is important to note that for non-identical particles it is significant which particle is first and which is second, as the signs of both $\vec{r}$ and $\vec{q}$ depend on the ordering. Therefore a convention is adopted that the first particle is always the one with lower mass - therefore in this work pions are always taken as first. If both particles have the same mass, the one with larger value of charge is taken as first.

The procedure of decomposition of $\vec{r^*}$ and $\vec{k^*}$ into *out*, *side* and *long* must also be described. First the pair is boosted to the Longitudinally Co-Moving System (or LCMS), that is a system where $p_{1,z} = -p_{2,z}$, along the z axis with velocity $\beta_z = \frac{|p_z|}{E}$. Then $k^*_{long} = p^{LCMS}_{1,z} = -p^{LCMS}_{2,z}$ in this reference frame, while $r^*_{long} = r_{1,z} - r_{2,z}$. The pair is then rotated so that its x axis is along the pair transverse momentum. Then the pair is boosted to the PRF along x axis with $\beta_t = \frac{|p_t|}{E^2 - p_z^2}$. In this reference frame two other components of k^* are defined: $k^*_{out} = p^{PRF}_{1,x} = -p^{PRF}_{2,x}$ and $k^*_{side} = p^{PRF}_{1,y} = -p^{PRF}_{2,y}$. Similarly $r^*_{out} = r^{PRF}_{1,x} - r^{PRF}_{2,x}$ and $r^*_{side} = r^{PRF}_{1,y} - r^{PRF}_{2,y}$. The initial separation in CMS $\vec{r}$ can also be decomposed into three components: r_{out}, r_{side} and r_{long}. Simple relations between the pair separations in CMS and PRF can be given:

$$r^*_{side} = r_{side} \tag{3.29}$$

$$r^*_{long} = \gamma_z \left(r_{long} - \beta_z \Delta t\right) \tag{3.30}$$

$$\Delta t_{LCMS} = \gamma_z \left(\Delta t - \beta_z r_{long}\right) \tag{3.31}$$

$$r^*_{out} = \gamma_t \left(r_{out} - \beta_t \Delta t_{LCMS}\right) \tag{3.32}$$

$$t^* = \gamma_t \left(\Delta t_{LCMS} - \beta_t r_{out}\right), \tag{3.33}$$

where $\gamma_z = \left(1 - \beta_z^2\right)^{-1/2}$ and $\gamma_t = \left(1 - \beta_t^2\right)^{-1/2}$.

3.2.2 Final State Interactions

Final state interaction is studied both to understand its effects on identical particle correlations, as well as to provide the possibility to study non-identical particle correlations. The formalism for the description of FSI is presented in the next sections. At the beginning terms from quantum dynamics, which will be used later, are introduced[71].

3.2.2.1 Scattering amplitude and differential cross-section

Of the interest here are the effects the FSI have on particular particle pair after last particles' collisions. The problem can be treated as an elastic scattering of particle m_1 on the particle m_2 schematically shown on Fig. 3.7. The problem can be reduced to considering the scattering of the quasi-particle with mass $\mu = m_1 m_2 / \left(m_1 + m_2\right)$ on the potential $V\left(\vec{r}\right)$, arising from the FSI. The scattering problem is best considered in the center of mass system (c.m.s.). The area where

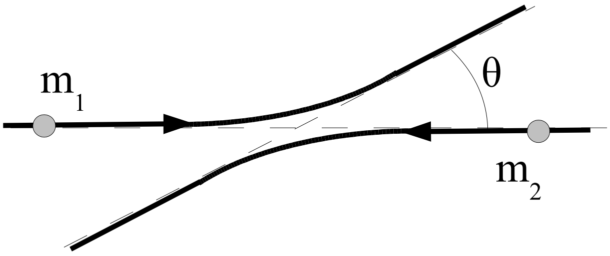

Figure 3.7: Two particles scattering elastically.

the potential V is non-zero is finite, outside of this region the particles can be described as plane waves:

$$\phi_a\left(\vec{r}\right)=\exp\left(i\vec{k}\vec{r}\right). \tag{3.34}$$

The Schroedinger equation for the problem

$$\left(\bigtriangledown^2+k^2\right)\psi\left(\mathbf{r}\right)=\frac{2\mu V\left(\mathbf{r}\right)}{\hbar^2}\psi\left(\mathbf{r}\right) \tag{3.35}$$

is solved by finding the Green function for the left-hand side of the Eq. 3.35 (the free-propagation operator). It is equivalent to finding the function, which fulfills the equation with point-like source:

$$\left(\bigtriangledown^2+k^2\right)G\left(\mathbf{r}\left|\mathbf{r}'\right.\right)=\delta\left(\mathbf{r}-\mathbf{r}'\right). \tag{3.36}$$

If this solution is known, then the general solution of the equation

$$\left(\bigtriangledown^2+k^2\right)\Phi\left(\mathbf{r}\right)=A\left(\mathbf{r}\right) \tag{3.37}$$

can be written as:

$$\Phi\left(\mathbf{r}\right)=\varphi\left(\mathbf{r}\right)+\int G\left(\mathbf{r}\left|\mathbf{r}'\right.\right)A\left(\mathbf{r}'\right)d^3\mathbf{r}'. \tag{3.38}$$

Where $\phi\left(\vec{r}\right)$ is the solution of Eq. 3.37 with right-hand side equal to 0. The solution corresponding to outgoing waves is:

$$G_{(+)}\left(\mathbf{r}\left|\mathbf{r}'\right.\right)=-\frac{\exp\left(ik\left|\mathbf{r}-\mathbf{r}'\right|\right)}{4\pi\left|\mathbf{r}-\mathbf{r}'\right|} \tag{3.39}$$

and therefore:

$$\psi_a\left(\mathbf{r}\right)=\varphi_a\left(\mathbf{r}\right)-\frac{\mu}{2\pi\hbar^2}\int\frac{\exp\left(ik\left|\mathbf{r}-\mathbf{r}'\right|\right)}{\left|\mathbf{r}-\mathbf{r}'\right|}V\left(\mathbf{r}'\right)\psi_a\left(\mathbf{r}'\right)d^3\mathbf{r}'. \tag{3.40}$$

It is an integral equation, which defines a wave-function $\psi_a(\vec{r})$, the solution of the scattering problem. For large distances $r \gg d$ one can assume that

$$k\left|\mathbf{r}-\mathbf{r}'\right| = kr - \mathbf{k_b}\mathbf{r}', \tag{3.41}$$

where $\mathbf{k_b} = k\frac{\mathbf{r}}{r}$ and $\psi_a(\vec{r})$ goes asymptotically to

$$\psi_a(\mathbf{r}) = \varphi_a(\mathbf{r}) - A_{ba}\frac{e^{ikr}}{r}, \tag{3.42}$$

where

$$A_{ba} = -\frac{\mu}{2\pi\hbar^2}\int \exp\left(-ik_b r'\right) V\left(\mathbf{r}'\right)\psi_a\left(\mathbf{r}'\right) d^3\mathbf{r}'. \tag{3.43}$$

Using the form of the wave-function from Eq. 3.34 one can write Eq. 3.43 in the form:

$$A_{ba} = -\frac{\mu}{2\pi\hbar^2}\left\langle\varphi_b\right| V \left|\psi_a\right\rangle.$$

The A_{ba} function is known as the *scattering amplitude*, it is proportional to the reduced mass μ of the quasi-particle and depends on the kinetic energy of the relative motion, the opening angle θ between k_a and k_b vectors and on the scattering potential V. In the limiting case of large distances from the area of non-vanishing potential, the scattered wave $\psi_a(\vec{r})$ is completely determined by the scattering amplitude.

One can also relate the scattering amplitude to the *total differential cross-section*, which is defined as a ratio of the number of particles scattered per unit of time in the element of the solid angle $d\Omega = \sin\theta d\theta d\phi$ to the density of the incoming flux. Radial density of the incoming flux is given as:

$$j_r = \frac{\hbar}{2\mu i}\left(\psi^*_{scatt}\frac{\partial\psi_{scatt}}{\partial r} - \psi_{scatt}\frac{\partial\psi^*_{scatt}}{\partial r}\right) = \frac{\hbar k}{\mu r^2}\left|A_{ba}(\theta,\varphi)\right|, \tag{3.44}$$

and therefore, for elastic scattering we have a relation between the scattering amplitude and the differential cross-section:

$$d\sigma = \frac{j_r r^2 d\Omega}{\left|\mathbf{j}_a\right|} = \frac{k}{k_a}\left|A_{ba}\right|^2 d\Omega. \tag{3.45}$$

3.2.2.2 Final state interaction - the strong potential

The formalism of the description of FSI is taken from [66, 67]. For a pair of particles with non-zero spin one defines the factor $g_0 = (-1)^{2j}/N(j)$, where $N(j)$ is the number of spin-states of the system. Then for a system without the

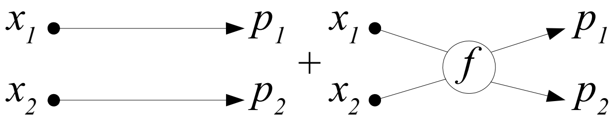

Figure 3.8: States contributing to the FSI calculation

final state interaction one can simply write:

$$W\left(p_1,p_2\right)=1+b\left(p_1,p_2\right), \tag{3.46}$$

where

$$b\left(p_1,p_2\right)=g_0\cos\left(qx\right). \tag{3.47}$$

where $\vec{q}=\vec{p_1}-\vec{p_2}$, $\vec{x}=\vec{x_1}-\vec{x_2}$, $qx=q_0t-\overrightarrow{q}\overrightarrow{r}$ and W is the weight attributed to the pair because of the correlation. Here the correlation comes only from Bose-Einstein or Fermi-Dirac statistics, but if particles do interact through FSI, one must consider two states shown on Fig. 3.8. If we assume that the initial production mechanism is spin-independent, we can rewrite the function b with the use of the Bethe-Salpeter amplitude corresponding to the given interaction:

$$\begin{aligned} b\left(p_1,p_2\right) &= \left\{\tfrac{j+1}{2(2j+1)}\left|\psi^*_{p_1p_2}\left(x_1,x_2\right)+\left(-1\right)^{2j}\psi^*_{p_1p_2}\left(x_1,x_2\right)\right|^2+\right.\\ &\left.+\tfrac{j}{2(2j+1)}\left|\psi^*_{p_1p_2}\left(x_1,x_2\right)-\left(-1\right)^{2j}\psi^*_{p_1p_2}\left(x_1,x_2\right)\right|^2\right\}-1. \end{aligned} \tag{3.48}$$

The first component describes states with even spin values, the second - with odd values.

For non-interacting (that is propagating freely) particles the Bethe-Salpeter amplitude is a composition of plane waves:

$$\psi^*_{p_1p_2}\left(x_1,x_2\right)=e^{-ip_1x_1}e^{-ip_2x_2}=e^{-ip(x_1+x_2)}e^{-iqx}, \tag{3.49}$$

where $p=\frac{p_1+p_2}{2}$. For interacting particles, the amplitude is a composition of a plane wave (corresponding to the case where particles did not interact), and the outgoing spherical wave (which is a solution of a scattering problem). For particles of equal masses:

$$\psi_{p_1p_2}\left(x_1,x_2\right) = e^{ip(x_1+x_2)}\left\{e^{\frac{iqx}{2}}+\phi_{p_1p_2}\left(x\right)\right\}, \tag{3.50}$$

$$\phi_{p_1p_2}\left(x\right) = \frac{8\pi\sqrt{p^2}}{\left(2\pi\right)^4 i}e^{ipx}\int\frac{e^{-i\kappa x}f\left(p_1,p_2,\kappa,2p-\kappa\right)}{\left(\kappa^2-m^2+i0\right)\left(\left(2p-\kappa\right)^2+m^2+i0\right)}d^4\kappa, \tag{3.51}$$

where $f\left(p_1, p_2, \kappa, 2p-\kappa\right)$ is an unsymmetrized scattering amplitude. The solution 3.50 requires an assumption of equal emission times (in the pair rest frame). For small relative momenta, only s-wave needs to be considered. If we assume the absence of Coulomb interaction and that the intrinsic range of interaction is smaller that the initial separation in the pair rest frame r^*, the formula in Eq. 3.51 factorizes:

$$\phi_{p_1p_2}\left(x\right) = f\left(k^*\right)\Phi_{p_1p_2}\left(x\right), \tag{3.52}$$

where $f\left(k^*\right) = \left(\exp\left(2i\delta_0\left(k^*\right)\right) - 1\right)/2ik^*$is the unsymmetrized s-wave scattering amplitude. One can then perform the integration of the function $\Phi_{p_1p_2}\left(x\right)$:

$$\Phi_{p_1p_2(x)} = i\frac{\sin k^*r^*}{r^*} + \frac{1}{2r^*}\left(1-i\right)\left\{e^{ik^*r'}\left[C_1\left(z_-\right) + iS_1\left(z_-\right)\right] + e^{-ik^*r'}\left[C_1\left(z_+\right) + iS_1\left(z_+\right)\right]\right\}, \tag{3.53}$$

where $z_\pm = \sqrt{\frac{m}{2|t^*|}}\left(r^* \pm \frac{k^*|t^*|}{m}\right)$ and $C_1\left(z\right)$ and $S_1\left(z\right)$ are the Fresnel integrals: $C_1\left(z\right) + iS_1\left(z\right) = \sqrt{\frac{2}{\pi}}\int_0^z e^{iy^2}dy$.

FSI is added to the correlations coming from Bose-Einstein/Fermi statistics. An equivalent of Eq. 3.47 is then:

$$b\left(p_1, p_2\right) = b_0\left(p_1, p_2\right) + b_i\left(p_1, p_2\right), \tag{3.54}$$

where b_0 is defined in Eq. 3.47 and

$$b_i\left(p_1, p_2\right) = g_i\left\{\left|f\left(k^*\right)\Phi_{p_1p_2}\left(x\right)\right|^2 + 2Re\left[f\left(k^*\right)\Phi_{p_1p_2}\left(x\right)\right]\cos\left(\frac{qx}{2}\right)\right\}, \tag{3.55}$$

where $g_i = 1 + g_0$, and $g_0 = \frac{(-1)^{2j}}{(2j+1)}$. Formula 3.55 can be generalized for the emission of polarized particles by performing the substitution:

$$g_0 = \sum_{S-even}\rho_S - \sum_{S-odd}\rho_S,\ g_i = 1 + g_0 = 2\sum_{S-even}\rho_S. \tag{3.56}$$

In principle $f\left(k^*\right)$ can depend on the total spin of the pair. The final, most general form of b_i is then:

$$b_i\left(p_1, p_2\right) = \sum_S\rho_S\left\{\left|f^S\left(k^*\right)\Phi_{p_1p_2}\left(x\right)\right|^2 + 2Re\left[f^S\left(k^*\right)\Phi_{p_1p_2}\left(x\right)\right]\cos\left(\frac{qx}{2}\right)\right\}. \tag{3.57}$$

For most common case when particle production does not depend on spin $\rho_S = \frac{(2S+1)}{(2j+1)^2}$.

3.2.2.3 Coulomb interaction

Another type of the FSI is the Coulomb interaction. It is usually approximated by Coulomb penetration factor (sometimes called the Gamov factor):

$$A_c\left(k^*\right)=\frac{2\pi}{k^*a_c}\left[\exp\left(\pm\frac{2\pi}{k^*a_c}\right)-1\right]^{-1}, \tag{3.58}$$

where k^* is the momentum of one of the particles in the pair rest frame and $a_c=1/\left(\mu z_1z_2e^2\right)$ is the Bohr radius of the system and its sign +(-) corresponds to repulsion(attraction). For πK system $a_c=\pm 83.6\ fm$. The higher the mass of the system, the more important is the Coulomb interaction. The factor $A_c=\left|\psi_{k^*}^{Coul}\left(0\right)\right|^2$ corresponds to the Coulomb interaction at zero distance between particles. For the purpose of this work, this approximation is not sufficient however, since it does not not take into account the dependence on the relative distance between emission points. This dependence is responsible for the sensitivity of the non-identical particle correlation function on the source size, the study of which is one of the main results of this work. A more accurate form of the pair wave-function ψ, which depends on the particle relative distance $\vec{r^*}$ is needed[67]:

$$\psi_{\vec{q}}\left(\vec{r^*}\right)=e^{i\delta_0^c}\sqrt{A_c\left(\eta\right)}e^{-i\vec{q}\vec{r^*}}F\left(-i\eta,1,i\xi\right), \tag{3.59}$$

where $\xi=qr^*+\vec{q}\vec{r^*}\equiv qr^*\left(1+\cos\theta^*\right)$, $\eta=1/\left(k^*a_c\right)$ and $\delta_0^c=\arg\Gamma\left(1+i\eta\right)$ is the Coulomb s-wave phase-shift. θ^* is the angle between particle relative momentum $\vec{q}$ and initial separation $\vec{r^*}$. The last term:

$$F\left(\alpha,1,z\right)=1+\alpha z+\alpha\left(\alpha+1\right)z^2/2!^2+\alpha\left(\alpha+1\right)\left(\alpha+2\right)z^3/3!^3+\dots \tag{3.60}$$

is the confluent hypergeometric function.

3.2.2.4 Combining strong and Coulomb interaction

For systems where particles interact through both strong and Coulomb interactions as for all charged meson-meson, meson-barion and barion-barion systems, both are needed in the form of pair wave-function $\psi_{p_1p_2}\left(x_1,x_2\right)$. The Coulomb FSI is introduced as a modification of the wave-function of the pair and modifies both the incoming plane wave (see Eq. 3.59) and the scattered wave, particularly the scattering amplitude becomes:

$$f_c\left(k^*\right)=\left[\frac{1}{f_0}+\frac{1}{2}d_0k^{*2}-\frac{2}{a_c}h\left(k^*a_c\right)-ik^*A_c\left(k^*\right)\right]^{-1}, \tag{3.61}$$

where in case of proton-proton interaction, $f_0 = 7.77\ fm$ and $d_0 = 2.77\ fm$, while for pion and kaon with opposite charge $f_0 = 0.137\ fm$, for pion and kaon with same charge $f_0 = -0.071\ fm$ and the effective radius d_0 is 0 for both. The function $h(x)$ has the form:

$$h(x) = \frac{1}{x^2} \sum_{n=1}^{\infty} \frac{1}{n(n^2 + x^{-2})} - C + \ln|x|. \tag{3.62}$$

The final form of the of the pair wave function for the pair of particles interacting strongly and by Coulomb force contains both the incoming plane wave and the scattered wave, both modified by the Coulomb interaction:

$$\psi_{-k^*}(r^*) = e^{i\delta_C} \sqrt{A_C(\eta)} \left[e^{-ik^* r^*} F(-i\eta, 1, i\xi) + f_C(k^*) \frac{\tilde{G}(\rho, \eta)}{r^*} \right], \tag{3.63}$$

where all the symbols were defined in the previous section and $\tilde{G}$ is a combination of the regular and singular s-wave Coulomb functions (for details, see [68]).

3.2.2.5 Origin of non-identical particle correlations

In section 3.1.2.1 the correlation function has been expressed as an integral of the source emission function, convoluted with the plane wave, describing the propagation non-interacting pair of identical particles. The formula can be generalized for the case of interacting non-identical particles[68]. Since non-identical particles are considered, single-particle emission function must be replaced by two-particle emission function $G_S(x_1, p_1; x_2, p_2)$. The plane wave must be replaced by the wave function of the pair, which includes all the interactions. The *smoothness* condition allows one to express the production cross section through the emission function $G_S(x_1, p_1; x_2, p_2)$ in the case of interacting particles. Thus, separating the two-particle c.m.s. motion in the phase factor $\exp[iPX]$ and using the *smoothness* condition to neglect here $\widetilde{q}$ compared with $p_{1,2}$ and substitute, in the amplitudes $\psi_{\widetilde{q}}^{S(+)}(x)$, the relative coordinates x and x' by their mean value $\bar{x}$, we can write two-particle cross-section in a simple approximate form:

$$\begin{aligned}
\frac{d^6\sigma}{d^3\mathbf{p}_1 d^3\mathbf{p}_2} &\approx \sum_S \int d^4x_1\, d^4x_2 G_S(x_1, p_1; x_2, p_2) |\psi_{\widetilde{q}}^{S(+)}(x)|^2 \\
&= \sum_S \int d^4x g_{PS}(x, \widetilde{q}) |\psi_{\widetilde{q}}^{S(+)}(x)|^2 \\
&\equiv (2\pi)^6 \gamma_1 \gamma_2 \frac{d^6\sigma_0}{d^3\mathbf{p}_1 d^3\mathbf{p}_2} \sum_S \mathcal{G}_S \langle |\psi_{\widetilde{q}}^{S(+)}(x)|^2 \rangle_{\widetilde{q}PS},
\end{aligned} \tag{3.64}$$

where g_{PS} is the emission function integrated over the c.m.s. space coordinates, $d^6\sigma_0$ is the production cross section of the non-interacting particles. The averaging $\langle \ldots \rangle_{\tilde{q}PS}$ is definned as:

$$\langle f(\tilde{q}, x) \rangle_{\tilde{q}PS} = \frac{\int d^4x g_{PS}(x,q) f(\tilde{q}, x)}{\int d^4x g_{PS}(x,q)} \tag{3.65}$$

and the initial spin factors $\mathcal{G}_S$ are defined as:

$$\mathcal{G}_S(p_1, p_2) = \frac{\int d^4x g_{PS}(x,q)}{\sum_S \int d^4x g_{PS}(x,q)} \tag{3.66}$$

The correlation function defined as a ratio $d^6\sigma/d^6\sigma_0$ then takes on the form:

$$\mathcal{R}(p_1, p_2) \doteq \sum_S \mathcal{G}_S \langle |\psi_{\tilde{q}}^{S(+)}(x)|^2 \rangle_{\tilde{q}PS}. \tag{3.67}$$

Recall that for identical particles the Bethe-Salpeter amplitudes $\psi_{\tilde{q}}^{S(+)}(x)$ should be symmetrized.

This definition is used to generate the theoretical correlation functions in the program `CorrFit`, which is described in the Appendix B. The program effectively performs the Monte-Carlo averaging of the particle wave-function squared for several bins in particle relative momentum k^*.

3.2.3 Asymmetry Measurement

For identical particle pairs, the average value of the projection of the separation vector in the pair rest frame on any direction $\langle \vec{r}_i^* \rangle$ is, by symmetry, equal to 0. However for non-identical particle pairs, this is not necessarily the case. Below we illustrate how the non-identical particle correlations can be sensitive to such asymmetries.

One can consider a system, where Coulomb FSI dominates. The correlation function then takes the form, following Eq. 3.59 and 3.67 [67]:

$$C(p_1, p_2) \quad = \quad A_c(\eta)\left[1 + 2\langle r^*(1 + \cos\theta^*)\rangle / a_c + \ldots\right]. \tag{3.68}$$

The correlation for opposite-sign pair is positive, since the Coulomb interaction is attractive. The term $1 + \cos\theta^*$ is always positive, while the Bohr radius a_c is negative. Therefore, in total, the term $2\langle r^*(1 + \cos\theta^*)\rangle / a_c$ will decrease the correlation. The decrease of the correlation is dependent on the θ^* angle, that is on the relative orientation of $\vec{k}^*$ and $\vec{r}^*$. More specifically the correlation will be stronger for cases, when both vectors point in opposite directions ($\cos\theta^* < 0$) and weaker for cases when $\vec{k}^*$ and $\vec{r}^*$ are aligned ($\cos\theta^* > 0$). This is immediately understandable when one realizes, that the former case corresponds to the situation where both particles, in the moment of their creation, are moving towards each other and consequently stay close together and interacting for a longer time. For pairs with identical charges the sign of A_c and a_c are inverted, and the situation is equivalent.

So far the method for measuring $\langle \vec{r}_i^* \rangle$ is not apparent. Only the direction of $\vec{k}^*$ is measurable. However there is one more independent variable that can be used - the total pair momentum $\vec{P}$ or, as it was originally used by Lednicky et al., the direction of pair velocity $\vec{v}$[62, 63, 67], which can be easily measured. One can divide the pairs of correlated particles into two groups: group a) with pair velocity $\vec{v}$ and pair relative momentum $\vec{k}^*$ aligned ($\cos\Psi > 0$) and group b) where they are pointing in opposite directions ($\cos\Psi < 0$). If the consideration is restricted to the transverse plane, the angle ϕ between vectors $\vec{r}^*$ and $\vec{v}$ (see Fig. 3.9) is connected to the other two by a simple relation:

$$\Psi = \phi + \theta^*. \tag{3.69}$$

Since we consider cosines of these angles, we also note:

$$\langle \cos\Psi \rangle = \langle \cos\phi \cos\theta^* - \sin\phi \sin\theta^* \rangle . \tag{3.70}$$

In cases when two vectors with angle α between them are aligned on the average, one has $\langle \cos\alpha \rangle > 0$ and $\langle \sin\alpha \rangle = 0$, in the opposite case when they are anti-aligned, one has $\langle \cos\alpha \rangle < 0$ and again $\langle \sin\alpha \rangle = 0$. In further considerations only the sign of the average cosines are used, therefore the following approximate formula can be used:

$$sign(\langle \cos\Psi \rangle) = sign(\langle \cos\phi \rangle) sign(\langle \cos\theta^* \rangle). \tag{3.71}$$

Experimentally only the Ψ angle is measurable. The asymmetry measurement technique is based on that fact, and the dependence of the strength of the correlation function on $\cos(\theta^*)$. One constructs two separate correlation functions - one with pairs having $\cos(\Psi) > 0$ (which is called C^+ and is a function of half of pair relative momentum k^*) and the other from pairs with $\cos(\Psi) < 0$ (C^-). In principle one can differ from the other. For illustration in this consideration it is assumed that $C^+ > C^-$ was observed (and the correlation effect is positive - e.g. when opposite charge particles are considered). This means that by selecting pairs with $\cos(\Psi) > 0$ a stronger correlation was obtained, which is only possible if $\langle \cos(\theta^*) \rangle$ for these pairs is less than 0. Relation 3.71 then implies, that $sign\,\langle \cos(\phi) \rangle < 0$. That means, that $\vec{r^*}$ vector and pair velocity $\vec{v}$ were anti-aligned. If the opposite case is observed, that is if $C^+ < C^-$, the

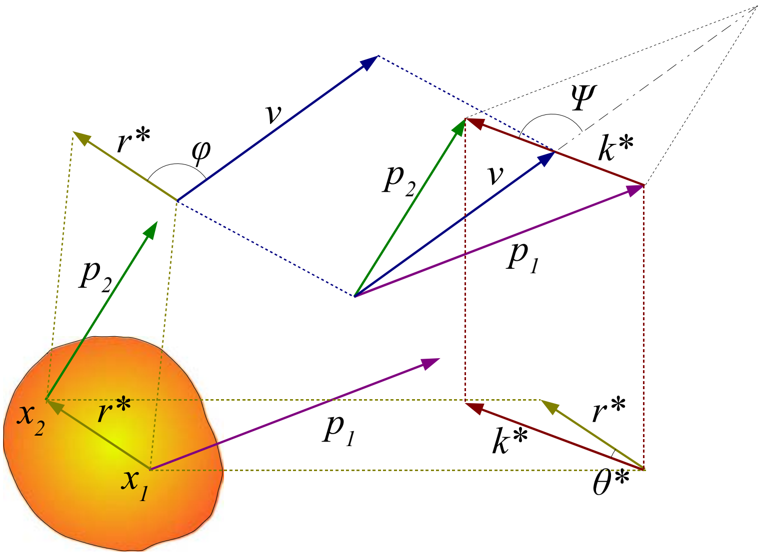

Figure 3.9: Dependencies between directions of pair velocity $\vec{v}$, pair relative momentum $\vec{k}^*$ and initial separation in space $\vec{r}^*$

same argument can be made, showing that $sign \langle \cos(\phi) \rangle > 0$ in this case. In summary, if a difference between C^+ and C^- is observed, it means that the average value of the projection of the separation vector between the considered two particle species is non-zero. If $C^+ > C^-$ the $\overrightarrow{r^*}$ and $\vec{v}$ are (on the average) anti-aligned, if $C^+ < C^-$ they are aligned. Further conclusions can be drawn from the consideration of Eq. 3.68 - if the average emission points of particles are the same (average projection of the separation vector in pair rest frame on the selected direction is zero), C^+ and C^- must be the same. Also the difference between C^+ and C^- will be monotonically (but not necessarily linearly) dependent on the size of the asymmetry $\langle r_i^* \rangle$. Obviously the same argument holds for same-charged particles - one only has to remember that in that case the correlation effect is negative, and the correlation function will be lower for pairs which are correlated more strongly, and vice-versa. In short, the asymmetry measurement technique uses: a) the fact the the strength of the correlation depends on the angle θ^* and b) one can experimentally distinguish pairs with $\cos(\Psi) > 0$ and $\cos(\Psi) < 0$ to obtain the information about the angle ϕ and the absolute size of average initial separation $\left\langle \vec{r_i^*} \right\rangle$. In principle in the asymmetry measurement technique it is enough to consider C^+ and C^-. However, the difference between the functions (or lack of it) is best illustrated by plotting the "double-ratio", that is C^+/C^-. If the double ratio differs from 1.0 at any value of k^* - the asymmetry is observed. If the ratio is equal to 1.0, there is no asymmetry.

Further consideration show, that if the interaction between two particles is dominated by Coulomb, a simple relation holds[64, 67]:

$$\frac{C^+}{C^-} \approx 1 + 2\left\langle \mathbf{r_i^*} \right\rangle / a_c,\ q \to 0 \tag{3.72}$$

The technique can be further advanced, if one decomposes the pair velocity $\vec{v}$ into the transverse $v_\perp$ and longitudinal v_L component (see Fig. 3.10). Pairs can be divided into two groups - one having $k^*_{out} > 0$ (that means aligned with $v_\perp$) and ones with $k^*_{out} < 0$ (anti-aligned with $v_\perp$). Correlation functions $C^+_{out}(k^*)$ and $C^-_{out}(k^*)$ can be constructed with the pairs from the two groups. Their ratio (the *out* "double-ratio") will be sensitive to the average separation in the *out* direction $\langle r^*_{out} \rangle$. Similar analysis can be done for the longitudinal direction, giving $C^+_{long}(k^*)$ and $C^-_{long}(k^*)$; their ratio (the *long* "double-ratio") will be sensitive to $\left\langle r^*_{long} \right\rangle$. By analogy one can try to do the similar analysis in the *side* direction, that is the direction perpendicular to both *out* and *long*. However, by definition, the velocity v has no *side* component, therefore there is no way to tell which direction in *side* should be called "positive" and which "negative". Some convention needs to be adopted, inferring the sign of the *side* component from the signs of *out* and *long*. The natural one is to assign it in such a way, that the resulting $out, side, long$ coordinate system will be right-handed. One can then construct correlation functions $C^+_{side}(k^*)$ and $C^-_{side}(k^*)$. However it can be shown that realistic sources must have, by azimuthal symmetry, zero *side* asymmetry $\langle r^*_{side} \rangle = 0$. Therefore these two function *must* be equal, and any difference between them must be an artifact of the experiment. This quality makes it worthwhile to construct them and use them as a quality assurance test in data analysis.

The consideration above was entirely done in the pair rest frame. In order to obtain the emission asymmetries in the the CMS frame, they need to be Lorentz boosted back to the CMS, according to Eqs. 3.29-3.33.

In summary the origin and the technique of the correlations of non-identical particles was presented in this chapter. It was shown that the FSI produce correlations which can be studied by techniques very similar to those used to measure Bose-Einstein or Fermi-Dirac correlations at small relative momenta for identical particles. It was also shown, that non-identical particle correlations can be used to study the relative averaged emission asymmetries $\langle \vec{r}^*_i \rangle$ between emission points of two particle types. The ratio between $C_i{}^+(k^*)$ and $C_i^-(k^*)$ was shown to be directly sensitive to the magnitude and direction of the asymmetry $\langle \vec{r}^*_i \rangle$.

So far it was shown that non-identical particle technique is sensitive to emission asymmetries, but the origin of such asymmetries is still not known. This topic is discussed in chapters 6 and 7.

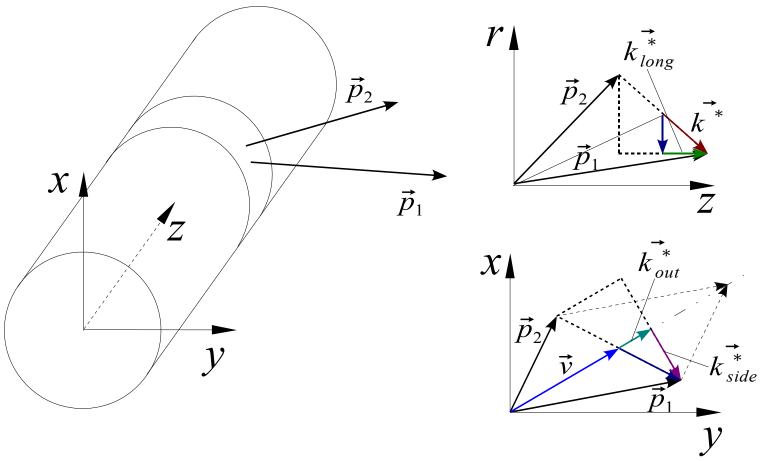

Figure 3.10: Decomposition of the half of the relative momentum of the first particle in the pair rest frame $\vec{k}^*$ into *out*, *side* and *long* components.

Chapter 4

STAR Experiment

4.1 RHIC Accelerator Complex

The Relativistic Heavy Ion Collider (RHIC) facility is located in Brookhaven National Laboratory (BNL) on Long Island, New York. It was designed and built to collide nuclei, from protons to gold, at energies up to $100 GeV/u$ for Au, or $500 GeV$ for protons. It is the first facility to collide heavy-ion beams. The collider setup makes it possible to achieve center-of-mass energies up to 10 times grater than in earlier, fixed-target experiments. Table 4.1 shows parameters of existing relativistic heavy-ion facilities.

RHIC consists of two semi-rings of beam-line, surrounded by super-conducting magnets (cooled to below $4.6K$), which focus and guide the beams and a radio-frequency (rf) system that captures, accelerates and stores those beams. The rings circumference is 2.4 miles, or 3.8 kilometers.

The RHIC complex, seen on Fig 4.1, uses existing facilities at BNL to produce and accelerate Au ions to RHIC injection energy (10.8 GeV/u). The

	AGS	AGS	SPS	SPS	SPS	RHIC	RHIC
Start year	1986	1992	1986	1994	1999	2000	2001
A_{max}	^{28}Si	^{197}Au	^{32}S	^{208}Pb	^{208}Pb	^{197}Au	^{197}Au
$E_P^{max}[AGeV]$	14.6	11	200	158	40	0.91e4	2.1e4
$\sqrt{s_{NN}} GeV$	5.4	4.7	19.2	17.2	8.75	130	200
$\sqrt{S_{AA}} GeV$	151	934	614	3.6e3	1.8e3	2.6e4	4e4
$\Delta y/2$	1.72	1.58	2.96	2.91	2.22	4.94	5.37

Table 4.1: Comparison of existing heavy-ion facilities; A_{max} is the maximum species mass number, E_P^{max} is the maximum (equivalent) fixed-target beam energy per nucleon, $\sqrt{S_{NN}}$ is the maximum center-of-mass energy per nucleon, $\sqrt{S_{AA}}$ is the total center-of-mass energy and $\Delta y/2$ is the separation between the beam and mid-rapidity region in units of rapidity [78].

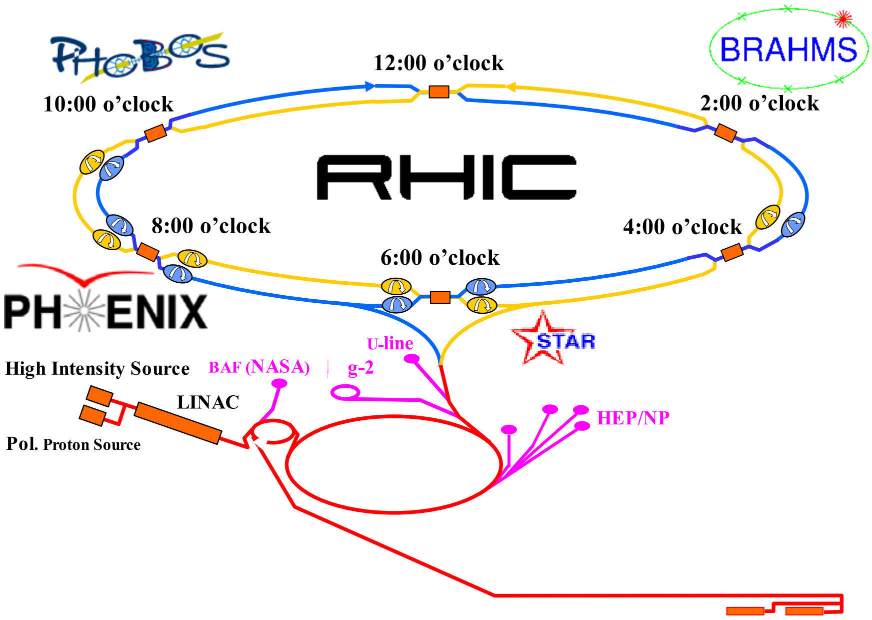

Figure 4.1: The RHIC facility

process starts at Tandem Van de Graaff, which acts as the ion source. The first device accelerates gold atoms at charge $Q = -1e$ to 15 MeV. Ions pass through a stripping foil, which knocks off electrons, so that their most probable charge becomes $Q = +12e$. The ions gain another 1 MeV as they accelerate through the second Van de Graaff. On exiting the Tandem, the ions pass through a second stripping foil bringing their charge to $Q = +32e$. They are then injected into the Booster synchrotron and accelerated to 95 MeV/u. Another stripper foil in the transfer line between the booster and the Alternating Gradient Synchrotron (AGS) increases their charge to $Q = +77e$. In the AGS the ions go through significant acceleration, bringing their energy to 10.8 GeV/u. They are then extracted, stripped of all the remaining electrons and injected into RHIC. Here they can be either stored at this energy, or accelerated up to top energy, which was 130 GeV/u for year 2000 (RHIC Year1) data taking and 200 GeV/u for year 2001 (RHIC Year2) data taking. The beams can be stored for up to 10 hours. In Run2000 the initial intensity of the bunch was $3.8 \times 10^9 ions$, after traversing the complex it was $0.9 \times 10^9 ions$, giving the total efficiency of 23%[79]. During the store the intensity decreases exponentially. Table 4.2 lists important parameters of RHIC.

Since the beginning of it's operation, RHIC generated collisions between gold nuclei at $\sqrt{S_{NN}} = 22$ (injection energy), $56, 130$ and 200 $AGeV$; between

Top AuAu $\sqrt{S_{NN}}$	200 GeV
Average luminosity $\mathcal{L}$ (10h store)	$\sim 2 \times 10^{26} cm^{-2} s^{-1}$
Bunches per ring	55
Gold ions per bunch	10^9
Crossing points	6
Beam lifetime (store length)	$\sim 10h$
RHIC circumference	3833.845 m

Table 4.2: Nominal parameters of the RHIC Au+Au operation

	Bunches	Ions/Bunch (store average)	Instantenous Luminosity $cm^{-2}s^{-1}$	Integrated Luminosity $\mathcal{L}\left[(\mu b)^{-1}\right]$
Year1 (2000)	55	0.5×10^9	2×10^{25}	$40 - 85$
Year2 (2001)	55	1×10^9	2×10^{26}	$3 - 6$

Table 4.3: The performance of RHIC during the 2000 (Year1) and 2001 (Year2) Au+Au run[79]. Integrated luminosities vary from experiment to experiment, hence the range in the last column.

protons at $\sqrt{S_{NN}} = 200\ AGeV$ as well as between deuterium and gold nuclei at $\sqrt{S_{NN}} = 200\ AGeV$. Table 4.3 shows the luminosity performance of RHIC during Au+Au operation.

Four experimental collaborations are using the RHIC facility. The BRAHMS collaboration with 44 members from 10 institutions, the PHENIX collaboration with about 430 members from 52 institution, the PHOBOS collaboration with 106 members from 8 institutions and STAR collaboration with 495 members from 50 institutions. The summary of RHIC experiments can be seen in Table 4.4. Two RHIC rings intersect at six points; at each of them collisions are possible. BRAHMS detector is situated at the 2 o'clock crossing point, STAR at 6 o'clock, PHENIX at 8 o'clock and PHOBOS at 10 o'clock.

4.2 The STAR Detector

The STAR (Solenoidal Tracker At RHIC) detector is situated in the 6 o'clock position in the RHIC ring. The subsystem layout is shown on Fig. 4.2. The main detector used in this work was the STAR Time Projection Chamber (TPC). It is placed inside the large solenoidal magnet[84], which was specifically designed for the experiment. The main constraints were imposed by the TPC. The field needs to be strong enough to bend the trajectories of high-momentum particles. The higher the field, the larger the momentum resolution for such particles. However field uncertainties (both in stability over time as well as homogeneity) produce

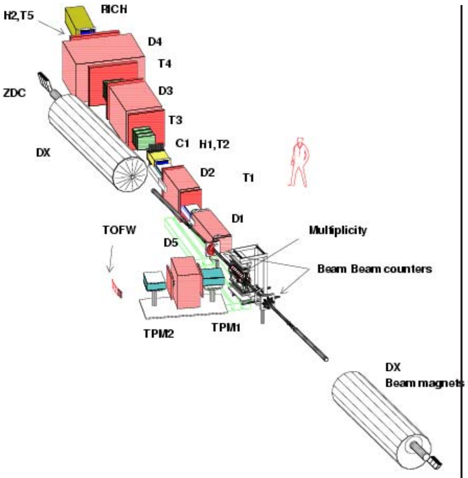 BRAHMS detector	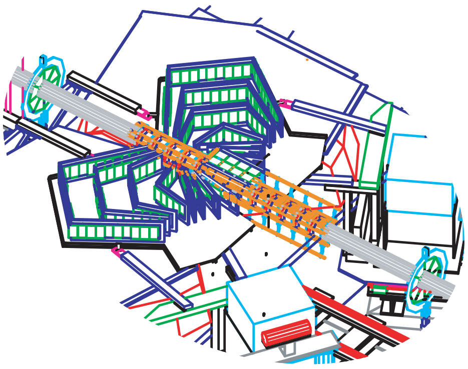 PHOBOS detector
Consists of two spectrometers measuring particles in wide range of rapidity ($0 < \|y\| < 4$) and p_t ($0.2 < p_t < 3$) GeV/c. Main goal: measure p_t spectra, especially in forward rapidity region[80].	PHOBOS silicon detectors have a full azimuthal and rapidity coverage. Two silicon spectrometer arms allow for tracking in limited acceptance. Main goals are multiplicity measurements, integrated and differential in azimuthal angle and rapidity[81] .
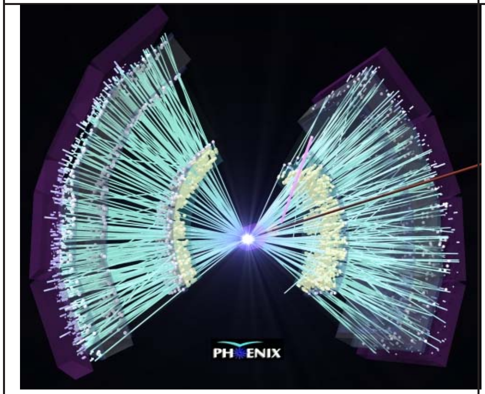 PHENIX event display	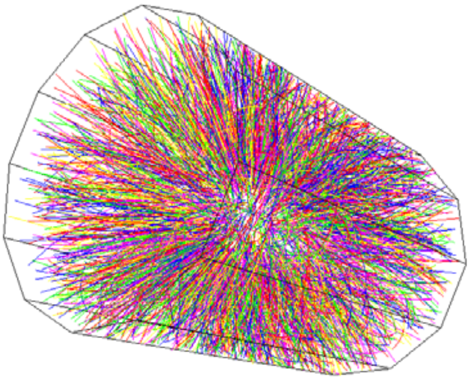 STAR Event display
Consists of a central arm ($\|\eta\| < 0.35$) with tracking systems for charged particles and EM calorimetry and two muon arms $1.2 < \|\eta\| < 2.4$. Main emphasis are J/Ψ measurements, high p_t physics (jets) and bulk properties of matter (HBT correlations). [82].	A solenoidal tracker with full azimuthal acceptance, $\|\eta\| < 2.0$ and $2.5 < \|\eta\| < 4.0$. Main parts are central TPC, two forward TPCs, silicon vertex tracker and electromagnetic calorimeter. Broad range of results produced, from global event characteristics, fluctuations, correlations, strange particle production to high p_T rare probes[83].

Table 4.4: Short description of RHIC experiments

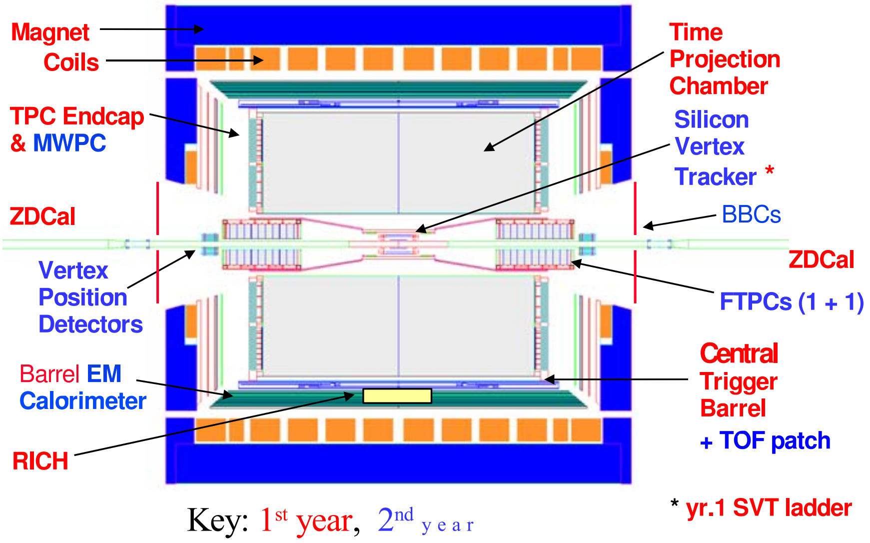

Figure 4.2: The STAR experiment layout as of 2001. The subsystems present during Year1 (2000) are described in blue. The subsystems added for Year2 run (2001) are described in red.

drift and position reconstruction distortions, that need to be minimized. It is crucial that the magnetic field is parallel to the TPC longitudinal axis, so that drifting electrons are not influenced by the Lorenz force. Additional constraints on the magnet construction was the need to accommodate several additional detectors (e.g. electromagnetic calorimeter) inside the magnet volume and to allow particles with pseudorapidity $|\eta| > 2.0$ to reach the trigger detectors outside of the magnet. The STAR magnet fulfills all those requirements and is able to operate at a “half-field” setting of $0.25T$ and at “full-field” setting of $0.5T$. The former facilitates tracking of low-momentum particles in the TPC, while the latter allows the TPC to reconstruct particles with high transverse momentum p_T, leaving the very low-p_T ($< 150\ MeV$) part for inner tracking systems (SVT). The STAR magnet is 6.85 m long and it’s outer radius is 7.32 m, the total power consumption is $3.5MW$. The deviations from field uniformity do not exceed 50 $Gauss$ for “full-field” setting.

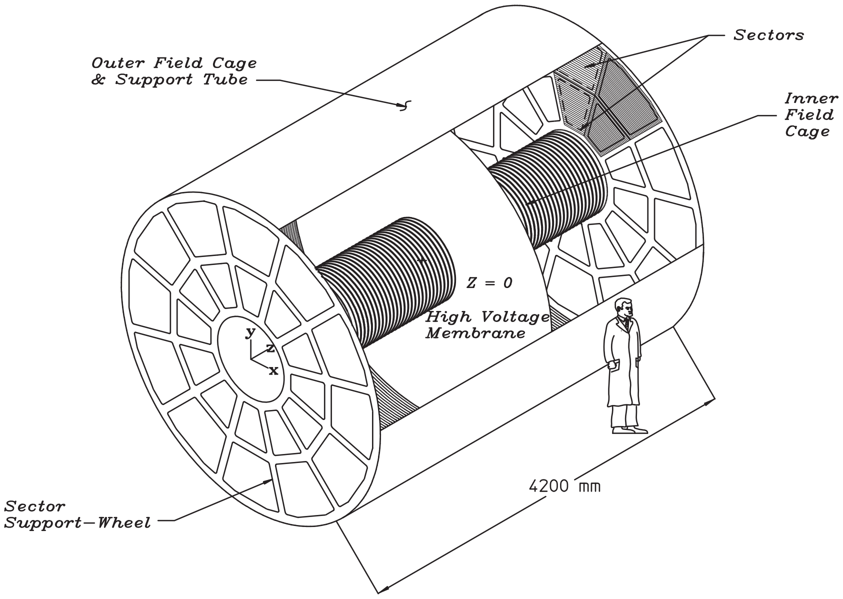

Figure 4.3: The schematic view of STAR TPC

4.2.1 Time Projection Chamber

4.2.1.1 Detector description

TPC is STAR's main tracking device[85]. It records the tracks of particles, measures their momenta and identifies them by measuring their ionization energy loss (dE/dx). It's acceptance covers ± 1.8 units of pseudorapidity through the full azimuthal angle and over the full range of multiplicities. The STAR TPC is shown schematically in Fig. 4.3. I is situated inside the STAR magnet and surrounds the beam pipe. The collisions take place near the canter of the detector. The TPC is 4.2 m long and 4 m in diameter. It is filled with P10 gas (90 % argon + 10 % methane) at 2 $mbar$ above atmospheric pressure. A well-defined, uniform, electric field of $\approx 135\ V/cm$ is produced by a thin conducting central membrane (CM) at the center of the TPC which is a cathode held at 28 kV. The concentric field cage cylinders help maintain the uniform field and the readout end caps are at ground potential. Field uniformity is critical, as electrons drift towards the end caps over the distance of up to 2.1 m.

The TPC is often compared to 3-dimensional digital camera. It is because it provides 3-dimensional pixel information and, unlike previous particle detectors such as e.g. bubble-chambers, is fully electronic. The main idea of operation

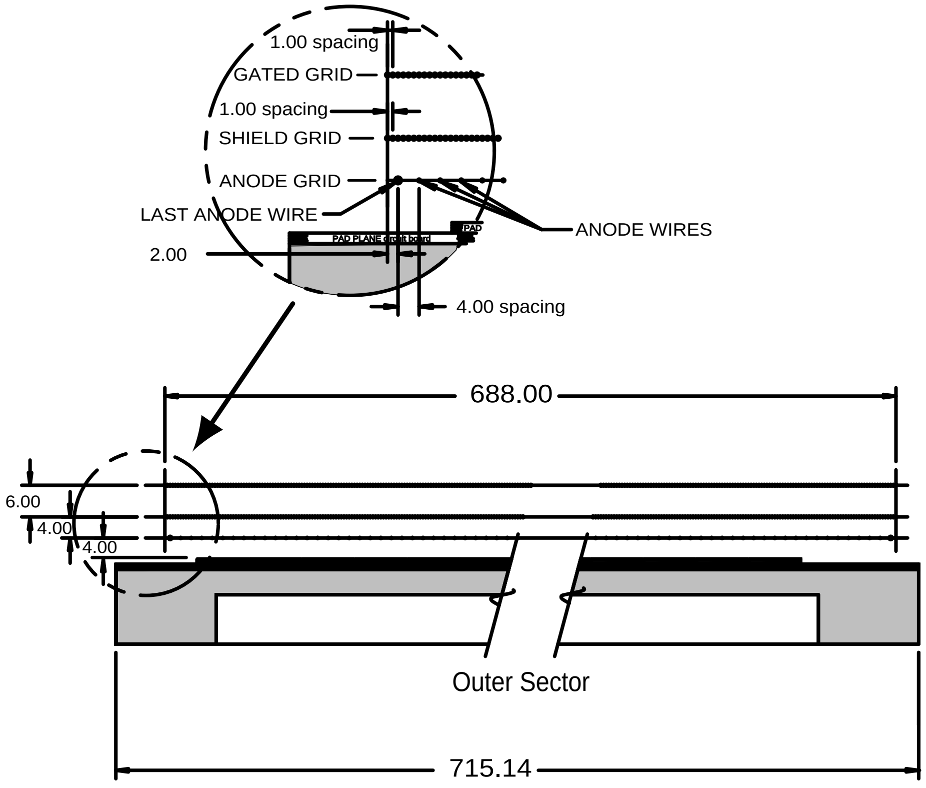

Figure 4.4: A cut-way view of an outer sector. The cut is taken along the radial line from the center of the TPC to the outer field cage so the center of the detector is to the right. The figure shows the relative position of the pad plane, anode wires, the grounding shield grid and the gated grid. All dimensions are in millimeters.

is as follows: as the charged particle traverses the TPC volume it loses it's energy by ionizing the gas, leaving along it's track a cloud of electrons. These electrons drift along the uniform electric field toward the end-caps, where they are read-out. This field cannot be strong enough to create avalanches, but must be strong, since it determines the drift velocity, and the time required for an electron to drift from the CM to the end-caps limits the rate of operation. The drift velocity in STAR TPC is 5.45 $cm/\mu s$.

The read-out system, shown on Fig. 4.4 is based on Multi-Wire Proportional Chambers (MWPC) with readout pads. The gating grid, located $6mm$ from the ground grid, has two modes of operation. Normally, when it's in "closed" state and it has alternating potentials of $\pm 75V$ on every wire, it prevents electrons from the TPC volume to enter the amplification MWPC region. When a decision is made by the trigger that an event is to be read-out, the gating grid is rapidly ($< 400ns$) switched to the "open" state when all the wires are at the

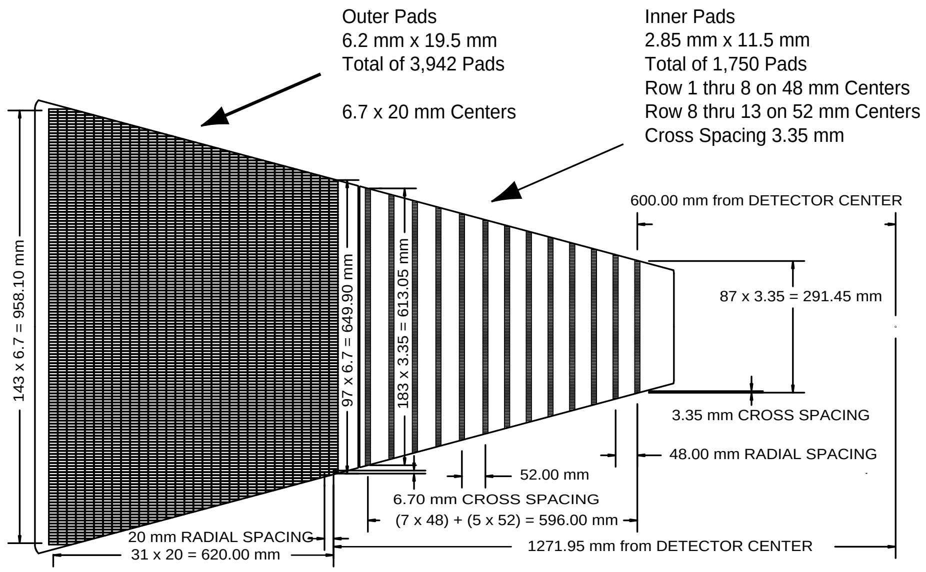

Figure 4.5: One full sector of an anode pad plane. The inner subsector, with widely spaced rows of small pads, is on the right. The outer subsector with continuous pad coverage is on the left.

same potential (typically 110V). Then the drifting electrons avalanche in the high fields between the shield (also called ground) grid and the $20\mu m$ anode wires providing an amplification of 1000-3000. The positive ions created in the avalanche induce a temporary image charge on the pads, which disappears as the ions move away from the anode wire. The image charge is measured by the preamplifier/shaper/waveform digitizer system. The induced charge from an avalanche is shared over several adjacent pads. The are a total of 136,608 pads in the read-out system, divided into 12 sectors.

Each of the TPC's read-out sectors (shown on Fig. 4.5) has an inner (closer to the beam) and outer pad plane. The latter has a continuous pad coverage, with pad 32 padrows placed perpendicular to the radial direction, which maximizes the transverse momentum resolution. The pad width of $6.7mm$ and the separation of $4mm$ between anode plane and pad plane was chosen, taking into account the amount of transverse diffusion the electron clouds suffer when drifting through the full $2m$ of gas, so that the typical signal would be shared among 3 pads, which maximizes the centroid position resolution to about 20% of the pad width. The $19.5mm$ length of the pad was constrained by the available front-end electronics packaging density. The continuous pad coverage is critical for accurate measurement of the energy loss of particles in the TPC.

The inner pad sectors are in the region of highest track density, and thus are optimized for good two-track hit resolution. Because of the limited electronics packaging density the padrows are separated by $48mm$ in radial direction. This means the inner sector mainly contributes to the position information but is less suited for dE/dx measurements. Single pad dimensions are $2.85 \times 11.5mm$.

The track in the TPC is identified by finding a string of ionization clusters along it's path. A single cluster has 3-dimensional information. A local coordinate system is used, with x direction along the padrows, y direction perpendicular to the padrow and z along the beam line. x cluster position information is inferred from the charge measured on several (most probably 3) adjacent padrows. The y-information is simply the radial position of the padrow. The time it takes the electrons to drift from the CM to the end-caps is divided into 512 time-buckets, approximately $100ns$ long. The z-direction information is determined by measuring the time it took the electrons to drift to the end-caps, and is inferred from how this charge was divided into several time-buckets. If the clusters do not overlap, the ionization energy is measured by summing the energy from all the pads. If clusters do overlap it is sometimes possible to disentangle them and get the position information; however such clusters do not contribute in the dE/dx measurement. Since there are 45 padrows, a track can have a maximum of 45 hits.

4.2.1.2 Performance

Several STAR TPC performance parameters were of special importance in this work. They included particle identification through dE/dx information, momentum resolution in the low-p_T ($< 1GeV/c$) region and two-track effects.

In central AuAu collision about 30% of the hits in the TPC overlap. In order to perform the tracking efficiently, these situations need to be resolved. A hit-separation study was performed. A distribution of a distance between two hits was done separately for pairs of hits coming from the same event and coming from different events. Taking their ratio one obtains the plot shown on Fig. 4.6. Since pad sizes in the inner and outer subsectors are different, the separation function is also different. Since x (along the padrow) and z (drift) information is obtained independently, the separation function in these directions is also different. The plot shows, that the hits can be completely resolved if they are separated by at least $0.8(1.3)cm$ in the inner(outer) sector in x direction and $2.7(3.2)cm$ in the z direction.

The software tracking procedure is then applied to the TPC hits. They are combined into tracks - collections of hits which are believed to be produced by a single particle. The transverse momentum p_T of the primary particle track is obtained by fitting a circle through the x, y coordinates of the vertex and the

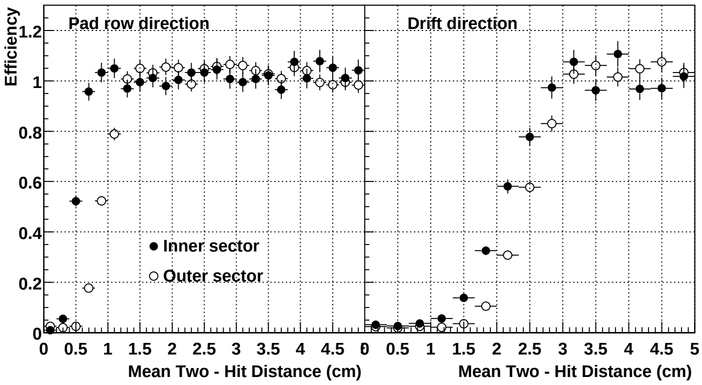

Figure 4.6: Two-hit resolution in the STAR TPC. The plots are mean two-hit distance distribution from the same event normalized to the equivalent distribution for two hits coming from different events.

hits generated by the particle and applying the standard formula:

$$p_T = r\,|q|\left|\vec{B}\right|,$$

where r is the circle radius, q is the particle charge and $\left|\vec{B}\right|$ is the strength of the magnetic field. The tracking also determines the polar (dip) angle θ the track has with respect to the beam axis, and the azimuthal angle ϕ with respect to the horizontal plane. These three coordinates determine the particle momentum. In order to obtain the momentum resolution of the particles a following procedure is performed. A simulated track with known momentum $\vec{p}_{orig}$ is embedded into real event at the hit level. Then the whole event is reconstructed and the reconstructed momentum $\vec{p}_{rec}$ of the simulated particle is compared with original one. The differences $\vec{p}_{orig} - \vec{p}_{rec}$ for all particles are histogrammed, and a Gaussian is fitted to this distribution. The main component of the momentum resolution - the p_T resolution of the STAR TPC is shown on Fig. 4.7. The θ and ϕ angle resolution is very good ($< 10^{-2} rad$).

Once a particle is tracked and its momentum is identified, the dE/dx information from all its hits is combined to obtain the most probable energy loss. Combined with particle momentum it is used to identify the particle. The STAR TPC is able to separate pions and protons up to $1.0 GeV/c$ and pions and kaons up to $0.55 GeV/c$. A relative dE/dx resolution of 7% is needed to achieve this. Fig. 4.8 shows the energy loss for particles in the TPC as a function of particle momentum, averaged over many particles.

Particle Identification (PID) procedure is described in more detail. For the full description see [87]. As seen on Fig. 4.8 each particle type forms a distinct

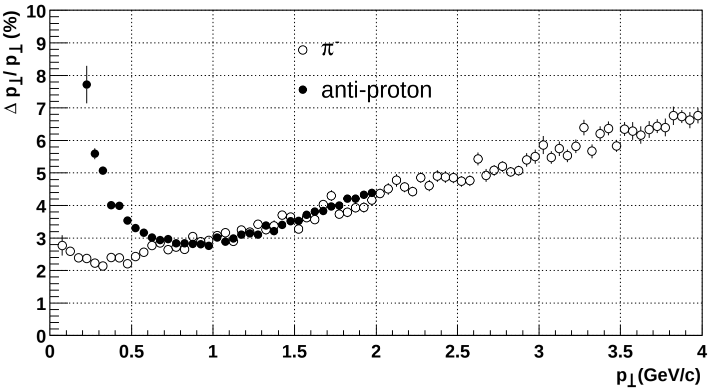

Figure 4.7: Transverse momentum resolution of the STAR TPC for π^- and $\overline{p}$ in the $0.25T$ magnetic field. Only tracks with minimum 15 hits are considered. Tracks are embedded into minimum-bias events. The Gaussian sigma is taken as the momentum resolution value.

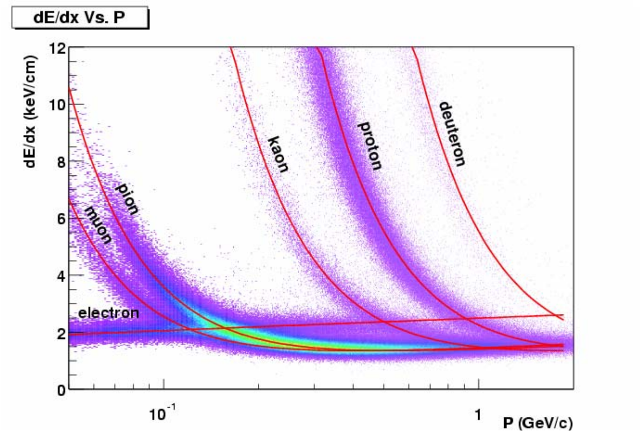

Figure 4.8: The energy loss distribution for particles in the STAR TPC as a function of the p_T. The magnetic field was $0.25T$. The lines show the theoretical Bethe-Bloch curves.

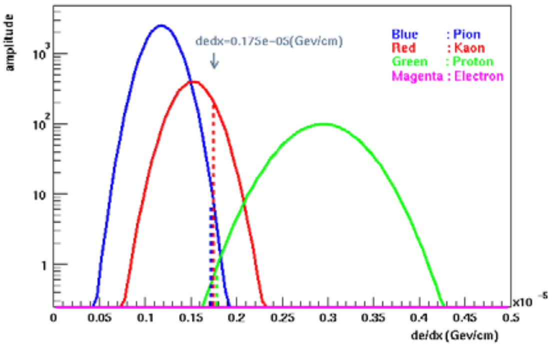

Figure 4.9: An example of the dE/dx vs. p_T plot slice for rigidity $p/z = 0.68$.

band on the $2D$ dE/dx plot. If one takes a number of counts in a bin as a third dimension, the bands will transform into "ridges" with a Gaussian cross-section, with the center of the Gaussian taken from the Bethe-Bloch formula. In areas where the bands do not overlap, the ridges can be fitted with Gaussians, and their height can be obtained. In areas where the bands do overlap, one can perform the fit to a sum of up to four Gaussians. From these fits one obtains the relative amplitude of each of the four "ridges" (pion, kaon, proton and electron) as a function of particle rigidity. When trying to identify a single particle, one does the following: given the rigidity p/z of a particle one can plot the band cross-sections as a function of dE/dx; an example is shown in Fig. 4.9. One then takes the particle's average energy loss dE/dx and gets the value of the four Gaussians (G_π, G_K, G_p, G_e) at this point. A probability for a particle to belong to the pion band (in other words - a *pion PID probability* of a given particle) is then defined as:

$$P_\pi = \frac{G_\pi}{\sum_{i=\pi,K,p,e} G_i},$$

and similarly for P_K, P_p and P_e. This definition ensures, that $\sum_{i=\pi,K,p,e} P_i = 1$.

4.2.2 Trigger Detectors

When RHIC operates, beams cross inside the STAR detector with the rate $\sim 10MHz$. A collision is possible at each crossing, but the STAR TPC detector can only operate at a moderate $100Hz$. Therefore a trigger system, utilizing "fast" detectors is needed to make a decision when and if to begin data taking for an event in the "slow" detectors. In STAR Run1(2000) and Run2(2001) two detectors were used for this purpose: Central Trigger Barrel (CTB) and two Zero-Degree Calorimeters (ZDC)[86]. The goals for the trigger were, among others:

- select central AA interactions based on charged particle multiplicity in STAR TPC acceptance
- reject background (e.g. beam-gas collisions)
- open TPC amplifier in $< 1.5\mu s$. Each $1\mu s$ of delay costs 2% of TPC data.

The STAR trigger is organized into four levels. The Level 0 trigger is the actual trigger, which determines if a given event matches the broadest criteria of an "interesting" event. If it does, a command is issued to all the detectors to begin data taking. This decision is made in less than $1.5\mu s$. At Level 1 and more fine-grained data is used, and more time is available. Level 1(2) makes it's decision in $\sim 100\mu s(\sim 5ms)$ and can abort data taking if the event turns out to be not interesting (e.g. a beam-gas interaction). Level 3 trigger, although operational, was not used in the trigger stream in Run1 and Run2. If the event is not aborted, it goes through a complete amplification-digitization-acquisition process and is stored for later analysis.

Central Trigger Barrel The Central Trigger Barrel measures charged particle multiplicity in $-1 < |\eta| < 1$. It consists of 240 scintillator slats with the coverage of $\pi/30$ in $\phi$and 0.5 in η. The slats are grouped in four cylindrical bands around the STAR TPC. Each slat consists of a radiator, a light guide and a photomultiplier tube (PMT). A particle crossing the CTB excites the scintillator medium, which produces light, which is then detected in the PMT. The average occupancy is 10 hits/single CTB slat in AuAu central collision. The signal from the CTB is directly proportional to the multiplicity of the collision. A sum of signals from all CTB channels is used in the Level 0 trigger.

Zero Degree Calorimeter Each of the RHIC experiments uses a pair of Zero Degree Calorimeters (ZDCs) located at $\pm 20m$ from the center of the TPC around the beam pipe, just beyond the point where two RHIC beampipes separate. Each ZDC consists of three modules; each module consists of series of tungsten plates alternating with layers of wavelength shifting fibers that route the Cherenkov light to a PMT. The ZDC measures the deposited energy of neutral particles (mainly neutrons) which are usually spectators from the collision. Charged particles are deflected by the beam steering magnets that are situated between the ZDC and the interaction region. The ZDCs provide the hadronic minimum-bias trigger, when a signal of at least 40% of single neutron signal is simultaneously detected in both. The timing difference between ZDC East

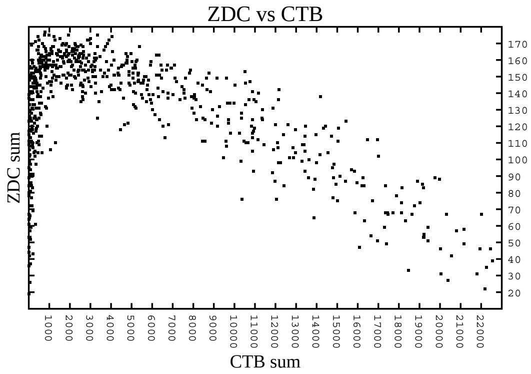

Figure 4.10: ZDC signal vs. CTB signal.

and ZDC West can be used to roughly determine how far from the interaction region center the collision occurred. Central collisions are selected using combined ZDC and CTB information, shown on Fig. 4.10. In the left part of the plot very peripheral events with strong forward neutron production and small number of mid-rapidity charged particles are situated. In the second part of the plot there is an anti-correlation of ZDC and CTB signals, as more and more neutrons participate in the collision, less reach the ZDC, and more charged particles produced reach the CTB. The most central events, used in the analysis described later in this work, are situated in the bottom right corner of the plot.

4.3 Managing STAR data files

In normal mode of operation STAR detector produces $\sim 100Mb/s$ of raw detector data. This data is then transfered through the optic fiber Gigabit Ethernet link to the RHIC Computing Facility (RCF)[88] where it is stored on High Performance Storage System (HPSS) tape silos in the form of "raw data" files. After the calibration information is collected, data is transfered to Central Reconstruction Server(CRS) Linux PC farm, where the reconstruction software converts it into the form usable in physics analyses. The main step of this process is tracking. The data is then transfered back to HPSS, now in the format of Data Summary Tapes(DSTs). The DST contain all the information that can be possibly used in the physics analysis. This makes the DST files fairly big ($\sim 400MB/file$, single file containing $\sim$ 100 events). However all of this data is rarely needed, so due to space and computing time limitations, smaller files, containing only essential information, are produced. These are called μDST files and usually have the size $\sim 40MB/file$, single file containing $\sim$ 100 events.

Copies of all of theses file types (“daq_raw”, “daq_dst”, “daq_MuDst”) are kept on the HPSS. However, in order to be analyzed these file must be transfered to the Central Analysis Server(CAS) farm of PCs, where each member of the STAR collaboration can access them. They can be stored on centralized NFS disk, server by Sun machines, governed by the Veritas filesystem. This storage space has limited capacity and the servers can slow down under heavy load. So the files can also be transfered directly to the local disks of the CAS PCs, where they can be accessed with minimum delay by the jobs running there.

From the above short description of the flow of data from the experiment to the experimentalists it is clear that huge number of files is produced and stored in various places. One should also consider the fact, that STAR usually has several productions of $\mu DSTs$ from a single set of DSTs, done with different reconstruction software versions. Adding to that, files on local CAS disks are frequently copied, moved, corrupted, deleted and repopulated. One is then presented with a non-trivial task of managing and keeping track of all of these files.

To help in this activity, the author of this work was assigned a task to design, test and implement a specific database, containing file information. Also a programmatical layer was needed, which would connect the database itself with userspace programs available for the STAR Collaborators.

The following design specifications were considered:

- create a database that would store information about all STAR data files, easily accessible by both human operators and utility software
- store as much physics-related information (e.g. the trigger with which the file was taken) as possible, as a description of each file, so that it can be easily available without the need to actually access the file
- provide the functionality to have the same file in several copies on possibly different storage types (HPSS, NFS disk, local disk) or even different storage sites (RCF, PDSF computing facility at NERSC, California).
- provide the functionality to store the following physics information: trigger type and number of events per each trigger type, information if the specific subdetector was in or out of the data stream, magnetic field setting, collision type, RHIC run number
- store not only information on files with experimental data, but also on files generated by detector simulation

- store software related information, such as file type or the version of STAR software the file was produced with

The design process resulted in the creation of the FileCatalog database. The detailed description of the project itself as well as the needed software is in Appendix C. The database was implemented and deployed on Linux server running MySQL database engine.

A software module simplifying the access to the database was also designed and implemented. PERL language was chosen for this task. It has several advantages, which make it the suitable choice: well developed MySQL communication API, superior string manipulation and handling - crucial for SQL query building and result parsing, immediate availability on all STAR PCs, which run Linux operating system. The PERL module `FileCatalog.pm` was implemented, tested and deployed. It offers methods to connect to the FileCatalog database, and to easily, securely and consistently add, update, delete or retrieve records from it.

Using these two building blocks programs can be written to use the FileCatalog database. A tool, accessible to all STAR Collaborators, which would give easy access to FileCatalog data, was needed. For this task `get_file_list.pl` PERL script was written[89]. It can be used to get any or all the information listed in the design specification. It accepts conditions on the dataset it returns. It can also be used from within other programs, or as a generator of file lists for user analysis jobs.

FileCatalog has been deployed both at RHIC Computing Facility (RCF) and Parallel Distributed Systems Facility (PDSF) computing center in California. It is constantly used by the STAR collaboration. It now stores information of ~ 4 million files, and the number is growing fast, as new data is collected by the STAR experiment. The PERL module and utility script are commonly used by STAR users. FileCatalog made it possible for STAR to utilize local disks on CAS computers for storing the analyzed data, a transition that proved essential when collected data volume exceeded the capacity of centralized NFS disks.

STAR also developed a Scheduler - a JAVA program, which facilitates parallel data analysis. It takes the user-supplied meta-description of an analysis job, then, using the FileCatalog, searches for requested data-files, locates them (preferably on CAS machines local-disks) and then creates the suitable file list. A number of jobs are then sent in parallel, each with its own generated file list to execute on the CAS nodes, that store that specific dataset.

In summary FileCatalog has proved useful and essential in STAR data analysis effort.

Chapter 5

Analysis

5.1 Data analysis overview

The data used in this work comes from the STAR experiment, working at RHIC. It has been collected during two RHIC runs - Run1 in the summer of year 2000 and Run2 from July to November 2001. The main detector used was STAR TPC, which detected and tracked the particles produced in the collisions of gold ions. In this work central gold-gold collisions were studied.

The analysis consisted of several steps. The first was the preparation of the analysis code as an extension of the existing STAR `HbtMaker` software. This module was designed and written for the analysis of correlations of two (or three) particles at small relative velocities (which, in the case of identical particles, correspond to small relative momenta, both in pair rest frame and laboratory frame), traditionally called "HBT correlations". The code was first tested and used for $\pi\pi$ HBT measurements[49]. Minor changes to the code as well as several additions were needed for the analysis preformed in this work. The main changes were: the introduction of the special mode of obtaining the correlation function background (or "mixing"), which ensured that for non-identical particles the ordering of particles was never changed (e.g. pions and kaons were always combined into pion-kaon, never kaon-pion pairs); the introduction of correlation function classes, which allowed the analysis of emission asymmetries by constructing the double ratios. Appendix A has a more detailed description of the `StHbtMaker` module and the changes made.

The next step was the data analysis itself. `ROOT4STAR` package, with `StHbtMaker` as it's part was run with the data μDSTs as its input. The results were the pion-kaon correlation functions, as well as a large set of quality assurance histograms. In an iterative process the data cuts were fine-tuned to produce the best possible correlation function without sacrificing the data quality. The details of the cuts used for the final analysis is found in section 5.2. The resulting correlation functions are shown in chapter 6.

With the correlation functions ready it was necessary to determine how our detector could distort them. Two such effects were studied: the TPC momentum resolution (see also 4.2.1.2) and the particle purity. The latter actually consisted of two contributions: first part coming from the PID probability (see 4.2.1.2) and the second being the percentage of primary pions and kaons. Based on these studies appropriate corrections were made to the correlation functions. Details are described in section 5.3.

As a final step of the analysis, the obtained correlation functions were fitted with the custom written software, which allowed the use of arbitrary source model parameterizations and utilized the current state of knowledge of the pion-kaon interaction (coming from strong and coulomb forces) in the calculation of the theoretical correlation function. The details of the fitting procedure is described in section 6.2. Systematic errors were also determined at this stage.

5.2 Data selection

The data selection was done at three levels. At the event level the decision was made for each event whether it was to be discarded or included in the analysis. Then the tracks from the accepted events were also tested, and accepted only if they met specific criteria. The accepted tracks were then combined into pairs. Cuts, based on pair-wise characteristics, were also developed and used to either accept or reject a given pair. In the following sections the detailed description of all the cuts used is given.

5.2.1 Event selection

There were two main event characteristics, which were important in data selection. Most importantly only central gold-gold collisions were included in the analysis. Based on the ZDC and CTB information (see section 4.2.2) all the events collected by STAR were divided into two main categories: “central” and “minimum-bias” datasets. Several other datasets, such as ultra-peripheral collisions, were also recorded, but were not considered in this work. For each event in these two main dataset the centrality was determined, based on the TPC information. For Year1(Run1) negative tracks, which produced more than 10 hits in the TPC, passed closer than $3cm$ from the event primary vertex and had $|\eta| < 0.5$ were counted. If their multiplicity was within the range $(174, 500)$ the event was accepted as central. For Year2(Run2) similar tracks criteria was used, but the positively-charged particles were also counted. If the multiplicity was within the range $(431, 1000)$ for runs with STAR magnet (see section 4.2) at “half-field” setting or $(409, 1000)$ for runs with “full-field” setting, the event was accepted as central. Glauber model calculations indicate that these cuts accepted 12(10)% of the total gold-gold cross-section for Run1(Run2).

The second important cut was needed to ensure good data quality. The RHIC bunches were spread over some distance, so when they crossed, the collisions occurred not only in the very center of the TPC, but also some distance up or down the beam-pipe. The event that occurred away from the TPC center could still be properly tracked, however it did not retain it's symmetry in rapidity, due to the obvious acceptance limitations. The cut was therefore implemented to discard events that occurred more than $150cm$ from the center of the TPC for Run1. In Run2 the beam collimation was significantly improved and cut was narrowed down to $50cm$. Furthermore special care was taken not to construct the background (“mix”) from events whose primary vertices were separated more than $10cm(4cm)$ for Run1(Run2).

5.2.2 Track-level cuts

The main purpose of the track level cuts was selecting the appropriate particle types (pions and kaons) and ensuring good data quality.

To ensure good track reconstruction and a reliable dE/dx measurement only tracks that produced at least 15 hits in the TPC were accepted. The analysis required only primary particles, so only tracks with DCA (distance of closest approach) to the primary vertex less than $3cm$ were accepted.

For Year1 the accepted rapidity range was $(-0.5, 0.5)$. In order to select the proper particle type, cuts on PID probability (see section 4.2.1.2) were used. A particle was accepted as pion(kaon) if it's PID probability to be a pion(kaon) was larger than 50%. The particle momentum was also restricted to be within $(0.08, 0.5)\, GeV/c$ for pions or $(0.3, 1.0)\, GeV/c$ for kaons. Figure 5.1 shows the pion and kaon data sample from Year1. There was an additional requirement where pions were required to pass within $1.5cm$ of the primary vertex.

For Year2 the z-vertex position was improved, so the rapidity range was extended to $(-0.7, 0.7)$. To further improve the dE/dx information a track was only accepted if at least 10 of it's hits was used in the dE/dx determination. The electron contamination was larger in this dataset, therefore the PID cuts were tightened. A particle was accepted as a pion(kaon) if it's PID probability to be a pion(kaon) was more than 60%, while the PID probability for each of the remaining particle types was less than 20%. The field setting was changed to “full-field” for the most of the run, therefore the momentum ranges ware also changed and were $(0.13, 0.5)\, GeV/c$ and $(0.3, 1.0)\, GeV/c$ for pions and kaons

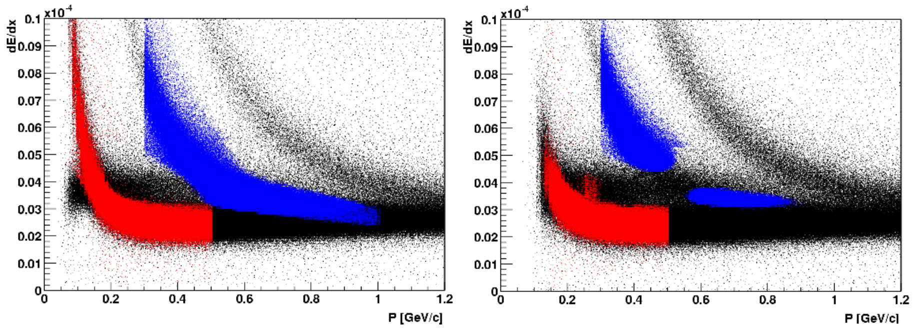

Figure 5.1: Distribution of dE/dx vs. momentum for accepted pions(red) and kaons(blue) overlayed over the background distribution of all particles for Year1(left) and Year2(right).

respectively. The resulting particle distributions are shown at Fig. 5.1.

5.2.3 Pair-level cuts

The cuts at the pair level dealt with issues that only arose for pairs of particles and were not possible to remove at the particle level. In other words these issues represented superficial correlations between particles. Since the purpose of this work was to study heavy-ion collision physics through pion-kaon correlations it was of critical importance to remove all fake correlations induced by the detector system itself.

The most effective tool in detecting such fake correlations was the Side "double-ratio" (see 3.2.3). By symmetry considerations it was required to be exactly equal to 1.0 for all values of k^*. Any deviation from such behavior was an indication of a detector effect. Indeed two such effects were found with the help of this method; they were later identified and specific cuts were developed to remove them. These effects and cuts are described below.

5.2.3.1 Removal of pairs with merged hits

STAR central event has a typical multiplicity of over 1000 charged particles, that traverse the TPC. It is common for tracks of these particles to be not far apart, or even cross. Indeed in central gold-gold collision at least 30% of the clusters, that form particle tracks, are merged. There are cases where these clusters cannot be successfully disentangled, and are therefore lost for the particle reconstruction software. This effect, known as "track merging" is known in identical particle HBT, and was extensively studied by STAR for $\pi\pi$ correlations[49]. It was believed that non-identical particles would be free of that problem, since

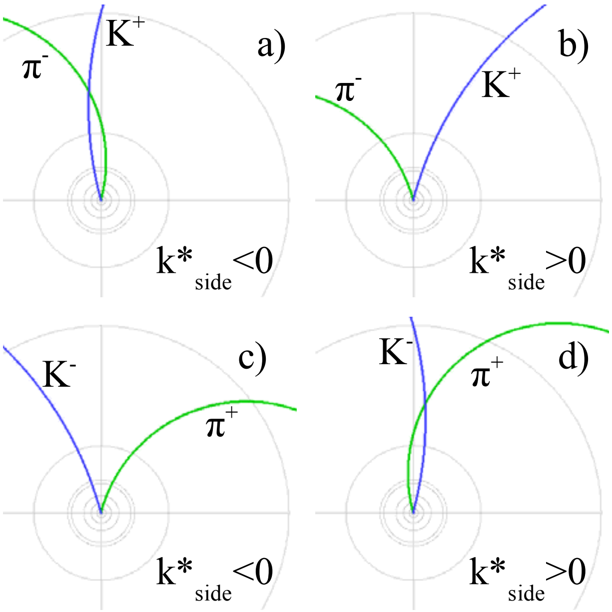

Figure 5.2: Tracks of pions and kaons may intersect inside the TPC volume, but only for pairs with the right configuration of charges and k^*_{side} sign. In the case shown on the plot merging would occur only for configurations a) and d).

pairs with low relative momentum would correspond to pairs with close velocities in laboratory frame. And this, for particles with different masses, would correspond to significantly different momenta and therefore tracks with different curvature, that would be well separated. However Side "double-ratio" indicated that some kind of track-merging problem persisted.

It was later understood that it was connected to the TPC tracking algorithm. As a first step of the algorithm so called "track seeds" were generated from hits in the outer padrows of the TPC. These seeds were later used in tracking. If a given particle's seed was not found, it could not have been tracked, even if it had significant number of good hits in the rest of the TPC padrows. If two tracks, also two non-identical particle tracks, would cross in the outer region of the TPC, their hits would be merged, the seeds would not have been found and the pair would not be reconstructed.

The occurrence of this phenomenon would be limited to pairs within small range of k^*_{side}. It is because k^*_{side} is directly proportional to the pair azimuthal angle difference $\Delta\phi$. For small $\Delta\phi$ the tracks would cross before the outer sectors of the TPC, and would not merge. For large values of $\Delta\phi$ the tracks would cross after traversing the TPC and would not merge either. Only for intermediate values of $\Delta\phi$ merging effect would occur. It is important to notice that for pairs

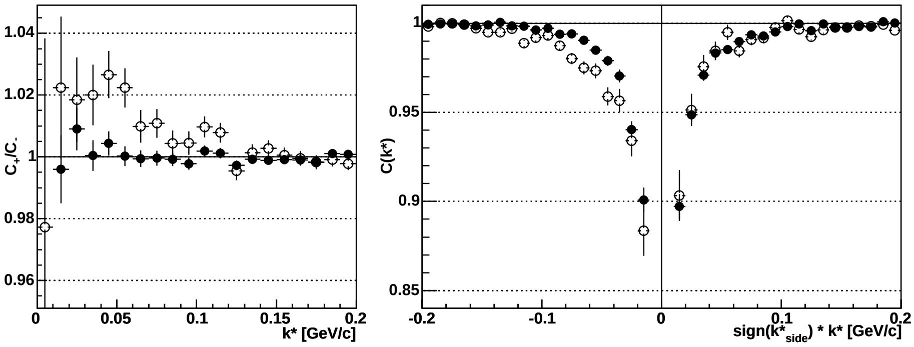

Figure 5.3: $\pi^- - K^-$ Side "double ratio"(left panel) and correlation functions (right panel) before (open circles) and after (closed circles) the application of the hit-merging cut.

with an opposite sign of k^*_{side} the $\Delta\phi$ would also have opposite sign, therefore the particle tracks would be bent away from each other by the magnetic field, would never cross, and would not merge either. This situation is shown schematically on Fig. 5.2. The net result would be that for correlation function numerator for pairs with a particular sign of k^*_{side}, there would be a depletion of pairs with respect to the denominator in a limited range of k^*. There would be no such effect in the correlation function for pairs with opposite sign of k^*_{side}, producing the above-mentioned non-unity Side "double-ratio", which was indeed observed in the data.

The described effect should be corrected for by the removal of pairs from the background. One should remove those pairs, which would be merged, if both particles came from the same event. A dedicated C++ class, so called "hit-merging" cut, was developed as a part of `StHbtMaker` to perform this task. Its operation is based on STAR TPC design and performance studies (see chapter 4.2.1). The basic idea is described below.

For both particles parameters of the reconstructed helices are taken. The helices are then projected onto the TPC pad plane, and points $x_{i,\pi}$ and $x_{i,K}$, where the helices cross the TPC padrows are found. For each padrow, the distance $\Delta x_i = |x_{i,\pi} - x_{i,K}|$ along the padrow is calculated. If the distance is less than the mean TPC two-hit separation distance (see chapter 4.2.1.2) for a given TPC sector, the two hits are tagged as "merged". An analog procedure is also carried out in the drift direction. Then all hits generated by the pair are counted, and a percentage of "merged" hits is calculated. If this percentage is higher than a preset number (for this analysis 10% was used), the pair is discarded as merged. This procedure is applied to both real and background pairs. The effect of the cut on the pion-kaon "double ratio" is shown on Fig. 5.3.

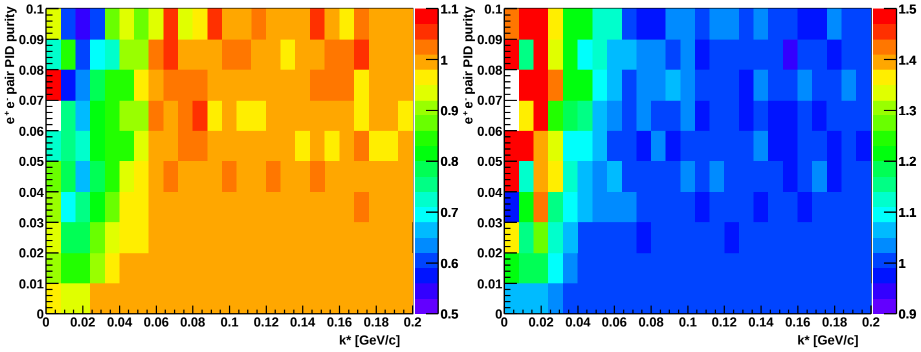

Figure 5.4: Side "double ratio" for π^+K^-(left) and π^-K^+(right) pairs as a function of pair e^+e^- PID purity.

The cut effectively removes unwanted correlations induced by track merging.

5.2.3.2 Electron-Positron pairs removal

After the removal of artificial correlations induced by hit-merging, Side "double ratio" was found to be equal to 1.0 for all values of k^* for like-sign pion-kaon pairs. For unlike-sign pairs some residual correlations remained that could not have been explained by track merging. They were identified as pairs of electrons and positions, coming from a γ conversion and misidentified as a pion and a kaon. Such a pair would be created at a conversion point between the collision vertex and the TPC volume. Then both particles would be misidentified as crossing, primary (coming from a primary vertex) tracks, creating a configuration similar to case a) and d) in Fig. 5.2. Such pairs would therefore be reconstructed as pion-kaon pairs with k^*_{side} of a specific sign (negative for π^+K^- or positive for π^-K^+), producing non-unity "double ratio". As the tracks need to cross before the TPC, this effect would show at k^* lower than the "hit-sharing" effect.

For Year1 this source of additional correlations was removed by imposing an additional cut on opposite-charge pion-kaon pairs. They were accepted only if the product of both particles electron PID probability was less than 0.1. It is important to note that electrons not coming from γ conversions, and therefore not having a correlated opposite charge companion, were not a problem in this analysis. Their contribution to the pion and kaon sample was estimated and accounted for with a simple purity correction procedure (see section 5.3.2).

In STAR Year2 additional material was placed between the TPC and the collision zone. The SVT detector increased the amount of potential γ conversion points, which resulted in a dramatic increase of e^+e^- pair production. The result can be seen on Fig. 5.4. The plot shows Side "double ratio" for unlike-sign pion-

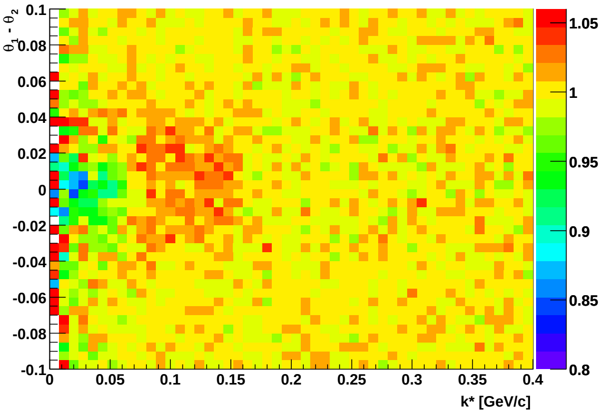

Figure 5.5: Side “double ratio” for $\pi^- K^+$pairs as a function of pair dip angle.

kaon pairs plotted as a function of pair e^+e^- PID probability. The artificial correlation is visibly enhanced as this PID probability increases. Even in the lowest bin of 1% it still is significant. Therefore the new cut on e^+e^- pairs was needed.

The cut, developed as a class of `StHbtMaker`, takes advantage of the fact, that e^+e^- pairs coming from a γ conversion have effectively zero opening angle. This corresponds to a small azimuthal angle difference $\Delta\phi$ of the pair, as well as small dip angle difference $\Delta\theta$. As $\Delta\phi$ is directly correlated with k^*_{side}, it was not a good variable to cut on, since it could induce indirect bias on the data. Therefore $\Delta\theta$ was selected. However simple cut to remove pairs with small dip angle was not possible, because it would remove too much statistics. A two step procedure was used. First a plot of the Side “double ratio” as a function of pair dip angle was created - see Fig. 5.5. It can be seen that pairs with dip angle < 0.05 show artificial correlations. Therefore pairs with a dip angle larger than this value need not be subject to the cut. For pairs with dip angle smaller, the e^+e^- PID purity is examined again, and if it is larger than a restrictive value of 0.01% it is considered to be a γ conversion pair candidate and discarded.

The effect of the anti-gamma cut can be seen on Fig. 5.6. The cut removes the artificial correlations produced by the electron-positron pairs in opposite-charge pion-kaon correlation functions. The cut is applied to both “real” and “mixed” pairs.

After both of the described pair cuts are applied, the artificial correlations in the Side “double ratio” are removed, and the next step in the analysis - the application of corrections, follows.

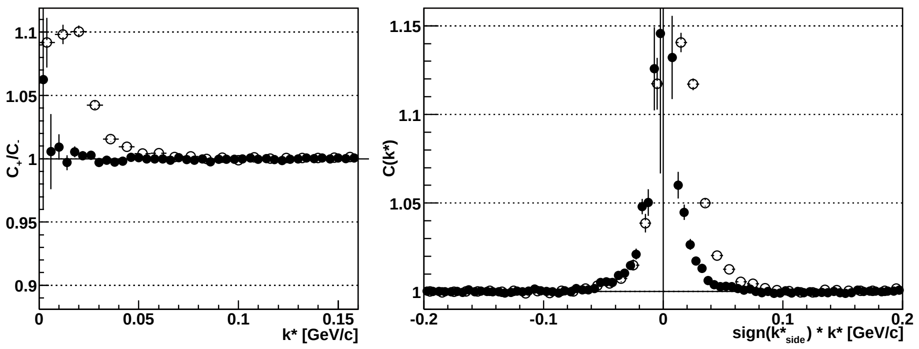

Figure 5.6: Side "double ratio"(left panel) and correlation functions(right panel) for $\pi^- K^+$ pairs before (open circles) and after (closed circles) the application of dip angle anti-electron pair cut.

5.3 Corrections

The corrections are procedures that attempt to account for such effects distorting the correlation functions that are known, but cannot be easily removed by particle or pair cuts. In the case of close-velocity non-identical particle correlations two of these effects were considered: particle momentum resolution and primary particle purity. The description of the respective corrections follows.

5.3.1 Momentum resolution correction

Particles reconstruction method in the TPC determines the momenta of the particles with a certain accuracy. This resolution is studied and known - for a description of a procedure see section 4.2.1.2. It affects the correlation function in the following way. Let's assume that a pion and a kaon have real momenta $\vec{p}^{\pi}_{orig}$ and $\vec{p}^{K}_{orig}$, and a relative momentum k^*_{orig}. The TPC reconstructs their momenta as $\vec{p}^{\pi}_{rec}$, $\vec{p}^{K}_{rec}$ and their relative momentum as k^*_{rec}. The probability that both differences $\Delta\vec{p}^{\pi} = \vec{p}^{\pi}_{orig} - \vec{p}^{\pi}_{rec}$ and $\Delta\vec{p}^{K}$ point in exactly opposite directions, producing $k^*_{rec} < k^*_{orig}$ is small. Therefore, on average, low k^* bins are the depleted of pairs, and therefore the correlations appears to be less strong in the low k^* region. On the other hand dN/dk^* distribution is a quadratic function of k^* at low k^*, so even though the production of a pair with smaller k^*_{rec} is less likely, there are more pairs that can produce it. These two effects balance each other, improving the situation.

The momentum resolution correction is done, but it is not applied to the data. Instead, momentum resolution effects are folded into the fitting procedure, that is applied to the data (see section 6.2). During this process simulated correlation functions are produced based on so called "pair weights". A weight is calculated based on the model-generated freeze-out coordinates of the particles, as well as their momenta $\vec{p}$(taken from the experiment), which are assumed to be their "real" momenta. Then the "reconstructed" momenta of the particles is determined by smearing the "real" ones with the simulation of the momentum resolution. The procedure is described below.

Momentum resolution parameterization has been performed, using the embedding technique and a detailed STAR TPC detector simulation (see section 4.2.1.2). Momentum resolution is described by the function of the form:

$$\begin{aligned}
\frac{\Delta p_i}{p_i} &= a_{p,i} + b_{p,i} p_i^{\alpha_i} + c_{p,i} p_i && (5.1)\\
\Delta \phi_i &= a_{\phi,i} + b_{\phi,i} \phi_i^{\alpha_i} && (5.2)\\
\Delta \theta &= a_{\theta,i} + b_{\theta,i} \theta_i^{\alpha_i}, && (5.3)
\end{aligned}$$

where i denotes a particle type. For each particle, based on its momentum p and angles ϕ and θ, corresponding smear sigmas $\sigma_{\Delta p}$, $\sigma_{\Delta\phi}$, $\sigma_{\Delta\theta}$ are found. Then a momentum resolution smears ∂p, $\partial\phi$ and $\partial\theta$ are generated from a Gaussian with a mean 0 and these sigmas. Finally new, "smeared" momenta are calculated using the following formulas:

$$\begin{aligned}
p_x^{smeared} &= p_x^{real} + \partial p_x && (5.4)\\
p_y^{smeared} &= p_y^{real} + \partial p_y && (5.5)\\
p_z^{smeared} &= p_z^{real} + \partial p_z, && (5.6)
\end{aligned}$$

where

$$\begin{aligned}
\partial p_x &= |p_x| \frac{\partial p}{p} + |p_y| \partial\phi + \left| p_x \frac{1}{\tan\theta} \right| \partial\theta && (5.7)\\
\partial p_y &= |p_y| \frac{\partial p}{p} + |p_x| \partial\phi + \left| p_y \frac{1}{\tan\theta} \right| \partial\theta && (5.8)\\
\partial p_z &= |p_z| \frac{\partial p}{p} + |p_z \tan\theta| \partial\theta. && (5.9)
\end{aligned}$$

Finally new $k^*_{smeared}$ is calculated with the "smeared" momenta of both particles in the pair, so the weight that is going into the histogram is calculates with the "real" momentum, but goes into the k^* bin corresponding to the "smeared" relative momentum. The results of this procedure can be found in Fig. 5.7, for parameters obtained from Year2 STAR TPC simulations with magnet at "full-field" setting. As can be seen, the momentum resolution affects mostly bins at low k^*. The figure also shows that the momentum resolution effect starts to be significant only when the simulated momentum resolution is unrealistically large (twice the magnitude predicted by embedding studies).

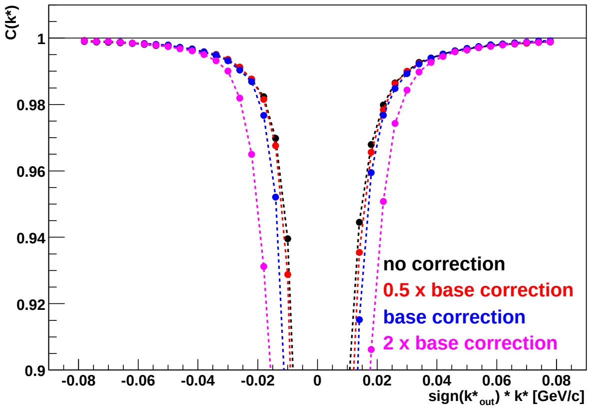

Figure 5.7: Momentum resolution affecting the simulated correlation function. Black points shows CF with no correction. Red, blue and magenta curves show this CF with momentum resolution smearing applied, where the smearing is half, equal or twice the amount determined by the STAR TPC performance simulations.

5.3.2 Particle purity correction

Particle purity correction is a procedure, which tries to account for the fact, that not all pairs of particles we detect contribute to the correlation effect. The are two possible reasons a pair would not be correlated. One of its particles may come from a decay of a particle, which occurred well outside of the source, that is a decay which is known not to occur on the $10^{-23}s$ time scale. For the purpose of this work all weak decays are assumed to be occurring outside of the source. It is not always possible to separate these particles from particles coming from the colliding AuAu system directly. A second case when a pair can be not correlated is when we misidentify a pion or a kaon for a different particle. Both of these effects modify the correlation functions in the same way, so they can be summed up to the overall purity parameter P, which is then used in the correction.

The contribution of the secondary pions to the pion sample cannot be obtained in a simple way, as many factors affect it: the multiplicity of weakly decaying particles, reconstruction efficiency as well as cuts applied to the data, especially the DCA cut (see section 5.2.2). The following procedure is used to estimate the fraction of secondary pions. Events are simulated with Hijing model and the multiplicities of primary pions, as well as pions coming from weakly decaying particles are plotted as a function of particle transverse momentum. The main source of secondary pions in STAR are K^0_S, strange hyperons Λ and Σ^0 and anti-strange hyperons $\bar{\Lambda}$ and $\bar{\Sigma^0}$. The generated particles are then put

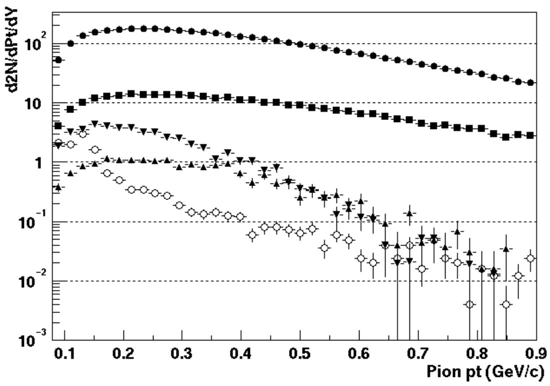

Figure 5.8: The scaled multiplicities of primary pions (black circles), K_s^0 (black squares), strange hyperons (up-pointing triangles), anti-strange hyperons (down-pointing triangles) and secondary pions (open circles) from Hijing.

through the full simulation of the STAR detector and then reconstructed. Then, they are propagated through the analysis software with all the cuts, that were described in this chapter. The final complication comes from the fact, that it is known, that Hijing does not reproduce particle multiplicities obtained in AuAu collisions observed at STAR. Therefore these resulting π, K_S^0 and hyperon spectra are additionally scaled in such a way, that their multiplicities correspond to the ones measured by STAR [90, 91, 92]. The resulting scaled distributions are shown on Fig. 5.8.

After this procedure, a percentage of primary pions can be obtained, by simply dividing the primary pion spectra by the full pion spectra. The effect is shown on Fig. 5.9. In addition to the weak decay products, some not correlated particles come from strongly decaying resonances that have a relatively long lifetime. The first is the ω resonance, decaying into charged pions. It's lifetime is $23.4 fm/c$, about 42% of them decay more than $20 fm$ from the source. Their multiplicity, relative to pion multiplicity, can be obtained from thermal model fits, and is estimated to be 9.2%. Therefore about 3.6% of pions can be considered as non-correlated products of the decay of the ω resonance. Similarly for kaons we have the ϕ. Its lifetime is $45 fm/c$, multiplicity relative to kaons is 14%, so about 9% of kaons are non-correlated ϕ decay products. This two contributions summed up constitute the first component of the particle purity.

The second component is the particle PID probability. The definition of this quantity and its origin is described in section 4.2.1.2. For the purpose of this correction we simply treat the particle PID probability as a fraction of true pions (kaons) in the group of particles that were selected as pions(kaons) by the

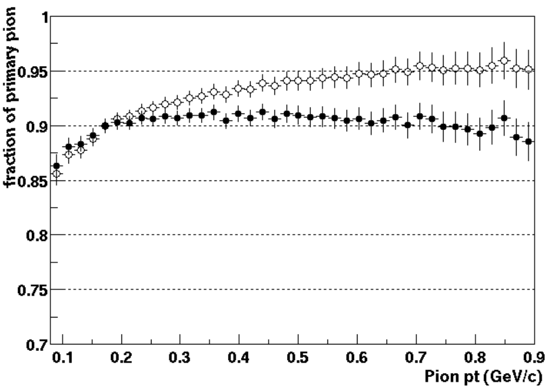

Figure 5.9: Fraction of primary pions from pure Hijing (open circles) and scaled Hijing (closed circles).

track cuts (see section 5.2.2). For each pair a *pair* PID probability is calculated as a product of the relevant *particle* PID probabilities of its constituents. Then the average of pion-kaon pair PID probability for all pairs used in the analysis is found as a function of pair relative momentum k^* multiplied by the sign of its k^*_{out} component.

The simulated primary particle purity described earlier is multiplied in the analysis code by the particle PID probability, then the results for a pion and a kaon from the same pair are multiplied to form the overall pair purity, which is then stored. Resulting purity histograms for all pion-kaon pair combinations are shown on Fig. 5.10.

This pair purity P is interpreted as a fraction of pairs, that do not contribute to the correlation effect. Therefore the observed correlation effect would be equal to the real correlation effect, scaled down by the purity:

$$C_{measured}\left(k^*\right) = \left(C_{real}\left(k^*\right) - 1\right) P\left(k^*\right) + 1, \tag{5.10}$$

therefore to recover the real correlation function one needs to apply a simple purity correction:

$$C_{real}\left(k^*\right) = \frac{\left(C_{measured}\left(k^*\right) - 1\right)}{P\left(k^*\right)} + 1 \tag{5.11}$$

This correction is applied to the experimental correlation functions on the bin-by-bin basis. All the functions shown in chapter 6 are corrected in this way.

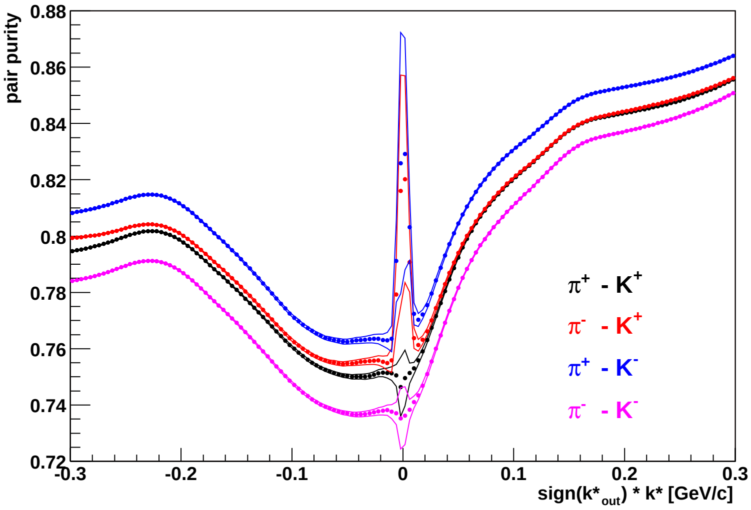

Figure 5.10: Summary pair purity histograms for all pion-kaon pair combinations. The plot is obtained from Year2 data. The symbols show the average pair purity in the bin, the bands reflect the PID purity spread.

Chapter 6

Results

6.1 Pion-Kaon correlations at 130 and 200 AGeV collisions

In this chapter the results of pion-kaon analysis at STAR (see chapter 4.2) in the form of the correlation functions and “double-ratios” are presented. They were obtained with the use of the procedures described in chapter 5.2. All presented functions are corrected for purity.

6.1.1 Correlation functions

The pion-kaon correlation functions obtained in Year1 data taking from STAR are presented on Fig. 6.1. Throughout this chapter the symbols have been consistently used in the following meaning: ●(closed circle) for π^+K^+ pairs, ○(open circle) for π^-K^- pairs, ■(closed square) for π^+K^- pairs and □(open square) for π^-K^+ pairs. The corresponding plot for Year2 data is shown on Fig. 6.2. The correlation functions show expected behavior: the pion-kaon interaction is dominated by the Coulomb force, so the correlation effect should be positive for unlike-sign combinations and negative for like-sign combinations. The good agreement between both like-sign correlation functions, as well as between unlike-sign correlation functions, suggests that the production mechanism of π^+ and π^- as well as K^+ and K^- are very similar, which is consistent with the fact that that spectra of the corresponding particles species are in agreement[94].

6.1.2 Asymmetry measurement

Emission asymmetries are measured using the “double-ratios”, which were defined in section 3.2.3. Figures 6.3 and 6.4 show the “double-ratios” measured in

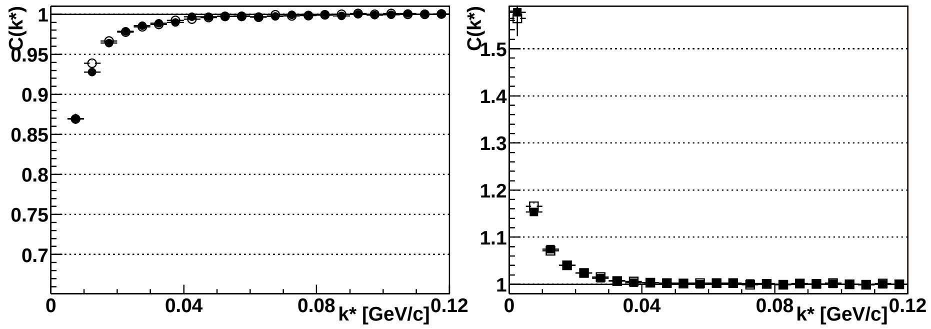

Figure 6.1: The pion-kaon correlation functions from STAR's Year1 data. See text for symbol explanation.

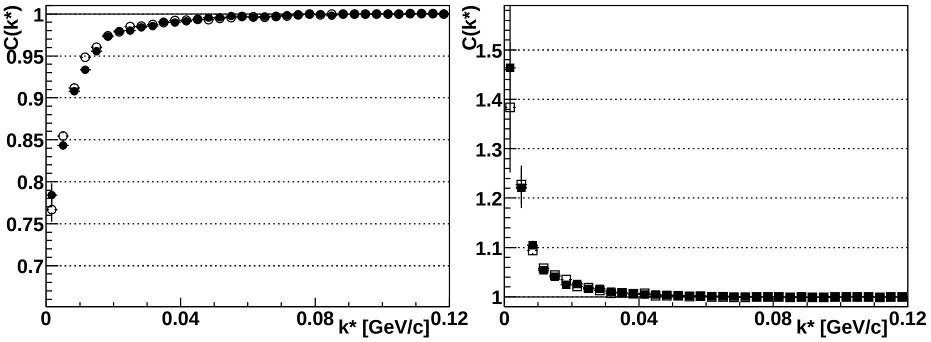

Figure 6.2: The pion-kaon correlation functions from STAR's Year2 data. See text for symbol explanation.

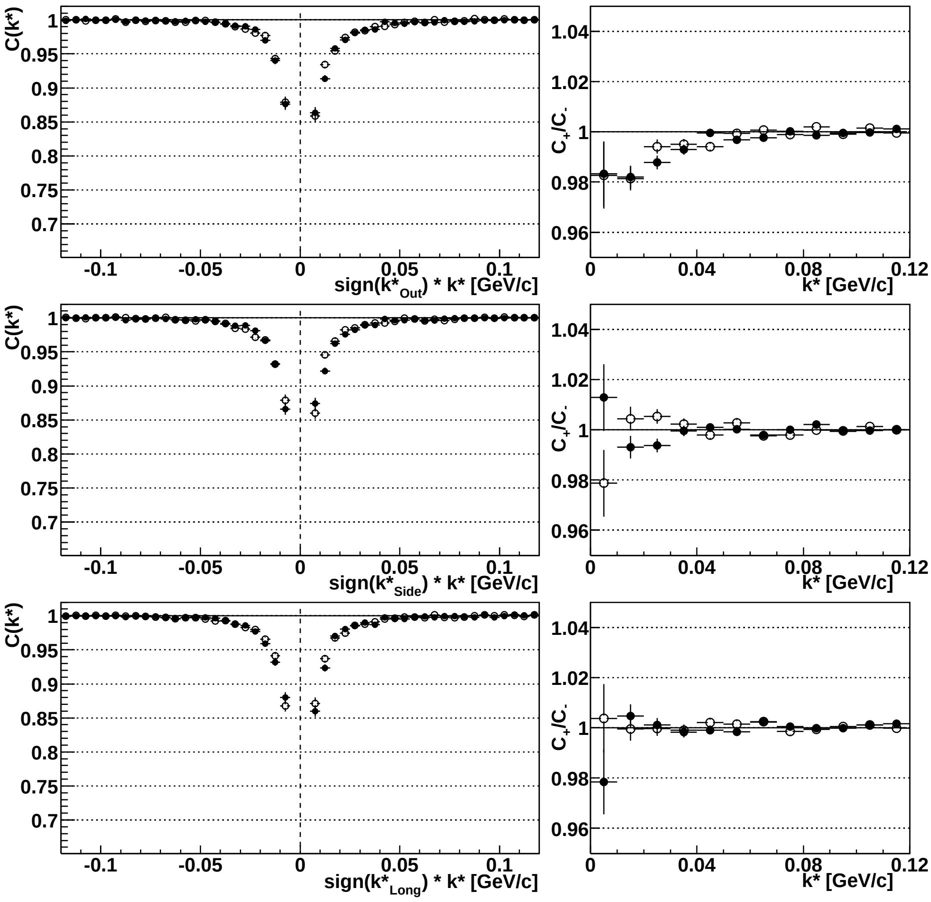

Figure 6.3: Asymmetry measurement in Year1 for like-sign pairs. Left panels show correlation functions, as a function of k^* multiplied by the sign of respective k^* components (from top to bottom: *Out*, *Side*, *Long*). Right panels show the "double-ratios" - they were obtained by dividing the right-hand sides (> 0) of the left panel plots by their left-hand sides (< 0).

the first year of STAR operation for all combinations of pion-kaon pairs. The corresponding figures for data from second year are shown on Figures 6.5 and 6.6.

The *Side* and *Long* "double-ratios" were used as a cross-checks, to ensure good data quality. The *Side* "double-ratio" is required to be unity by symmetry considerations (see section 3.2.3). It was used as a tool to tune the data-quality cuts described in section 5.2. On all the plots it can be seen that this "double-ratio" is flat and equal to 1.0 for all combinations of pion-kaon pairs, both for Year1 and Year2 data. Similar considerations show that the *Long* double ratio is expected to be flat at unity for a symmetric colliding system measured with a detector symmetric with respect to $y = 0$. Both requirements are fulfilled at

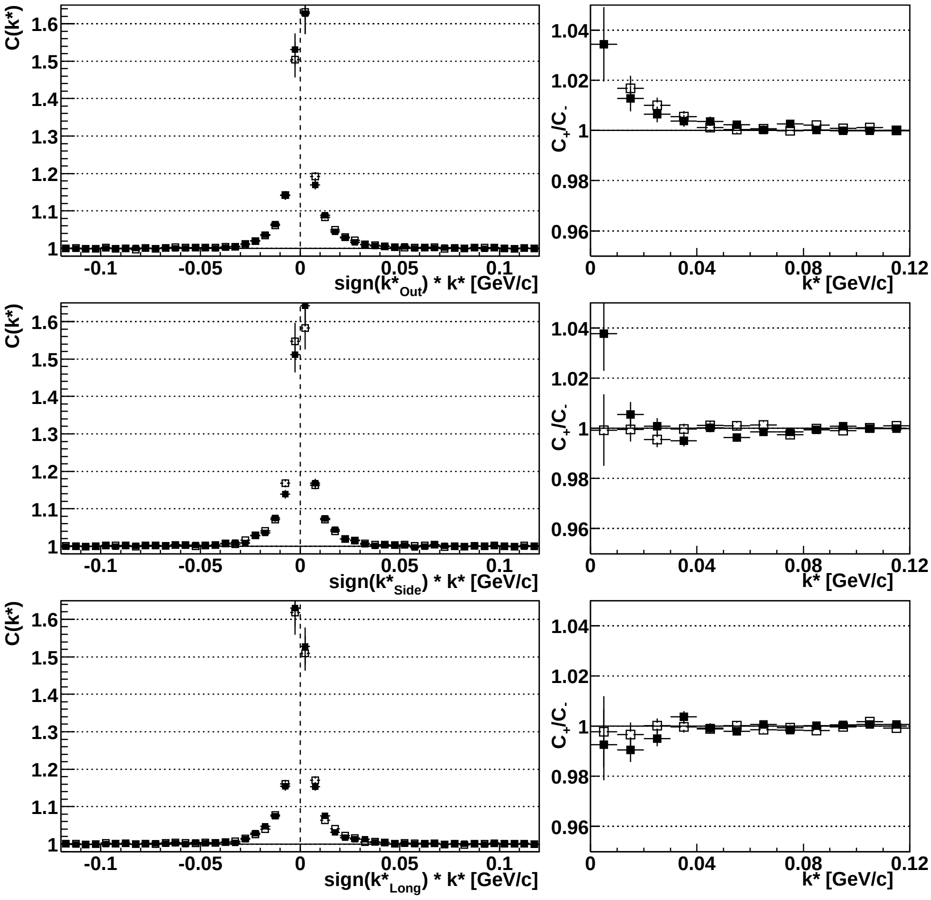

Figure 6.4: Asymmetry measurement in Year1 for opposite-sign pairs. Left panels show correlation functions, as a function of k^* multiplied by the sign of respective k^* components (from top to bottom: *Out*, *Side*, *Long*). Right panels show the "double-ratios" - they were obtained by dividing the right-hand sides (> 0) of the left panel plots by their left-hand sides (< 0).

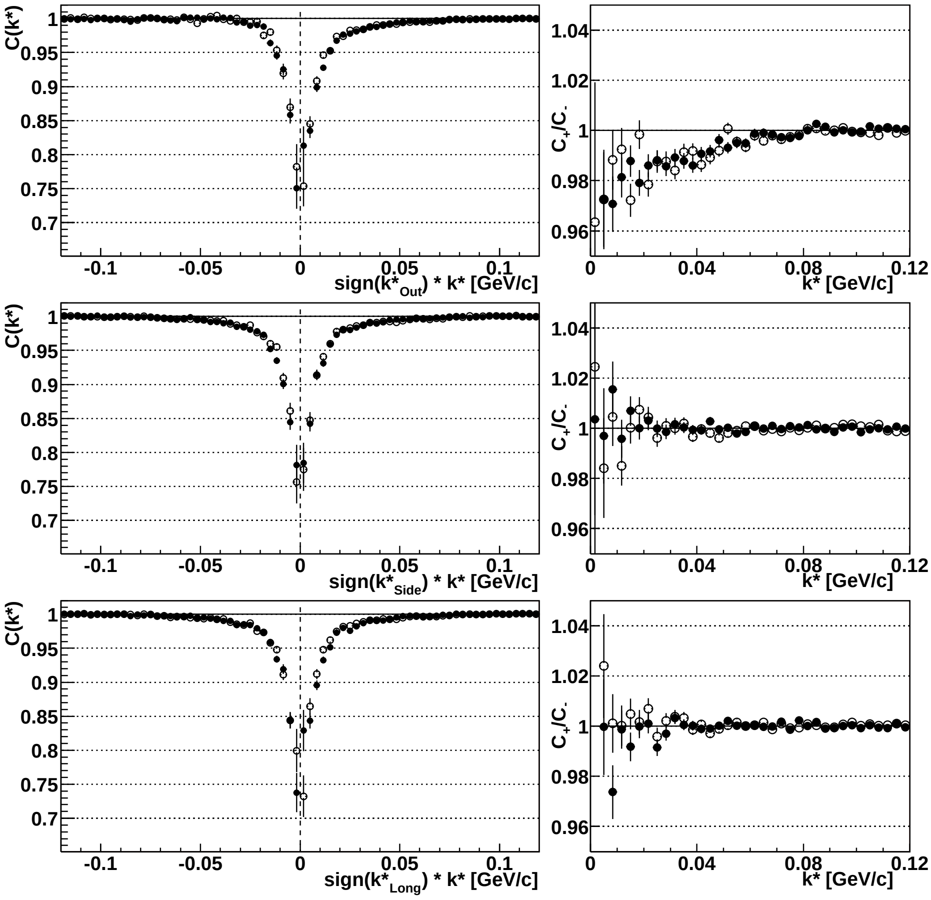

Figure 6.5: Asymmetry measurement in Year2 for like-sign pairs. Left panels show correlation functions, as a function of k^* multiplied by the sign of respective k^* components (from top to bottom: *Out*, *Side*, *Long*). Right panels show the "double-ratios" - they were obtained by dividing the right-hand sides (> 0) of the left panel plots by their left-hand sides (< 0).

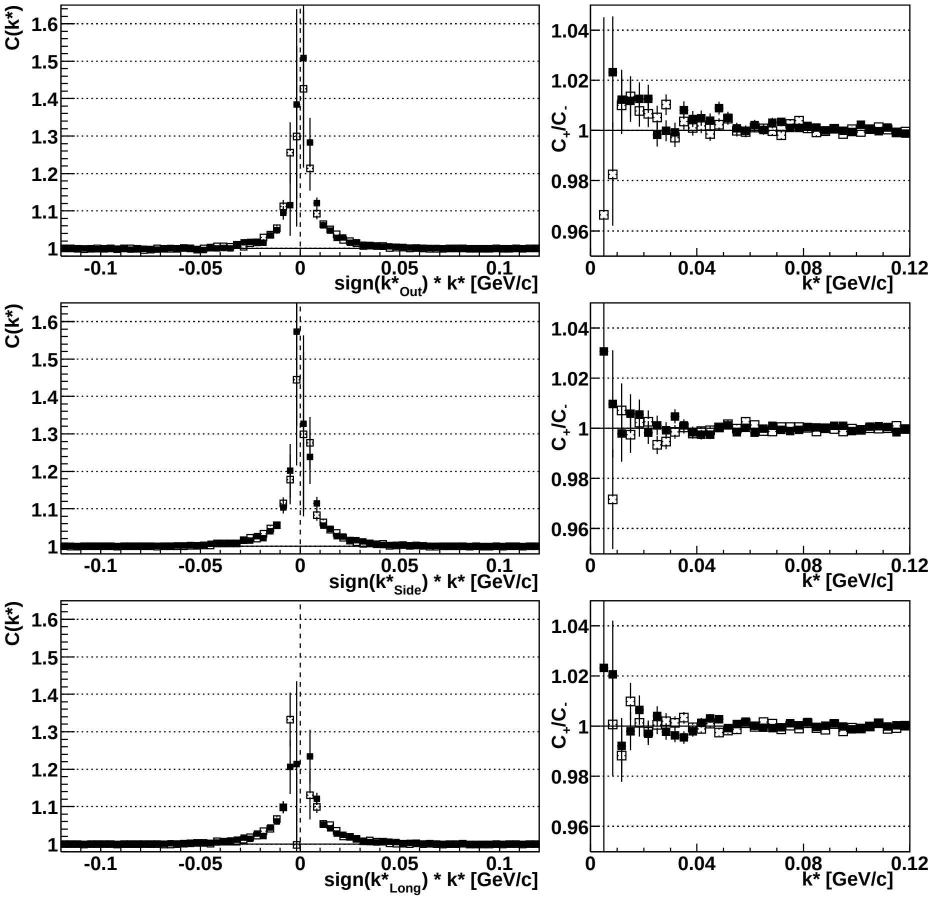

Figure 6.6: Asymmetry measurement in Year2 for opposite-sign pairs. Left panels show correlation functions, as a function of k^* multiplied by the sign of respective k^* components (from top to bottom: *Out*, *Side*, *Long*). Right panels show the "double-ratios" - they were obtained by dividing the right-hand sides (> 0) of the left panel plots by their left-hand sides (< 0).

STAR, and indeed the *Long* "double-ratios" for all combinations of pion-kaon pairs for both Year1 and Year2 data show no asymmetry.

The only direction where the asymmetry is expected is the *Out* direction. And indeed for all combinations of pion-kaon pairs, both for Year1 and Year2 data samples such asymmetry is observed. The correlation effect for like-sign pairs is negative, while for opposite-sign pairs it is positive. Therefore, if it is assumed that the asymmetry for all pair combinations is the same, then the "double-ratio" would be above unity for one charge combination, and below for the other - and such effect is indeed observed in the data: the double ratio goes above unity for opposite-charge combinations and below unity for same-charge combinations. This means that pions are, on the average, emitted closer to the center of the system produced in the collision, or that they are emitted later.

6.2 Fitting the correlation functions

In order to quantify the observed asymmetry as well as estimate the size of the emitting source, the fitting procedure is applied to the data. The correlation function for non-identical particles does not have an analytical form, that can be used to fit it and extract the source parameters directly. Instead, the numerical procedure, based on Monte-Carlo methods, is applied. It is described in detail in this chapter. The procedure finds such parameter values for a given source model that produce the theoretical correlation function that best matches the experimental one. A χ^2 test is used as an estimator of the quality of the fit. The procedure is more complicated and numerically demanding than regular fitting, but also allows for greater flexibility, as one is not limited to source models, that can be integrated analytically and new source models can be tried with little effort. A specialized software, `CorrFit`, was created specifically for the task of fitting. Its technical description can be found in Appendix B.

The theoretical correlation function is constructed from two sets of information. The first is the momenta of the pairs used in the CF construction. Since they are measured in the experiment, we can use them directly. The second are the coordinates of the emission points of the particles in each pair. Since the pair wave-function depends only on the relative position of the two particles, only four coordinates (r^*_{out}, r^*_{side}, r^*_{Long}, Δt) are needed. These coordinates are generated according to the selected source model.

Obviously one cannot hope to reconstruct a freeze-out coordinate of every particle. One can only deduce the overall characteristics of the coordinates' distributions. In order to do that, these distributions need to be parameterized - such a parameterization will be called a "source model" (SM). Then a relative freeze-out coordinates of each pair can be obtained by simply generating random numbers distributed according to the SM.

Each SM has a limited number of parameters. In the case of the asymmetry analysis, where two correlation functions $C^{+}(k^{*})$ and $C^{-}(k^{*})$ are available, only SM with two parameters will produce a non-degenerated fit. Therefore it is most convenient to have one of the parameters describe the strength of the correlation effect and correspond to the size of the source, while the second will describe the difference between C^{+} and C^{-} and will represent the average emission asymmetry between two particle species. An example is a simple SM - the source is assumed to be a three-dimensional Gaussian in the pair rest frame. The width of this Gaussian σ is the first parameter. This Gaussian is centered at $r^{*}_{side} = 0$ and $r^{*}_{long} = 0$, and $r^{*}_{out} = \mu$, where μ is the second SM parameter.

The description of the algorithm of the fitting process is given below. Each parameter of the SM was varied within a reasonable range. For each (discrete) combination (σ_i, μ_j) the following procedure was applied. For each pair the momenta of a pair $(\vec{p_1}, \vec{p_2})$ were taken from the experiment. The relative freeze-out coordinates $\vec{r^{*}}$ were generated according to the selected SM, with the parameters set to the above-mentioned values. Based on this data the modulus squared w of the pair wave-function (which includes both the strong and coulomb interaction part) was calculated. This weight w was put into the so-called "numerator" histogram, at the value of pair relative momenta k^{*} (see section 5.3.1 for the description how this procedure was modified to account for detector momentum resolution). At the same time a weight of 1.0 was put into the "denominator" histogram at the same value of k^{*}. After all pairs have been processed, the resulting "numerator" and "denominator" histograms were divided to obtain the theoretical correlation function (ThCF), which corresponded to the given combination of values of the SM parameters. The procedure is the numerical implementation of the formula **??**. This ThCF was then compared to the experimental one by a simple χ^2 test. The result of the test was then stored in the χ^2 map, at the coordinates (σ_i, μ_j). The procedure was repeated for each discrete point on the $\sigma - \mu$ plane until the χ^2 map was filled.

The minimum $(\sigma_{fit}, \mu_{fit})$ of the produced χ^2 map was then found and interpreted as a result of the whole fit procedure. Exemplary results for $\pi^{-}K^{-}$ pairs from Year1 data can be found on Fig. 6.7, where the minimum was found at $\sigma = 10.9 \pm 0.4\ fm$, $\mu = -4.9 \pm 1.0\ fm$. The described procedure performed for each bin is, in essence, a Monte-Carlo based numerical integration of the source emission function.

In this work the experimental correlation function was fitted using three different source models. The first was PRFGauss initially used by STAR to fit non-identical correlation functions[93]. It assumes the source is a 3-dimensional Gaussian in the pair rest frame (PRF), with equal width σ in all directions

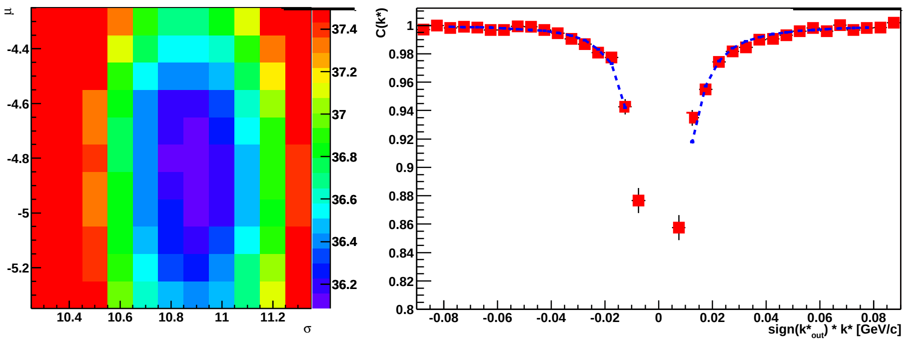

Figure 6.7: An example of the fitting results. A χ^2 map is shown on the left panel. An experimental correlation function (red squares) and the fitted theoretical correlation function (blue dotted line) are show on the right panel.

(*out*, *side* and *long*). It also assumes there is a shift μ between average emission points of pions and kaons in the *out* direction. An example distribution is shown on Fig. 6.8 as red lines.

The second model was CMSGaus. It was developed in order to take into account two observations, which were made in model studies (see chapter 7). It was observed that for simulated sources the σ of the Gaussian in the PRF was significantly larger in *out* direction when compared to *side* and *long*, due to the Lorentz boost in the *out* direction, which is necessary when going from CMS to PRF. Therefore having equal widths in all directions in PRF was not adequate. The widths were much more similar in the CMS frame. It was also noticed that the *out* distribution was not symmetric, having different slope for values of r_{out} smaller and larger than $\langle r_{out} \rangle$. To account for these effects, the CMSGaus model assumed the source was a 3-dimensional Gaussian in the source rest frame, or center of mass (CMS) frame. The parameter of the model was the base width σ of the Gaussian. In the *out* direction the distribution was described by the Gaussian with width σ for $r_{out} < \langle r_{out} \rangle$, and a width σs_{out} for $r_{out} > \langle r_{out} \rangle$. In the *side*, *long* and *time* directions the widths were σs_{side}, σs_{long} and σs_{time} respectively. The s_{out} multiplier was fixed at 0.8, and the s_{time} at 1.0, based on the results of RQMD and blast-wave simulations (for a detailed discussion see section 7.2). The s_{side} and s_{long} multipliers were taken as ratios of STAR pion-pion Bose-Einstein R_{out} as well as R_{side} and R_{long} values[49], and were fixed at 0.92 and 1.05 respectively. An example of pair space separation distributions produced by the CMSG model is shown in Fig. 6.8 as blue lines.

The last model used, CMSEH, was developed in an attempt to account for another feature of freeze-out r_{out}, r_{side} and r_{long} distributions observed in model studies: the fact that they do not decrease as fast as a Gaussian distribution. On a log scale, the behavior of these distributions away from the mean is more

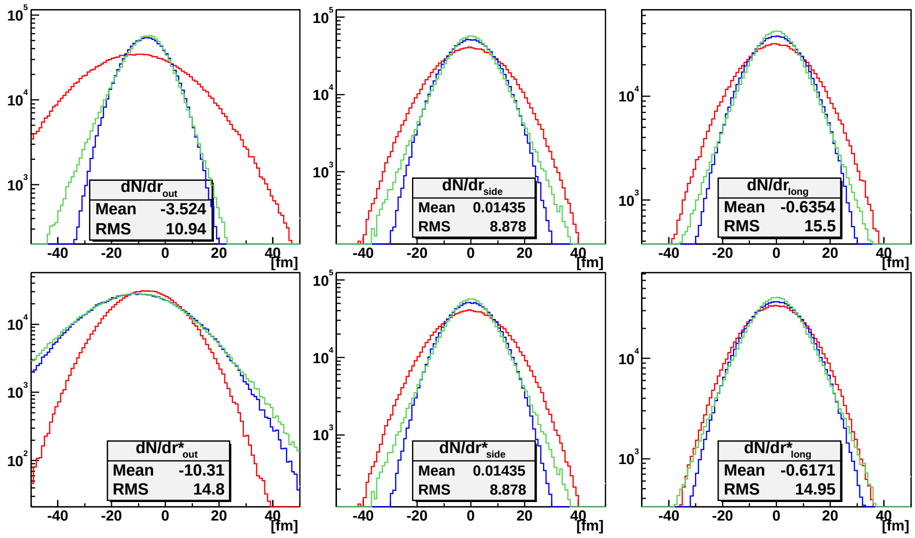

Figure 6.8: Examples of SourceModel distributions. Lines correspond to the PRFG SourceModel (red), CMSG (blue) and CMSEH (green). Upper plots show the resulting pair separation distributions in the source center-of-mass system (lab frame). Lower plots show pair separation distributions in Pair Rest Frame (PRF).

linear than quadratic. At the same time near the mean there is a smooth parabola-like transition from the rising to the falling part of the plot. A fairly simple function that reproduces this behavior is an inverted hyperbola in log space, or an "exponential hyperbola" (EH), that is a function of the form:

$$f_{EH}\left(x\right)=N\exp\left(\alpha\right)\exp\left(-\sqrt{\frac{\left(x-\mu\right)^{2}}{\sigma^{2}}+\alpha^{2}}\right).$$

The mathematical details of the formula are described in Appendix E.1. The function has three parameters: mean x value μ , a width of the distribution σ and a parameter α which controls the sharpness of the peak as well as a width of the distribution. An example of pair separation distributions produced by CMSEH are shown on Fig. 6.8 as green lines. The parameters α and σ are correlated, their change has a similar effect on the distribution. Therefore an attempt to fit the correlation function with three parameters μ, σ and α is likely to produce a degenerated fit. The solution is to fix the value of an α parameter to some value and fit only σ, which is similar to a σ parameter for a Gaussian distribution. In the CMSEH α was fixed to 2.0. Scaling parameters s_{out}, s_{side}, s_{long} and s_{time} were also used with values exactly the same as for the CMSGaus model. In order to compare the resulting width parameter to the Gaussian σ

	CMSEH	CMSGaus	PRFGaus
fit σ	$6.0^{+0.1+0.6\,syst.}_{-0.1-0.6\,syst.}$	$10.8^{+0.3+1.1\,syst.}_{-0.2-1.3\,syst,}$	$12.9^{+0.2+1.2\,syst.}_{-0.3-1.3\,syst,}$
half-width [fm]	$10.8^{+0.2+1.2\,syst.}_{-0.2-1.2\,syst.}$	$10.8^{+0.3+1.1\,syst.}_{-0.2-1.3\,syst,}$	$12.9^{+0.2+1.2\,syst.}_{-0.3-1.3\,syst,}$
mean shift μ [fm]	$-3.2^{+0.4+1.3\,syst.}_{-0.6-1.4\,syst.}$	$-4.5^{+0.3+1.2\,syst.}_{-0.5-1.2\,syst.}$	$-4.9^{+0.6+0.9\,syst.}_{-0.4-1.2\,syst.}$
χ^2/dof	1.20	1.21	1.20

Table 6.1: Summary results for fits of Pion-Kaon correlation functions from Year1

	CMSEH	CMSGaus	PRFGaus
fit σ	$6.5^{+0.3+1.1\,syst.}_{-0.1-0.7\,syst.}$	$11.4^{+0.3+2.5\,syst.}_{-0.2-0.9\,syst.}$	$14.7^{+0.4+3.2\,syst.}_{-0.3-1.7\,syst.}$
half-width [fm]	$11.7^{+0.5+1.9\,syst.}_{-0.2-1.3\,syst.}$	$11.4^{+0.3+2.5\,syst.}_{-0.2-0.9\,syst.}$	$14.7^{+0.4+3.2\,syst.}_{-0.3-1.7\,syst.}$
mean shift μ [fm]	$-4.2^{+0.7+3.8\,syst.}_{-1.3-4.1\,syst.}$	$-4.8^{+0.5+0.5\,syst.}_{-0.6-7.8\,syst.}$	$-8.2^{+0.4+3.3\,syst.}_{-0.9-5.4\,syst.}$
χ^2/dof	2.9	3.1	3.1

Table 6.2: Summary results for fits of Pion-Kaon correlation functions from Year2

one has to calculate the half-width of the distribution (see section E.1).

The results of the fitting of the correlation functions are summarized in Tables 6.1 and 6.2. The presented statistical errors were estimated based on the χ^2 map curvature. The systematic errors were obtained from two sources. One was the agreement between four correlation functions for all combinations of charges of pion and kaon. The second was the stability of the result with respect to the purity correction. The correlation functions were corrected for purity scaled by 90% and 110% of the value obtained from the experiment. The differences between these fit results and the result for 100% purity correction were taken as systematic errors due to this correction. The two contributions were added quadratically to obtain the final systematic error. The detailed values used in this procedure are shown in Tables 6.3 and 6.4.

	All	π^+K^+	π^-K^-	π^+K^-	π^-K^+	Purity 90%	Purity 110%
CMSEH σ	6.0	5.6	5.9	6.4	6.1	6.5	5.5
CMSEH μ	-3.2	-4.5	-3.6	-1.7	-2.6	-3.7	-3.0
CMSGaus σ	10.8	10.2	10.9	11.2	11.0	10.7	9.6
CMSGaus μ	-4.5	-5.7	-4.9	-4.1	-3.3	-4.8	-4.4
PRFGaus σ	12.9	12.2	13.3	12.9	13.1	14.0	11.8
PRFGaus μ	-4.9	-6.1	-5.3	-4.2	-4.0	-5.1	-4.7

Table 6.3: Determining systematic error of the fitted source model parameters for Year1 data. First column is a result of the fit to all four correlation functions simultaneously. Next four columns show fits to four functions separately. Last two columns show fits to correlation functions corrected for purity scaled to 90% and 110% of the standard value.

	All	π^+K^+	π^-K^-	π^+K^-	π^-K^+	Purity 90%	Purity 110%
CMSEH σ	6.5	6.9	7.5	6.0	6.2	6.9	6.0
CMSEH μ	-4.2	-8.3	-8.3	-2.9	-0.5	-3.3	-4.6
CMSGaus σ	11.4	13.0	13.5	10.7	11.7	12.8	10.8
CMSGaus μ	-4.8	-10.6	-12.5	-4.3	-4.3	-6.1	-4.9
PRFGaus σ	14.7	15.8	17.5	13.5	14.8	16.3	13.5
PRFGaus μ	-8.2	-13.5	-13.5	-4.9	-5.4	-9.4	-7.8

Table 6.4: Determining systematic error of the fitted source model parameters for Year2 data. First column is a result of the fit to all four correlation functions simultaneously. Next four columns show fits to four functions separately. Last two columns show fits to correlation functions corrected for purity scaled to 90% and 110% of the standard value.

The detailed discussion of the fit results, the fit quality as well as the applicability of each of the source models is presented in the next chapter.

Chapter 7

Results discussion

In this chapter the results of non-identical pion-kaon correlations are discussed. First the fit results and the quality of the fits are discussed. Then a comparison to models is made and the origins of asymmetry are discussed.

7.1 Comparing source models

In the fitting process, three models, described in section 6.2, were used. They were: PRFG, CMSG and CMSEH. The exemplary resulting source distributions are shown on Fig. 7.1. The PRFG model was used in the first non-identical particle correlations publication from STAR[93], so it was needed in order to compare the results from Year1 and Year2. It differs significantly form the other two, and this difference can be seen in the fit results. The obtained source size σ_{PRFG} is consistently significantly larger than the other two (σ_{CMSG} and σ_{CMSEH}). This is easily explained, when one takes into account the relation between sizes in all directions in the source center-of-mass system:

$$\sigma = \sqrt{\sigma_{out}^2 + \sigma_{side}^2 + \sigma_{time}^2 + \sigma_{long}^2} \tag{7.1}$$

and the fact, that while boosting to PRF, the size in *out* direction is significantly enlarged (see Eq. 3.32). Therefore, even though the sizes in *side* and *long* directions are the same for PRFG and CMSG, the larger size in *out* produces the larger average size. The difference is on the order of 10-15%. Part of the difference may also come from the fact, that the spread in *time* is assumed to be 0 in PRFG, so the spread in emission time in lab frame must also be accounted for by the σ_{PRFG}, while it is explicitly included in other models. There is also a difference in mean shifts $\mu = \langle r_{out} \rangle$ in the *out* direction between PRFG and other models. This comes from a feature introduced in CMSG and CMSEH -

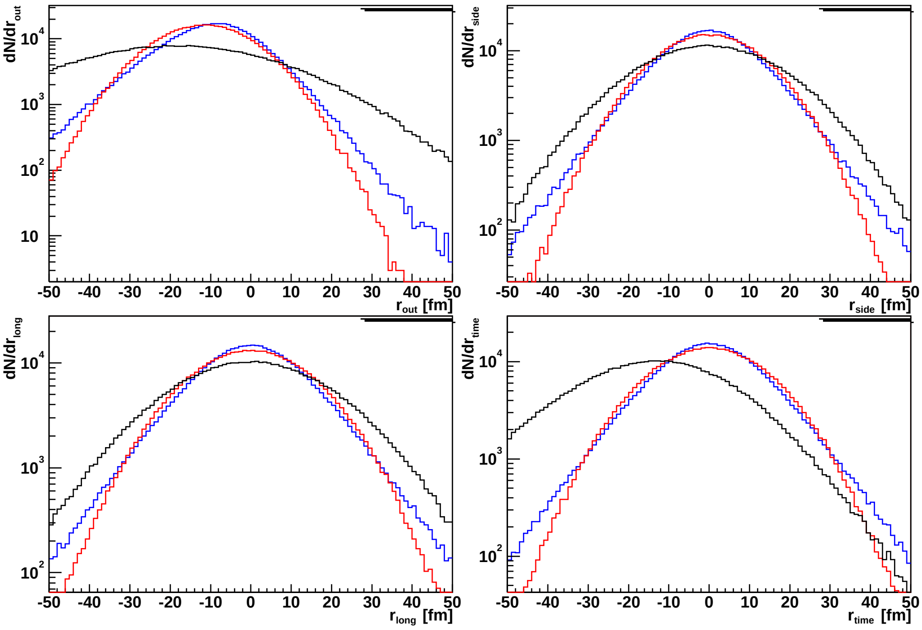

Figure 7.1: The source distributions in CMS for the “best-fit” values for Year2 π^+K^+ data obtained for PRFG(black), CMSG(red) and CMSEH(blue) source models.

the slope of the r_{out} differs for $r_{out} > \langle r_{out} \rangle$ and $r_{out} < \langle r_{out} \rangle$. Therefore part of the asymmetry in these models will be accounted for by the asymmetry of slopes and μ will be reduced.

The CMSG model assumes the source has similar size in all directions in CMS. It also assumes the asymmetry in *out* direction comes not only from the shift of the peak value (which is controlled by the μ fit parameter), but also from the asymmetry of slopes (controlled by the s_{out} value). From identical particle correlations we expect the size of the source to be similar in all directions in CMS, therefore the CMSG is thought to better describe the source produced in AuAu collisions.

The CMSEH model has different functional form than PRFG and CMSG. It is therefore different than the traditional form used so far in particle correlations as the majority of HBT results are given with the assumption that the source is a sphere with gaussian density profile (see section 3.1.2.3). The tails of the distribution fall almost linearly, which is consistent with the results of RQMD simulations (see next section), and is believed to be caused by the fact that some particles come from strongly decaying resonances. They will decay at mean distance $c\tau$ from the source, where τ is the decay time of the resonance. Since the decay time has exponential shape, so will the distance of the decay from the

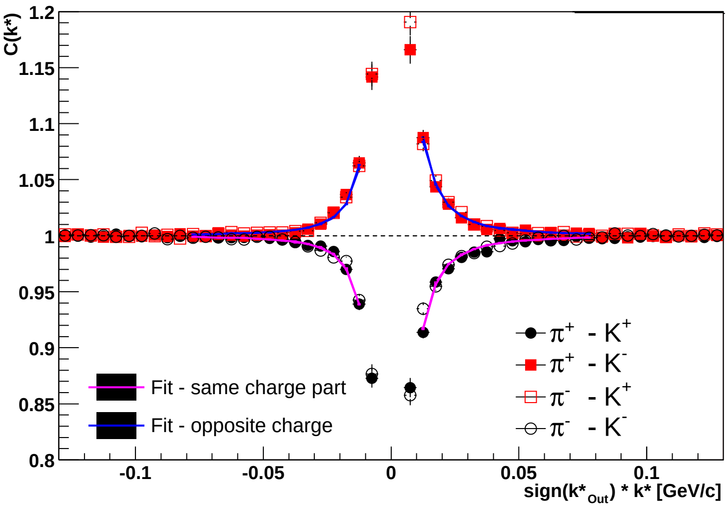

Figure 7.2: Experimental pion-kaon correlation functions for Year1 data and the fitted theoretical correlation functions obtained for PRFG model with "best-fit" parameters

source - therefore the source distribution is expected to have exponential tails. It is important to note, that the half-widths of the CMSEH agree exactly with the half-width from CMSG, therefore the size of the source is determined by the part of the source distribution around the mean, where most of the particles come from and where the two models do not differ significantly.

Judging the quality of the fit from the χ^2 values obtained, two conclusions can be drawn. In Year1 data, the quality of data does not allow to conclude which source model describes the data best. They are all valid, and describe the correlation functions fairly well. In Year2 data the statistics is significantly larger. The χ^2 values favor the CMSEH model, suggesting that the actual source produced in AuAu collisions does not have a Gaussian shape.

In this section the actual fitted correlation functions are also shown. On Figs. 7.2, 7.3, 7.4 the "best-fit" theoretical correlation functions for Year1 data and PRFG, CMSG and CMSEH models respectively are shown. Similar plots for Year2 data are shown on Figs. 7.5, 7.6, 7.7. Please note that the bins for $k^* < 10\ MeV$, which are most affected by the momentum resolution and have the smallest statistical significance due to low number of entries, were not included in the fit. Their inclusion does not change the results of the fit, but increases the duration of the fitting procedure.

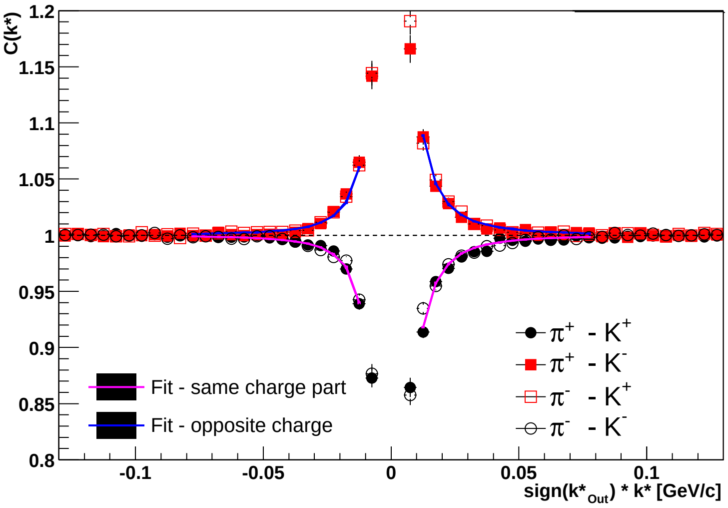

Figure 7.3: Experimental pion-kaon correlation functions for Year1 data and the fitted theoretical correlation functions obtained for CMSG model with “best-fit” parameters

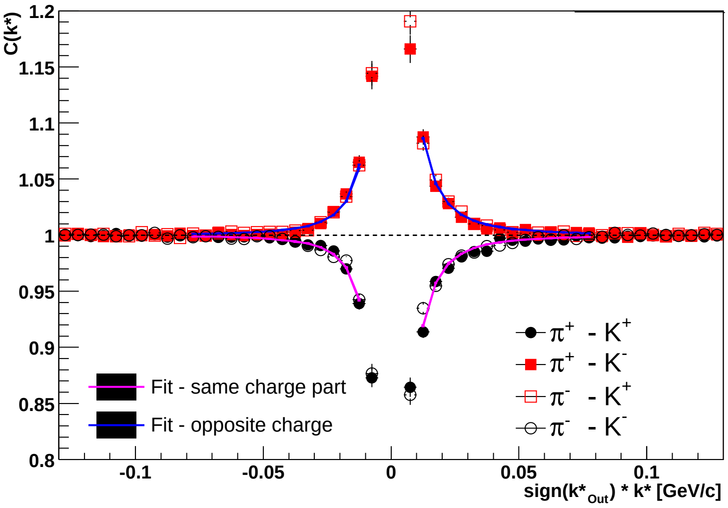

Figure 7.4: Experimental pion-kaon correlation functions for Year1 data and the fitted theoretical correlation functions obtained for CMSEH model with “best-fit” parameters

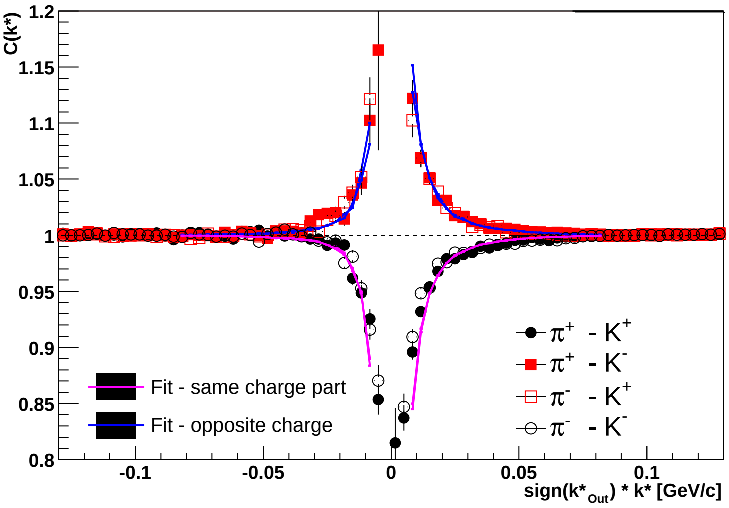

Figure 7.5: Experimental pion-kaon correlation functions for Year2 data and the fitted theoretical correlation functions obtained for PRFG model with "best-fit" parameters

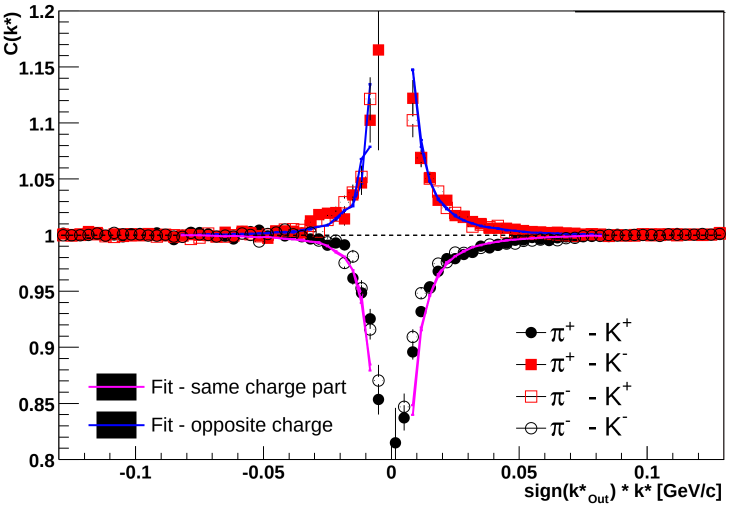

Figure 7.6: Experimental pion-kaon correlation functions for Year2 data and the fitted theoretical correlation functions obtained for CMSG model with "best-fit" parameters

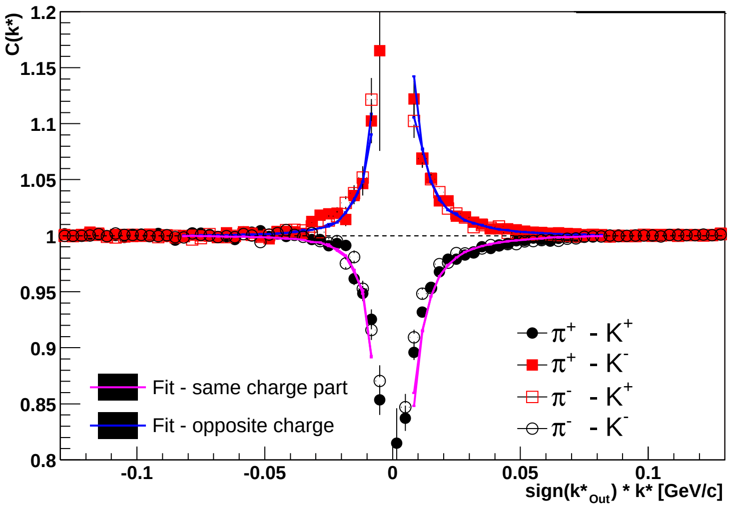

Figure 7.7: Experimental pion-kaon correlation functions for Year2 data and the fitted theoretical correlation functions obtained for CMSEH model with "best-fit" parameters

7.2 Comparing data and model predictions

7.2.1 Blast-wave parameterization and the origins of asymmetry

The theoretical basis of the blast-wave parameterization is described in section 2.4.2. Its main feature important for non-identical particle analysis is the hydrodynamics-like flow, which is embedded in the formulas. With the help of "blast-wave" the origins of asymmetry in the *out* direction can be explained.

Figure 7.8 shows the space-time density of pion and kaon emission points obtained for pion-kaon pairs from blast-wave calculations. The most important feature of the plot is the fact, that average emission points of pions $\langle r^{\pi} \rangle$ and kaons $\langle r^{K} \rangle$ are different. Closer examination shows, that $\langle r^{\pi}_{side} \rangle = \langle r^{K}_{side} \rangle = 0$ in agreement with the symmetry argument for the side asymmetry being 0. The only difference is in the *out* direction. It can be explained by the following argument. If a system with ideal flow is produced it implies a zero temperature in "blast-wave", which automatically gives $\phi_s = \phi_p$ (spatial angle is equal to momentum angle) in Eq. 2.13. In this case all particles are emitted along the radial direction. That means that particles with a given ϕ_p can only be emitted from space-points with $\phi_s = \phi_p$. In this case the radial coordinate of the average emission point is simply equal to the mean of the flow profile (given by Eq. 2.7) and is the same for particles with different masses. However in "blast-wave"

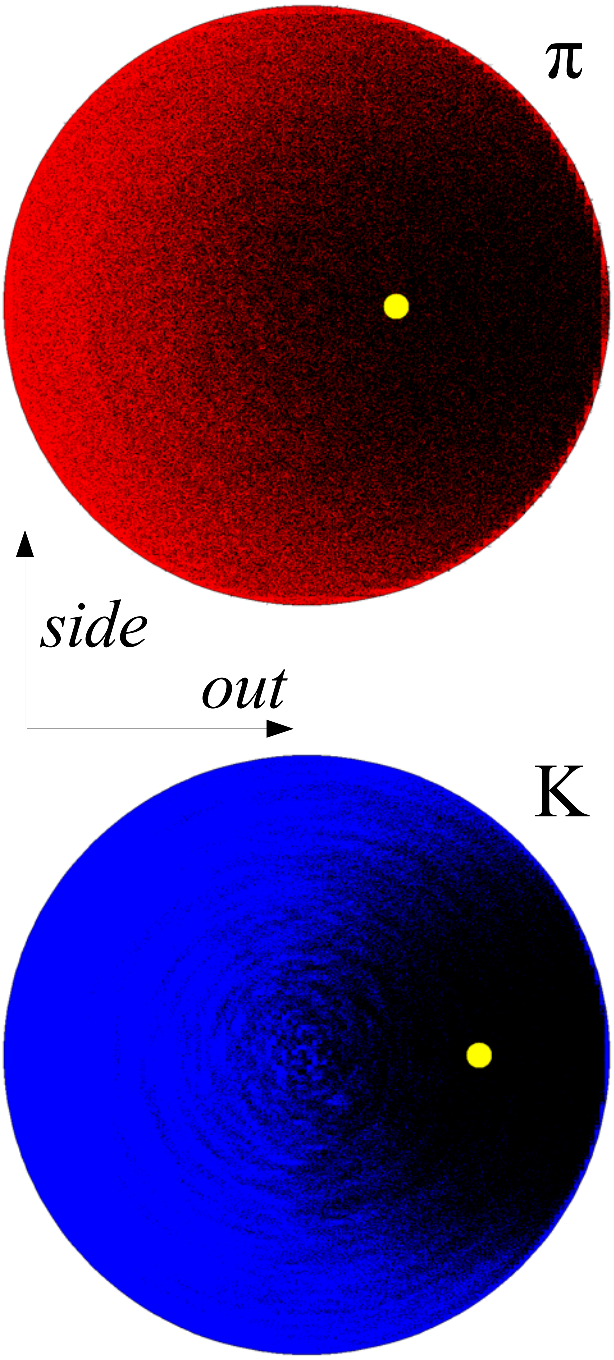

Figure 7.8: Spatial density of emission points of pions (top) and kaons (bottom) obtained from the "blast-wave" parameterization calculation with Year2 parameters. Yellow dots show the average emission points.

an additional randomization of particle momenta is introduced in the form of temperature. In this case the observed velocity β of the particle is the sum of the flow velocity β_f, which is completely determined by the flow field and the thermal velocity β_T which is directed randomly. Then particles emitted with a given ϕ_p can be emitted from space-points that have ϕ_s not necessarily equal to ϕ_p. How big the difference can be is determined by the relative magnitude of β_f and β_T. One can consider a pair of particles - a pion and a kaon. Their β_f will be the same, as the flow fields does not depend on particle mass. The thermal distributions is also the same for pions and kaons, but will produce the same momenta, not velocities. Since pions have smaller mass the resulting average β_T will be relatively larger for them. This means that the spread of emission points will be larger for pions, than kaons. This means that the average emission point of pions will be closer to the center of the source than the average emission point for kaons. This is exactly what is seen on Fig. 7.8. It is important to note that in the limiting case of no flow (or the equivalent case of infinite temperature), both average emission points are in the center of the source and there is no asymmetry. In summary: the existence of finite flow and finite temperature in "blast-wave" produces non-zero shift in the *out* direction between average emission points of particles with different masses, e.g. between pions and kaons.

There is no straightforward way to compare the predictions of the blast-wave parameterization with the results of the STAR experiment. In this work the following procedure was applied. First the particles were generated with the Monte-Carlo based "blast-wave" particle generator (see Appendix D for a detailed description). Then generated pions and kaons were mixed into pairs, and a theoretical correlation function was constructed with the help of the weight method, described in A.2. These correlation functions were then fitted with the CorrFit program (described in Appendix B), using exactly the same source models, as in the fitting procedure for the data. The simulation and fitting was performed for several bins in pair velocity β_t separately, to study the dependence of the effects on pair total momentum. The results of this procedure, and the comparison to the data is shown on Figs. 7.9, 7.10 and 7.11 for PRFG, CMSG and CMSEH models respectively. The input source separation distributions, as well as the fitted ones are shown on Fig. 7.12.

The most prominent feature seen on the plots is the significant underprediction of the size of the source by the "blast-wave" simulation with given parameters. It leads to significantly smaller σ and μ for all models, compared to the data. The size of the source in "blast-wave" fit is driven by the identical particle correlations, and is fixed for this study. It is however clear, that in order for the blast-wave to agree with non-identical particle correlation data, the parameters R_X and R_Y must be significantly larger. Also introducing larger

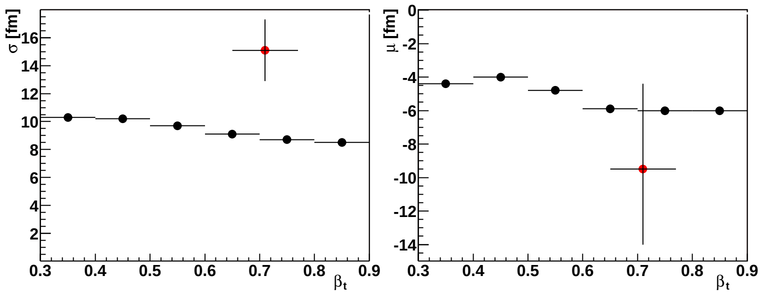

Figure 7.9: Results of "blast-wave" simulation fitted with PRFG model (black points), compared to Year2 STAR data fit results (red point).

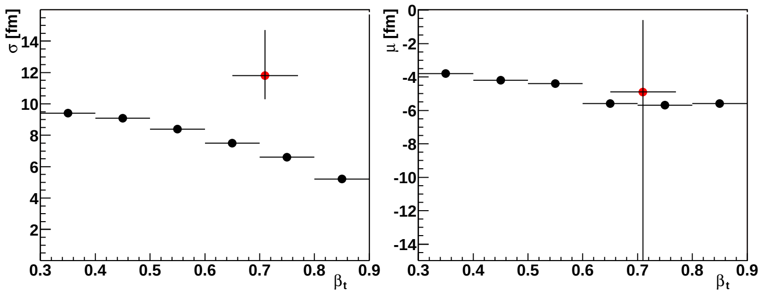

Figure 7.10: Results of "blast-wave" simulation fitted with CMSG model (black points), compared to Year2 STAR data fit results (red point).

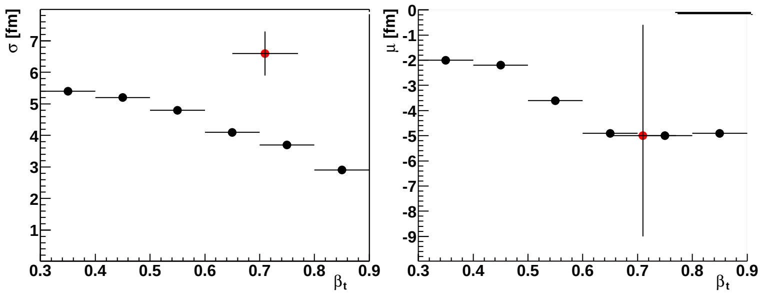

Figure 7.11: Results of "blast-wave" simulation fitted with CMSEH model (black points), compared to Year2 STAR data fit results (red point).

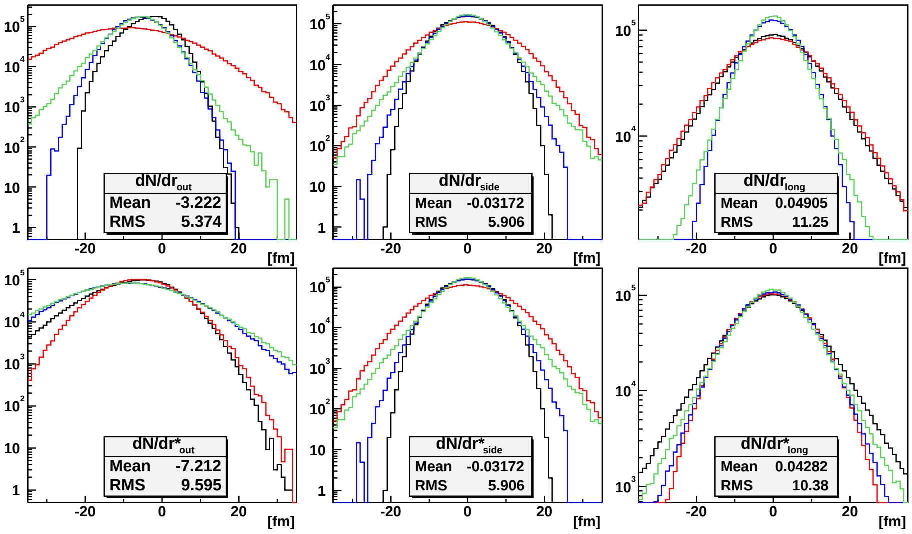

Figure 7.12: The pair separation distributions simulated in "blast-wave" (black lines), are compared to the fitted distributions coming from PRFG(red), CMSG(blue) and CMSEH(green) source models. Upper plots show distributions in the source center-of-mass system (lab-frame), lower plots show distributions in pair rest frame (PRF).

smearing a_s will increase the source size. However both these changes would make the predictions of "blast-wave" inconsistent with pion-pion Bose-Einstein correlation results.

It is also interesting to compare the amount of asymmetry produced by the blast-wave with that obtained from the fit to the data. Because of the significant disagreement of the σ's one cannot compare μ's from the model and data fits directly. However the argument at the beginning of this section showed, that the shift produced in "blast-wave" depends on the flow field ρ, which is linearly scaled with normalized radius $\tilde{r}$ (see Eq. 2.7). Therefore the ratio of μ normalized to σ can be a good measure of the asymmetry coming from flow, and is independent of the absolute value of the radius. Performing simple calculation we get the results shown in Table 7.1. It shows, that while the asymmetry produced in "blast-wave" is in agreement with the one in the data (within errors), it tends to be at the upper limit. This suggests that the asymmetry from flow in blast-wave is strong, possibly too strong, as part of the asymmetry in the data is expected to come from the shift in the average emission times.

A comparison of the fitted distributions to the distributions obtained from "blast-wave" are shown on Fig. 7.12. If a SourceModel would have the same functional form as the real source, the fitting process would produce the source distributions that would match the simulated ones exactly. Therefore by com-

	PRFG	CMSG	CMSEH
Data	$(-0.76, -0.38)$	$(-0.90, -0.40)$	$(-0.61, 0.03)$
"Blast-wave"	-0.69	-0.80	-0.70

Table 7.1: Comparing normalized asymmetry σ/μ between pions and kaons from data and from the "blast-wave" parameterization.

paring modeled and fitted distributions one can judge how well SourceModel functional form represents the one obtained from the model. It can then be used to discuss the strengths and limitations of the SourceModels used. The PRFG model is the simplest - it assumes equal widths of the distributions in *out*, *side* and *long* directions in PRF. However this assumption is also the main limitation. The "blast-wave" produces a source with significantly different RMSes in these directions. Therefore the "best-fit" PRFG distributions are the worst in reproducing dN/dr^*_{side} and dN/dr^*_{long}. In CMS system the PRFG is the worst in reproducing dN/dr_{out} and dN/dr_{side}. As a conclusion one might say that PRFG is probably not adequate for fitting the correlation functions.

The next model used was CMSG. It's functional form was motivated by two factors. The first is that the standard Bose-Einstein two-particle correlations fitting procedure relies on the assumption, that the source is a gaussian in CMS frame. The so called "HBT radii", usually given as the results of the fit are to be interpreted as the gaussian widths of the single-particle space-time distributions. In CMSG, the width σ_{CMS} is the gaussian width of the distribution of the two-particle separation $r^{\pi K}_{out}$:

$$r^{\pi K}_{out} = r^{\pi}_{out} - r^{K}_{out} \tag{7.2}$$

and is connected to the single-particle distributions by a simple relation:

$$\sigma^{\pi K}_{CMS} = \sqrt{(\sigma^{\pi}_{single})^2 + (\sigma^{K}_{single})^2}. \tag{7.3}$$

If single particle r_{out} distributions are gaussians, than the two particle distribution must also be a gaussian. In the fitting procedure we aim to find the SourceModel, that best describes the emitting source. The only source of experimental data that might help in this task are the identical particle Bose-Einstein correlation results (see section 3.1). From there one can get the important information that the source size in *out*, *side* and *long* directions is similar, but not the same. Therefore additional parameters s_{side} and s_{long} can be introduced, that account for this fact. Their values must be constrained by the data, so that we do not introduce additional model dependence. Therefore $s_{side} = R_S/R_O$ and $s_{long} = R_L/R_O$.

The results of the fit are much closer to the model predictions than for PRFG. The features of the dN/dr_{out} and dN/dr_{side} distributions are reproduced. The

dN/dr_{long} distribution is underpredicted, showing that the s_{long} parameter fixed by HBT data is not adequate for the description of the "blast-wave" source distributions.

The last model, CMSEH, uses a different functional form, an exponential hyperbola. It can be seen, that it is more close to the model distributions, especially for the dN/dr_{long} distribution. The strengths of this model are however more prominent when comparing with RQMD predictions, as it aims to reproduce the long exponential tails (coming from particles originating from resonances decaying strongly), which are absent in "blast-wave".

One comment is also necessary to explain the difference of the mean shift between the fit and the model distributions. It comes from the fact, that in "blast-wave" small, but non-zero shift in time between pions and kaons exists, while both CMSG and CMSEH assume it is zero. Therefore the time shift must be added to the space one and the sum will be reflected in the μ fit parameter.

7.2.2 RQMD

The RQMD model was used to simulate AuAu collisions at 200 AGeV and to study the space-time evolution of the source. RQMD, unlike "blast-wave" is a true model - it aims to describe the heavy-ion collision from the initial state up to freeze-out. It is of special interest in studying non-identical particle correlations, as it reproduces features that are believed to be responsible for the emission asymmetries. Through hadronic rescattering it is able to produce radial flow responsible for the spatial asymmetry in the production of pions and kaons. It also describes the creation and propagation of hadronic resonances, which may decay into pions and kaons not necessarily at the beginning of the collision and may be responsible for the difference of average emission times between pions and kaons. The emission times simulated in RQMD are shown on Fig. 7.13. It is clearly seen that pions are, on average, emitted later than kaons, which is not surprising, as there are more hadronic resonances decaying into pions than kaons. The plot clearly shows that the emission asymmetry in RQMD has to come, at least in part, from the shift between mean emission times.

In order to compare results of RQMD simulation and data, a procedure similar to the one used for "blast-wave" calculations was performed. RQMD-simulated correlation functions were constructed with the weight method and fitted with CorrFit. The results are shown on Figs. 7.14, 7.15 and 7.16 for PRFG, CMSG and CMSEH models respectively. The input source separation distributions, as well as the fitted ones are shown on Fig. 7.17.

As in the case of "blast-wave", the size of the source is underpredicted, al-

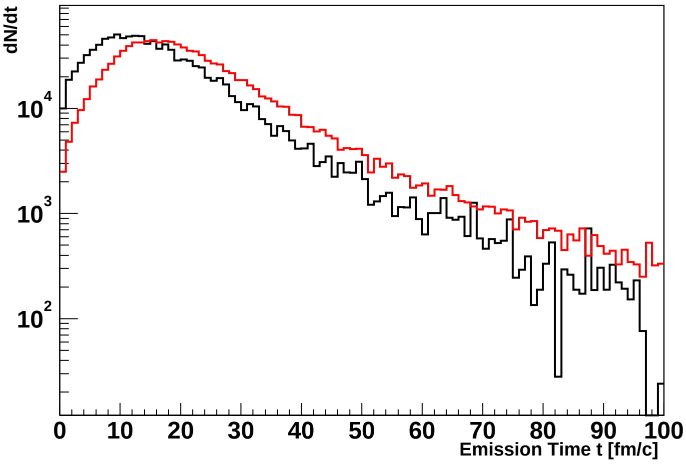

Figure 7.13: Emission time of pions (red) and kaons (black) simulated in RQMD model.

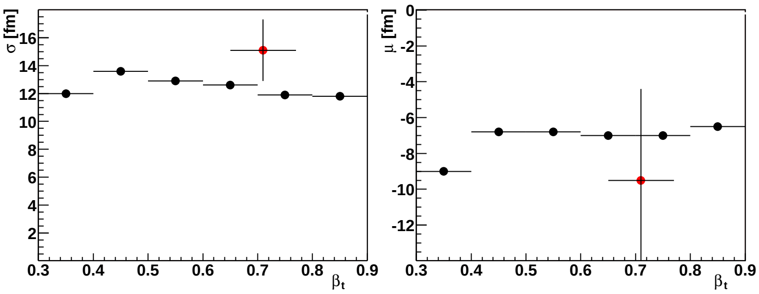

Figure 7.14: Results of RQMD simulation fitted with PRFG model (black points), compared to Year2 STAR data fit results (red point).

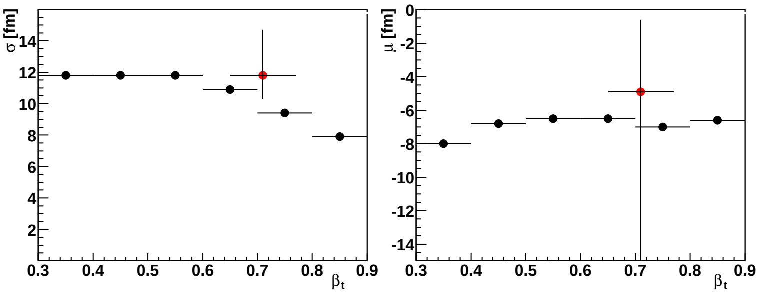

Figure 7.15: Results of RQMD simulation fitted with CMSG model (black points), compared to Year2 STAR data fit results (red point).

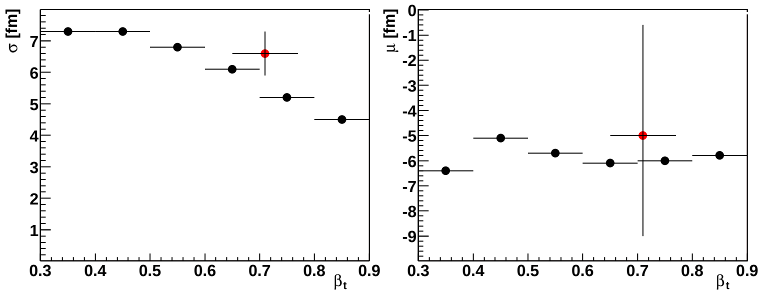

Figure 7.16: Results of RQMD simulation fitted with CMSEH model (black points), compared to Year2 STAR data fit results (red point).

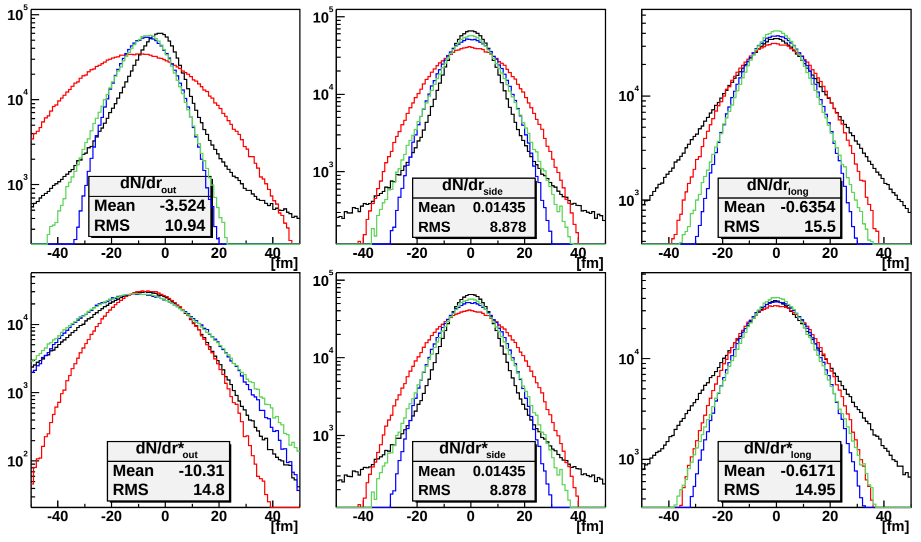

Figure 7.17: The pair separation distributions simulated in RQMD (black lines), are compared to the fitted distributions coming from PRFG(red), CMSG(blue) and CMSEH(green) source models.

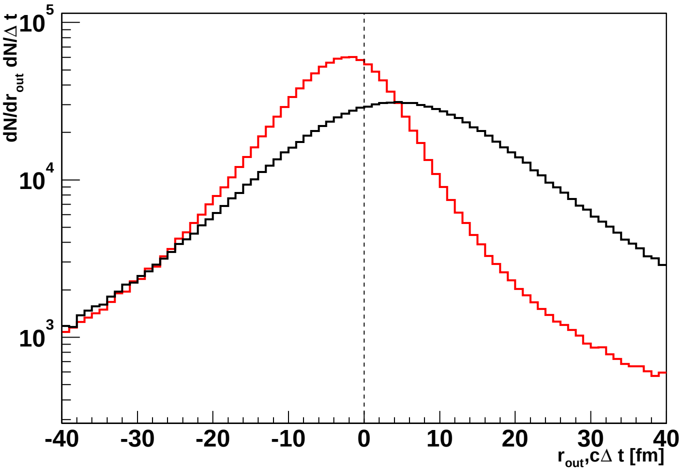

Figure 7.18: The r_{out}(red) and $c\Delta t$(black) distributions from RQMD simulations for pion-kaon pairs.

though to a much smaller degree. The shift between pions and kaons is in agreement with the experimental data, which suggests that in the observed asymmetry both the time and space effects contribute. It can be better seen on Fig. 7.18. Two source distributions are shown on the picture. The red plot shows the r_{out}, that is the distribution of spatial separation between particles in the *out* direction. It is clear that the distribution mean is not at zero. What is more, the distribution is asymmetric - it has larger slope for positive values of r_{out}. These two features were accounted for in the CMSG and CMSEH source models. That means that particle's average emission points are shifted in space - a feature already seen in blast-wave. In the case of RQMD this shift is also attributed to the existence of radial flow. The second distribution is the Δt. Its mean is also shifted from 0, and the distribution is slightly asymmetric. That means that the observed asymmetry r^*_{out} (see Eq. 3.32) will have both time and space components, and they will be contributing with the same sign, enhancing the observed asymmetry.

The discussion of the SourceModel applicability can be also given, similar to the one from the previous section on "blast-wave". It is again apparent that PRFG fails to describe the source distributions from RQMD. CMSG and CMSEH are doing a better job, especially striking is the difference between the two and PRFG for dN/dr^*_{out}. It is clear that the special features of the model - the asymmetry between the slope of the distribution for $r > \langle r_{out} \rangle$ and $r < \langle r_{out} \rangle$ is crucial for better reproducing of the model distribution. The agreement for

dN/dr_{out} and dN/dr_{side} distributions is relatively good, but again the s_{long} parameter value of 1.05 turns out to be too low to reproduce the difference in the RMSes of the *out* and *long* distributions.

The motivation for introducing CMSEH SourceModel is clearly shown in this plot. Long exponential tails exist for all pair separation distributions. CMSEH is better at reproducing them than CMSG, which can be seen e.g. on dN/dr_{long} or dN/dr^{*}_{side} plots. However the tails are even larger than predicted by CMSEH. Their detailed description requires even more complicated functional form. The determination of the detailed form of this function will be a subject of a separate study which will be performed in the future.

Chapter 8

Summary and conclusions

In this work the analysis of non-identical meson-meson correlations performed in the STAR experiment is presented. All systems of charged pion-kaon pairs have been selected. By the simultaneous analysis of all the charge combinations a consistency test has been carried out as well. All the stages of the analysis have been performed and described: the data taking process, methodical data processing, the specific aspects of the non-identical particle analysis, the experimental results as well as the modeling and comparison to theoretical expectations.

In this work the first pion-kaon correlations and emission asymmetry analysis ever performed is presented. It is also one of the first in the of field of asymmetry measurements through non-identical particle correlations. Thanks to the development of this method, a new observable - the space-time emission asymmetry between different particle species is available for study and can enlarge our knowledge of the matter produced in the relativistic heavy-ion collision and its dynamic evolution. It can also serve as an independent check for the predictions of dynamical models, aiming to describe such evolution.

The measurements were performed at the Relativistic Heavy-Ion Collider (RHIC), located in Brookhaven National Laboratory in New York state, USA. The Solenoidal Tracker At RHIC (STAR) detector system was used. The work was performed in the frame of the STAR Collaboration.

The technical part of this work consisted of two distinct elements. The first was the development of the software tools necessary for the analysis. This included both the software used for the processing of the experimental data, as well as the one used in the modeling of the non-identical particle correlations. Also, as a part of the service work for the STAR Collaboration, author developed a database used for storing information about STAR data files. The second part was the development and tuning of the experimental selection criteria, which produce the most reliable and pure correlation function. This included the technique to account for the pair of tracks merged due to the hit merging in the STAR TPC detector as well as elimination of the correlated pairs of misidentified e^+e^- originating from γ conversions. The determination of pair purity, that is the fraction of true primary pions and kaons was also of crucial importance.

The physics part of this work consists of two parts as well. The first was the construction of the correlation functions and "double ratios" for all combinations of pion-kaon pairs from $AuAu$ collisions registered in the first and second year of STAR operation. They enabled a detailed analysis of the source emitting pions and kaons, more specifically its size, the dynamics of its expansion and the ordering of the emission of these particles in time.

The second and final step was the comparison of the experimental results with the predictions of the models aiming to describe the dynamical evolution of the expanding system created in ultra-relativistic heavy-ion collisions. First the data was compared to the results of the "blast-wave" parameterization, which appeared to be successful in describing other features of the collision visible in the STAR data. Then RQMD dynamical model results were also compared, with special emphasis on the emission time of pions and kaons and the possible time shift between those particle species.

The following conclusions can be drawn from this work:

- A deviation from unity of the "double-ratio" in the *out* direction is observed for all combinations of pion-kaon pairs, both from Year1 and Year2 data sample from STAR. The directions of the deviations are self-consistently showing the real physics effect, more specifically, that the average space-time emission points of pions and kaons are not the same, which is a new fact that cannot be observed by any other measurement technique. The data implies that pions are, on the average, emitted from space points closer to the center of the source and/or that they are emitted later.

- The observed asymmetry is qualitatively consistent with the predictions of the "blast-wave" parameterization, meaning that an asymmetry in average space emission points exists between pions and kaons. The origin of this asymmetry can be understood in the frame of the "blast-wave" parameterization as arising from the *space-momentum* correlations produced by the radial flow embedded in this description. This is the most direct measurement of such correlations, as the two-particle correlation technique combines the space and momentum part of the phase-space, while other methods were based on the momentum part only. The space emission asymmetries can be explained by the radial flow hypothesis and the relation between the collective and thermal movement of hot and dense matter created in relativistic heavy-ion collisions. It is an independent information, enlarging our knowledge about these effects.

- The RQMD model, with its complete treatment of hadronic resonance states, was used to study the effect of time delays in emission of pions and kaons. It was found that the difference in the mean emission time indeed exists and does contribute to the observed emission asymmetry. However the predicted magnitude of the asymmetry is consistent with the experimental results only if both space and time asymmetry is considered. Therefore a conclusion can be drawn that both space and time components are present in the observed emission asymmetry between pions and kaons.
- The quantitative comparison of source sizes and emission asymmetries between experimental data and models was also made. A discrepancy in the predicted size of the system was observed, which is not fully understood yet, and will be a subject of further studies. Also model calculations disfavor the fully gaussian source parameterizations.
- The generic fitting procedure developed in this work enables to test new, non-symmetric, non-gaussian source parameterizations in order to resolve the observed discrepancies. One of such parameterizations was proposed and tested in this work and found to better describe the correlation function than the traditional one.

The results presented in this work are a new, independent, quantitative observable that need to be considered by models aiming to reproduce spatial and temporal characteristics of the source in a consistent way. The presented analysis techniques and results obtained show, that the STAR detector is ideally suited to study the non-identical particle correlations. The work performed and the developed tools open a new possibility to study particle correlations in STAR as the analysis technique can be used in the future studies.

Considering the possibilities of future analysis, the emission asymmetries and source sizes can be measured as a function of centrality to search for the onset of radial flow. Different particle species can be studied: pion-proton and kaon-proton correlations can provide the complete picture of the emission process of the most abundant particles, while pion-Ξ correlations can possibly answer the question about a collective behavior of multiply-strange barions. New detectors in STAR (more specifically the TOF - Time Of Flight) will enable the analysis of correlations as a function of pair velocity, which will provide a way to study the flow profile in more detail. Other data samples, more specifically pp and dAu collisions can also be analyzed, giving the insight into the jet structure and to answer the question if the flow is already present in such elementary processes.

Appendix A

Correlation analysis software - StHbtMaker

A.1 General overview

StHbtMaker is a part of the analysis software of the STAR experiment. It was designed and implemented to perform analysis of two-particle close-velocity correlations. It is integrated with the rest of STAR off-line software caller root4star[96]. It is based on the ROOT framework[95] and is almost entirely written in the C++ programming language.

The short description of the analysis process follows. It is an implementation of the experimental function definition shown in Chapter 3. The analysis of the correlation functions is managed by the class StHbtManger. It has a link to a StHbtReader class, which is responsible for reading events from mass storage. StHbtManager can manage multiple analyses, which are performed by instances of the StHbtAnalysis class. Each StHbtAnalysis has links to the following classes:

- StHbtEventCut - a class that is responsible for accepting the events read by StHbtReader. Each event is evaluated, based on specific criteria, e.g. the centrality or the z-position of the primary vertex and a decision is made to accept or reject it. Only particles from accepted events are used in the rest of the analysis.
- StHbtParticleCut - in case of identical particle correlations one instance of this cut is used, in case of non-identical particle correlations - two. This cut is responsible for accepting or rejecting each particle in a given event. The decision can be made based on any particle characteristic - either a

"physical" one (e.g. rapidity, transverse momentum or particle type), or detector one (e.g. number of hits produced in the TPC).

- StHbtPairCut - each particle pair is evaluated and accepted or rejected by this class. The pair-wise characteristics considered may include: pair opening angle, possibility to be an electron-positron pair, possibility that the pair is merged etc.
- StHbtCorrFctn - stores accepted pairs in the numerator and the denominator for "real" and "mixed" pairs respectively. At the end of the analysis, numerator and denominator are divided to obtain the correlation function, which is then correctly normalized. Other uses of "real" and "mixed" pairs are also possible, an example is described in the next section.

It is important to note, that StHbtReader, StHbtAnalysis, StHbtEventCut, StHbtParticleCut, StHbtPairCut and StHbtCorrFctn are all abstract base classes. The actual classes used in the analysis derive from them. This design concept allows for easy scalability and extendibility of the code. The description of the cut classes and the cuts used in this analysis is in Chapter 5. As an addition, so called CutMonitors can be attached to each of the cuts. It stores separately the relevant characteristics of the objects that passed and failed the cut. They are very useful in developing and tuning the experimental cuts. They also provide important physical information, e.g. multiplicities of events used in the analysis, of dE/dx vs. p dependence for accepted and rejected particles.

The flow of the data in StHbtMaker is as follows. The event is read by StHbtReader. It is then passed by StHbtManager to all the instances of StHbtAnalysis. In each of them, StHbtEventCut decides whether to accept or reject a given event. Particles from accepted events are then passed to the StHbtParticleCuts. Accepted particles are stored in a one (two) collection for identical (non-identical) particle analysis. Then particles from the same events are mixed together into "real" pairs and passed to StHbtPairCut. If accepted they are sent to multiple StHbtCorrelationFunctions. After all pairs are processed the event is stored in the mixing buffer. If enough events are in such a buffer - particles are combined into "mixed" pairs - that is one particle is taken from the current event and another is taken from the event in the mixing buffer. Such pair needs to pass through StHbtPairCut as well, and is then stored in the StHbt-CorrelationFunction. When all events are processed, the final calculations (e.g. normalization of correlation functions) is done, the results are saved and the process ends.

A.2 Theoretical classes and Lednicky's weight calculator

The original function of StHbtMaker was to allow for the analysis of the STAR experimental correlation functions. As the analyses progressed a need arisen for the software which can be used within STAR framework to simulate particle correlations. The open design of StHbtMaker allowed for easy integration of the theoretical part of the code with the already existing experimental part. This section gives a short description of the theoretical classes of StHbtMaker.

The main purpose in writing the theoretical classes for StHbtMaker was to enable the use of the pair weight calculator from Richard Lednicky. It is the same calculator as the one which is used in the CorrFit software (see Appendix B). Its theoretical basis is described in section 3.2. The weight technique requires a few conceptual changes in treatment of the correlation functions:

- To calculate the weight, the freeze-out point of each particle needs to be known. It can be obtained from a model calculation or it can be randomly generated from a predefined distribution. More importantly there must be a way to store this position for later use - there is no such possibility in a standard StHbtParticle class.
- In the weight formalism, the correlation function is generated slightly differently than in normal case: only "mixed" pairs are used. The numerator is created by binning the weight of each pair in the corresponding k^* bin, while in the denominator each pair has weight equal to 1.0.
- In the theoretical case, when one uses e.g. the data simulated by a model there is a possibility that two momenta are known for each particle - that the "real" momentum given by the model and the "reconstructed" one, which is obtained from the reconstruction software. It is desirable to store both momenta, which allows for the study of momentum resolution and its influence on the correlation functions.

The differences described above have been taken into account when designing the theoretical classes of StHbtMaker. As a result, the following decisions have been made:

- To create the StHbtHiddenInfo class, which is referenced by the StHbtParticle. This class can store arbitrary additional information, but is usually used to store particle freeze-out coordinate, particle real momentum and particle true type (PID). The convention was adopted that StHbtParticle itself always stores the particle reconstructed momentum. The creation of StHbtHiddenInfo requires several other additions. StHbtReaders which are aware of StHbtHiddenInfo and are able to fill it with data obtained from model calculations need to be created. Also, in case when freeze-out coordinates are not available, they need to be generated for each particle randomly - usually it is done by a specialized StHbtThPair class.

- To create the StHbtThPair class, which is the adaptation of StHbtPair class for theoretical purposes. It is aware of StHbtHiddenInfo's of particles, can calculate all the usual pair characteristics (like relative momentum, pair momentum, decomposition to *out*, *side*, *long* etc.) for both "real" and "reconstructed" momenta. It can also generate StHbtHiddenInfo when needed.
- To create the StHbtFsiLednicky class - a C++ wrapper of the Fortran weight generation code from Richard Lednicky. It serves only one, well defined function - given pair momenta p_1 and p_2 as well as pair freeze-out coordinates x_1, x_2 it returns the pair weight. All the flexibility of the Fortran code is retained - the possibility to independently switch on/off each of the interactions (strong, Coulomb and quantum statistics) and to calculate weights for any system. StHbtThPair class is the one that manages the weight calculation.
- The creation of StHbtThCorrFctn classes, that properly create theoretical correlation functions with the use of mixed pairs and pair weights. They are also aware of particle's "real" and "reconstructed" momenta and can be used to create and compare correlation functions with and without the momentum resolution distortion.

The theoretical calculation is managed by the StHbtThManager class. It has a link to the instance of the StHbtThPair class, as well as the theoretical correlation functions. In the standard scheme of StHbtMaker is a class derived from StHbtCorrFctn and is used as one.

There are two most common cases in which theoretical classes are used. First is the simulation of the correlation function from a model, which provides freeze-out coordinates of particles, but does not simulate the Bose-Einstein/Fermi-Dirac, nor the FSI correlations. Examples are the RQMD model (see section 2.4.1) and the blast-wave parameterization (see section 2.4.2). The correlation functions presented in Chapter 7 were obtained in this manner. Below the creation of the RQMD correlation function is described as an example.

The first component is the StHbtReader for RQMD output files. A specialized class derived from StHbtEventReader: KaiRqmdReader has been developed to read RQMD output file 13 and convert it into StHbtEvent and StHbt-

Particles. At the same time the reader reads in the freeze-out coordinates of each particle and stores them into StHbtEvtGenHiddenInfo class instance. Also StHbtManager is instantiated. It has a link to StHbtEvtGenPair instance - a class derived from StHbtThPair. The pair maintains it's own copy of StHbtFsiLednickyWeight, with the correct parameters of the interaction set. Then the event goes through a normal procedure of event, particle and pair cuts. The real and mixed pairs are then sent to the StHbtThManager. It passes the mixed pairs to the StHbtEvtGenPair, which calculates their weights, and then send the information to the ThNonId3DCF - a theoretical correlation function derived from StHbtThCorrFctn, written especially for non-identical particle analysis. One more theoretical specialized correlation function is used - the PosCorrFctnUt. It is aware of particle HiddenInfo and can use it to store various space-time and momentum source characteristics. Examples of them are shown in Chapter 7. As a result, a theoretical correlation function is calculated. It is equivalent to the correlation function which would be produced by RQMD, if quantum statistics and FSI effect were implemented in it. The function can be treated in exactly the same way as an experimental one, e.g. it can be fitted by CorrFit (see Appendix B).

A second common use of the theoretical classes is the simulation of a single theoretical function when no freeze-out information is available. In this case a normal reader can be used. HiddenInfo must be created later - usually by a specialized derivative of the StHbtThPair class, such as StHbtThPairDoubleGaus. This class assumes a source is a 3-dimensional sphere with a Gaussian density profile.The StHbtThManager and StHbtFsiLednicky is set up in the same way as in previous case. Then for each pair passed to StHbtThPairDoubleGaus the class checks each particle. If it does not have a HiddenInfo yet, it is generated, which the freeze-out position randomly assigned from the described distribution. Then the weight generation and correlation function construction can proceed as in the previous case. This use of theoretical classes may have one more important application. The StHbtThPairDoubleGauss class can also generate "real" particle momenta and store them in the HiddenInfo. It is done with the help of a StHbtMomRes class. Given the particle measured momentum, and a parameterization of STAR TPC momentum resolution (see section 4.2.1) an approximation of the particle "real" momentum is obtained by smearing the measured one. Then the weight is calculated according to "real" momentum, but it is stored in the correlation function according to the measured one. By switching on and off the smearing procedure, two correlation functions can be produced, with and without the momentum resolution effect. They can later be compared and an estimate of the momentum resolution effect on the correlation function can be obtained.

Appendix B

CorrFit - fitting correlation functions

In order to extract the information from two-particle close-velocity correlation functions, a fitting procedure must be applied. In this chapter the software "`CorrFit`" is described. Its main purpose is to provide a way to fit arbitrary two-particle correlation functions, using a complete knowledge of the interaction potential for a given system.

In a traditional HBT measurement the quantitative information of the source is obtained under several assumptions, states in chapter 3.1. The correlation function fitted must contain only Bose-Einstein or Fermi-Dirac correlations, all the FSI must be corrected out. The source sizes r_{out}, r_{side} and r_{long} can only be obtained if a 3-dimensional Gaussian form of the source is assumed (for details see section 3.1.2.3). In the case of non-identical particle correlations both of these assumptions are not valid. The FSI cannot be treated as a correction, as is is the source of the correlation itself (see section 3.2). Also if one wants to measure emission asymmetries, which are the effect of source dynamics, a static 3-dimensional Gaussian centered at zero cannot be assumed as a model of the source. Therefore a new method of fitting correlation functions was needed.

The `CorrFit` program has been originally created in order to fit non-identical particle (pion-kaon) correlation functions obtained in the STAR experiment[93]. It was necessary to develop a program, which would use the full information of the interaction potential (both coulomb and strong interaction, as well as quantum statistics for identical pairs) and an arbitrary source model. The "best-fit" correlation function is found through the minimumχ^2 method. The program was later extended to allow for fitting of the correlation of any system, including identical particle HBT. Special care was also taken to create the program in an modular and extensible way and to make user-friendly in order for it to be useful for the community.

B.1 Physics concept

The concept of fitting the arbitrary correlation function comes from the formulation in the Eq. 3.67. It shows that the correlation function can be described as simply the *average pair weight* W, where the weight is the squared two-particle amplitude, which includes, in its most general form, the quantum statistics for identical particles, Coulomb interaction for charged particles, and strong interaction for hadrons. This concept significantly simplifies the problem, as one does not need to treat the correlation function as a whole, or perform analytic integrals. Instead one deals with two-particle interaction on a pair-by-pair basis. For the calculation of W, the relative distance of emission points (also called initial separation) $\vec{r^*}$ and pair relative momentum $\vec{k}^*$ is needed. Knowing them, and the type of the pair, which makes 8 independent values, is sufficient to calculate W. However the ultimate goal of the fitting process is not to study two-particle interaction in the pair rest frame, but to study the source emitting these particles. Therefore the full information about the two particles, that is their momenta $\vec{p_1}$ and $\vec{p_2}$ as well as their emission points $\vec{x_1}$ and $\vec{x_2}$, which makes 16 independent values, needs to be used.

One now has to consider the way to perform the averaging in Eq. 3.67. In the ideal case, one would like to reproduce exactly the two-particle momentum distribution and freeze-out configuration of all the pairs, which created the correlation function. This is of course not possible. Instead one can perform a stochastic procedure, equivalent to Monte-Carlo numerical integration, which will be now described. The best estimate available of the real momentum distribution is the momentum distribution measured by the experiment. Therefore one can simply use the momenta of the pairs, that were used to construct the background of the fitted correlation function (see chapter 6). Then one selects the parameterization of freeze-out, that will be used to fit the correlation function. This can be as simple as a 3-dimensional Gaussian used in regular HBT, or as complicated as the parameterization of the RMQD model output. The freeze-out coordinates of the particles is generated, using the Monte-Carlo method, using this parameterization as the probability density. Now the weight W can be calculated for each pair. Iterating the procedure for as many pairs as needed (the number is practically limited only by the available computing power and operating memory) the theoretical correlation function, for a given source parameterization, is calculated. The χ^2 test determines how well it describes the fitted (experimental) correlation function. One can change the parameters of the source parameterization and perform the procedure many times, searching for the parameters that produce the theoretical correlation function that best describes the experimental one. In this way the fitting of arbitrary two-particle correlation functions is possible. What is also important, the arbitrary source model can be used.

B.2 Software design specifications

The following requirements have been considered when designing the CorrFit software:

- Using the full knowledge of particle interaction in the form of "weight calculators". Possibility to use interchangeably multiple calculators. Possibility to add new calculators.
- Use of arbitrary source models, describing the emitting source. Each source model needs to be parametrized. Possibility to use models with any number of parameters. Easy addition of the new source models by the end user.
- Use of arbitrary correlation function types (1-dimensional, 3-dimensional, "double-ratios"). Possibility to add new correlation function types.
- Only data normally available in the experiment should be used in the fitting procedure - that is the correlation functions and the pair momentum distribution.
- Program execution is controlled by the parameter file, which is automatically generated. The end user only needs to fill the data relevant to his analysis.

The program would be distributed in the source form, available for use and extendibility by anyone.

B.3 Implementation

The program was designed to be fully object-oriented. It is written in C++ language, with the use of classes and file formats from the ROOT package[95].

B.3.1 Algorithm description

The program starts by reading the parameter file. If it does not exists, it is automatically created for the user, which then needs to supply the necessary

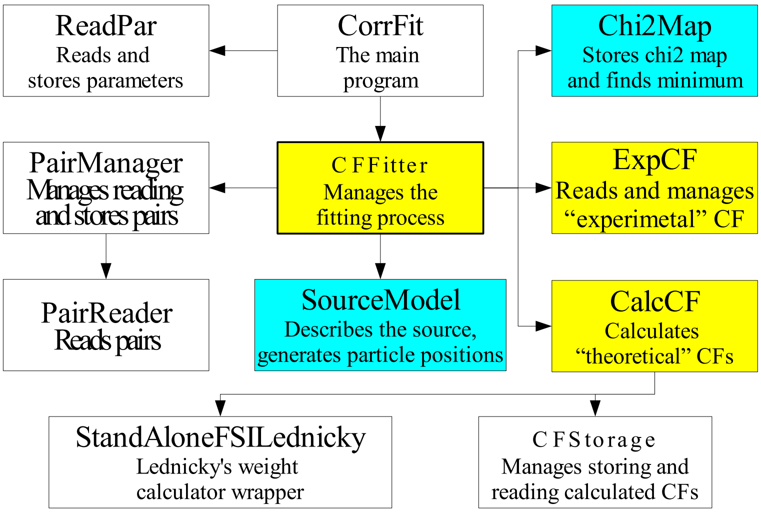

Figure B.1: Functional diagram of the CorrFit classes

values. Then the input data is read - the experimental correlations functions (ECF) and the pairs. Also the source model (SM) and the range of its parameters is determined. A χ^2 map (C2M) is then created, with model parameters on the axes. The map has as many dimensions, as there are parameters of the SM. Then the program progresses through all of the C2M bins sequentially. In each of them, the following actions are carried out. First the SM parameters are read from the axes of C2M, and set. For each pair, the momenta is read from the pair input file, the position is generated by the SM, according to the current parameters, and a pair amplitude squared (called "a weight") for such a pair is calculated. The Calculated Correlation Function (CCF) is constructed as the average of these weights in each k^* bin. At the end a χ^2 value for a given bin is calculated by comparing the ECF and the CCF. When the whole map is filled in this way, the minimum of the map is sought, and the the values of the parameters, which produced the bin with lowest χ^2 value are taken as the "best fit".

In the current version of the program, after the first, coarse map is done, a second map, centered in the minimum of the coarse map, smaller but also with smaller bin width, is filled in the same way to get the "best-fit" parameters with better accuracy.

B.3.2 Main classes

The main building classes of the "`CorrFit`" program are shown on Fig. B.1. The CFFitter class manages the whole fitting process. It initiates the procedure of pair reading (through `PairManager` class), manages the C2M filling (through `Chi2Map` class) and has the knowledge of the ECFs and CCFs used in current analysis. The `CFFitter` is an abstract base class, with the actual fitter classes inheriting from it. In principle each type of correlation function class needs its own fitter. At the time of this writing fitters where written for:

1. `CFFitter1DHBT` - 1D identical particle correlation functions
2. `CFFitterNonId` - 1D non-identical correlation functions with double ratios
3. `CFFitterNonIdMult` - several 1D non-identical correlation functions with double ratios fitted at the same time with the same model

Each of these fitters can have (and usually has) a separate ECF and CCF class.

The ECF class `ExpCF` handles reading and storing of the experimental correlation function. It also takes care of momentum resolution and purity corrections. `ExpCF` is an abstract base class, each CF type requires its own ECF class.

The CCF class `CalcCF` handles calculation of the theoretical correlation functions. It manages the weight generator, which calculates the weights for pairs. It is also possible (through `CFStorage` class) to store and retrieve previously calculated CFs with the specific SM and SM parameter values. `CalcCF` is also an abstract base class; each CF type requires its own CCF class.

The weight calculator (WF) takes as an input pair momenta (p_1, p_2) and freeze-out coordinates (x_1, x_2), as well as particle types, then calculates the squared pair amplitude (a weight) for this pair. At the time of this writing two WFs were implemented - one based on Fortran code by Richard Lednicky, the other based on the code provided by Scott Pratt.

The SM class `SourceModel` is responsible for providing the freeze-out coordinates (x_1, x_2) for the pair, given its momenta (p_1, p_2). The `SourceModel` is an abstract base class, the real models should be built on top of it. The SM can have any form - from a simple gaussian distribution to the parameterization of complex physics models. This class is the most important from the physics point of view, as it includes the description of the emitting source necessary for the interpretation of the fit results. New SM classes can be trivially added by the end user. At the time of this writing several SMs were implemented, the most important are:

1. `SourceModelGaus` - the source is assumed to be a 3-dimensional sphere with Gaussian profile. In the most general form it can have different parameters (r_x, r_y, r_z and τ) for each particle. No source dynamics is assumed.

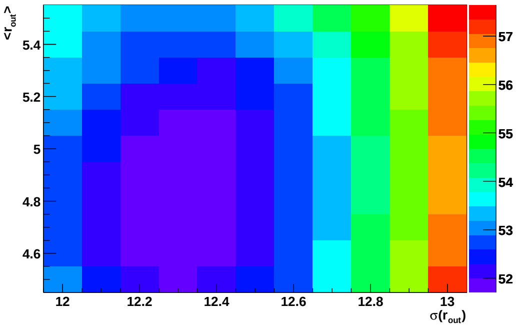

Figure B.2: An example of a χ^2map produced by CorrFit

2. `SourceModelGausCMS` - the source model is assumed to be a 3-dimensional gaussian in lab frame. The variable described by a Gaussian is an initial pair separation $\vec{r}$ in the lab frame (or source frame), not the independent, single particle emission points. The parameters of the source are: the size in the *out* direction r_{out}, mean shift in the *out* direction μ_{out}, size in the *side* direction (used as a multiplier of r_{out}) s_{side}, s_{long} and s_{time}.

3. `SourceModelGausROut` - the model originally used to fit pion-kaon correlation function in [93]. It assumes the source is a 3-dimensional sphere with gaussian profile in pair rest frame (PRF). The parameters of the model are: the size of the source r^* and mean shift in the *out* direction μ_{out}.

4. `SourceModelCMSHyper` - the source is assumed to be described by a 3-dimensional exponential hyperbola (see Appendix E) in the source rest frame. The parameters are: the size of the source in the *out* direction σ_{out}, the mean shift in the *out* direction μ_{out}, and s_{side}, s_{long} and s_{time}, similar to `SourceModelGausCMS`. The α parameters in all directions were fixed to 2.0.

Two `CFStorage` classes are also implemented - `CFStorage` stores the calculated correlation functions stores CCFs in the ROOT file, while `CFStorageMySQL` stores CCFs in a MySQL database, allowing for the significant parallelization of the calculations.

B.4 Program output - examples

The CorrFit program produces several results. It outputs the "best fit" parameters for the given fit run. It stores the C2M's it produced during it's run. An example of such a map is shown on Fig. 4.9. The axes of the map are the

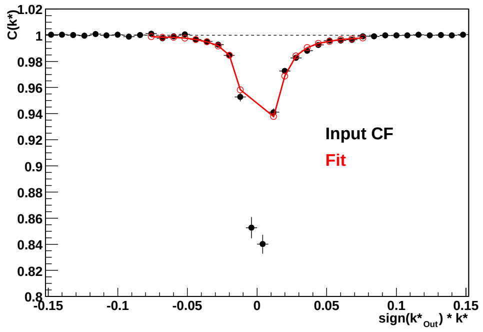

Figure B.3: Comparison of the experimental (input) and theoretical (fitted) correlation functions

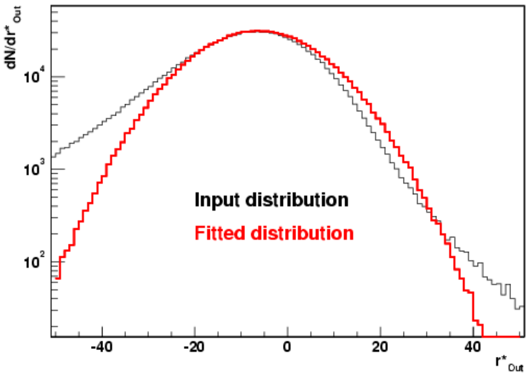

Figure B.4: A comparison of input and fitted source distributions

parameters of the model (in this case a sigma and mean of a gaussian in r_{out} variable). The value in each cell is the χ^2 value between the fitted ECF, and the CCF generated with a given SM parameter values. Such a map can be later used to judge the quality of the fit, as well as to determine the systematic error. The program also generates a "best fit" correlation function which can be directly compared to the experimental one. An example of such comparison is shown on Fig. B.3.

The output of the program can be easily extended. For example for theoretical model studies in might be desirable to compare the theoretical source distributions with the fitted one. In this case the CorrFit program can save the source distribution it generated through the SM class. An example of such comparison for RQMD study is shown on Fig. B.4. This plot can be used to judge how well the assumed SM describes the actual source distribution.

B.5 Summary

A stable, fully functional version of the CorrFit software exists and can perform the basic tasks of fitting an arbitrary correlation function with an arbitrary source model, although many improvements to the software will be made in the future. At the moment it is the only method to obtain quantitative information from non-identical particles correlations.

Appendix C

Managing large sets of data files - file Catalog database

This documents describes briefly the FileCatalog database and the PERL module "FileCatalog" which can be used to access and manipulate data in this database.

C.1 The database

The diagram C.1 shows the structure of the database. It contains a number of “dictionary” tables - the ones that do not reference any other tables and usually hold only one useful field. They are: FileTypes, StorageTypes, StorageSites, ProductionConditions, TriggerWords, TriggerSetups and RunTypes.

There are also special tables:

- EventGenerators - holding the data about various Event Generators and their simulation parameters.
- SimulationParams - parameters pertaining to the specific simulation run.
- CollisionTypes - the type of particles colliding and their energy. Holds also special values like "cosmic" etc..
- DetectorConfiguration - holds a detector configuration used to collect specific data. For simulation it holds the geometry version used.
- TriggerCompositions - holds data about the number of events collected with a specific TriggerWord, that are included in a given file.

These are also three main tables holding data about the files and run parameters, and binding all the other tables together.

- RunParams - parameters of a single physics run. Each run is identified by its run number.
- FileData - data about a specific file, without any information about its physical location. Each file is identified by a combination of a file name, file type, file sequence, production conditions and the run number it is connected to. File Data can be connected to a run number it comes from.
- FileLocation - data describing a specific file location and its physical storage - the file path, the owner, protection etc.

In general the database is supposed to be hidden from the user. It is to be modified only through the PERL module and the corresponding functions. Manual changes to the database should not, in principle, be necessary.

C.2 The "FileCatalog" PERL module

The FileCatalog perl module is intended to provide access to the database both for data querying and retrieval as well as data insertion and modification.

It is completely based on the concept of keywords and context. The user first sets the context variables to a desired value, and then uses special commands to get/insert/delete/modify data in the database based on current context. The context consists of keywords eg. "filename", "path", "storage" that may have values assigned to them. If a keyword has a value assigned to it, e.g. by issuing a command set_context("site = HPSS"), we say it is set to this value. The current context is a combination of all the keywords set.

The following subroutines are available in the FileCatalog module:

- new(): create new object FileCatalog, on which all the following operations would be carried out. It is necessary to issue this command before any other operation with the module can be carried out.
- connect() : connect to the database FilaCatalog
- destroy() : destroy object and disconnect from the database FileCatalog
- set_context() : set one of the context keywords to the given operator and value
- get_context() : get a context value connected to a given keyword

The following methods require a connection to the database and are meant to be used outside the module First the methods of everyday use:

- insert_file_location() : after setting the whole context this method inserts the file location record. If it doesn't find the corresponding file data or run parameters it insert the necessary information into the database as well. It also ensures data integrity and refuses to insert a record if some critical data was not specified in the context.
- run_query() : get the data from the database. As a parameter to this procedure user gives a list of keywords - the returned data is an array of strings. Each string corresponds to one record in the database. The string consists of all the fields corresponding to the list of keywords concatenated by "::"

This subroutines are database specific, and should be used rarely and only if necessary.

- check_ID_for_params() : returns the database row ID from the dictionary table connected to this keyword
- insert_dictionary_value() : inserts the value from the context into the dictionary table
- insert_detector_configuration() : inserts the detector configuration from current context
- get_current_detector_configuration() : gets the ID of a detector configuration described by the current context
- insert_run_param_info() : insert the run param record taking data from the current context
- get_current_run_param() : get the ID of a run params corresponding to the current context
- insert_file_data() : inserts file data record taking data from the current context
- get_current_file_data() : gets the ID of a file data corresponding to the current context
- insert_simulation_params() : insert the simulation parameters taking data from the current context
- get_current_simulation_params : gets the ID of a simulation params corresponding to the current context
- delete_record() : deletes the current file location. If it finds that the current file data has no file locations left, it deletes it too.

- update_record() : modifies the data in the database. The field corresponding to the given keyword changes it value from the one in the current context to the one specified as an argument
- bootstrap() : database maintenance procedure. Looks at the dictionary table and find all the records that are not referenced by the child table. It offers an option of deleting this records.

Here are the keywords that can be used in the context:

- filetype - The type of the file, eg. "daq", "MC" etc.
- extension - The extension of the file - directly connected to type (each file type has an associated extension)
- storage - The storage medium, eg. HPSS, NFS, local disk
- site - The site where the data is stored, eg. BNL, LBL
- production - The production tag with which a given file was produced. Can also be "raw" or "sim"
- library - The library version this file was produced with
- triggername - The name of the trigger
- triggerword - The triggerword itself
- triggersetup - The name of the triggersetup - for real data each triggersetup is a collection of triggerwords
- runtype - the type of the run - eg. "physics", "laser" and also "simulation" for simulated datasets
- configuration - The detector configuration name. A detector configuration is a combination of detectors that were present during data taking in a given run.
- geometry - The geometry definition for a given simulation set.
- runnumber - The number of the run. Arbitrary for simulations.
- runcomments - The comments for a given run.
- collision - The collision type. Specified in the form of <first particle><second particle><collision energy>, e.g. “AuAu200”
- datetaken - The date the data was taken. Arbitrary for simulation.

- magscale - The name of the magnetic field scale, e.g. FullField
- magvalue - The actual magnetic field value
- filename - The name of the data file
- size - The size of the data file
- fileseq - The file sequence as determined during data taking by DAQ. Arbitrary for simulation and processed files.
- filecomment - The comment to the file.
- owner - The owner of the file.
- protection - The protection or read/write permissions, given in a format similar to UNIX 'ls -l'
- node - The name of the node where data is stored (mostly useful with "local disk" storage)
- available - is the file available?
- persistent - is the file persistent?
- createtime - the time a file was created
- inserttime - the time a file data was inserted into the database
- path - the path to a specific copy of the file
- simcomment - The comments for the simulation
- generator - The event generator name
- genversion - Event generator version
- gencomment - Event generator comments
- genparams - Event generator params
- tpc - was the TPC in the datastream when specific data was taken?
- svt - was the SVT in the datastream when specific data was taken?
- tof - was the TOF in the datastream when specific data was taken?
- emc - was the EMC in the datastream when specific data was taken?
- fpd - was the FPD in the datastream when specific data was taken?

- ftpc - was the FTPC in the datastream when specific data was taken?
- pmd - was the PMD in the datastream when specific data was taken?
- rich - was the RICH in the datastream when specific data was taken?
- ssd - was the SSD in the datastream when specific data was taken?
- triggerevents - *SPECIAL.* This keyword is a shortcut for adding a collection of triggerwords and number of events to one file. It can be used for data insertion only. It is specified in the form of <triggerword> <number of events> [; <triggerword> <number of events>]. E.g. "triggerevents = central 77; minbias = 65; laser = 1000", means that a given file contains 77 events recorded with central trigger, 65 with minbias trigger and 1000 with a laser trigger.
- events - Number of events in the file for a given triggerword.

Here are the keywords not connected to a specific field in the database. They change the behavior of the module itself.

- simulation - Is the data a simulation?
- nounique - Should the module return all fields, instead of only unique fields?
- noround - Turns off rounding of magfield, and collision energy.
- startrecord - The PERL module will skip the first startrecord records and start returning data beginning from the next one.
- limit - The PERL module will return the maximum of limit records.

C.3 The command line utility to access the FileCatalog database

Below the description of the command line utility to access data in the FileCatalog database is given. The utility is called get_file_list.pl. If issued without any arguments it will print the following usage message:

```
   get_file_list.pl [-all] [-distinct] -keys field{,field} [-cond field=value{,field=value
[-start <start record number>] [-limit <number of output records>]
[-delim <string>] [-onefile]
```

The parameters to the command are described below:

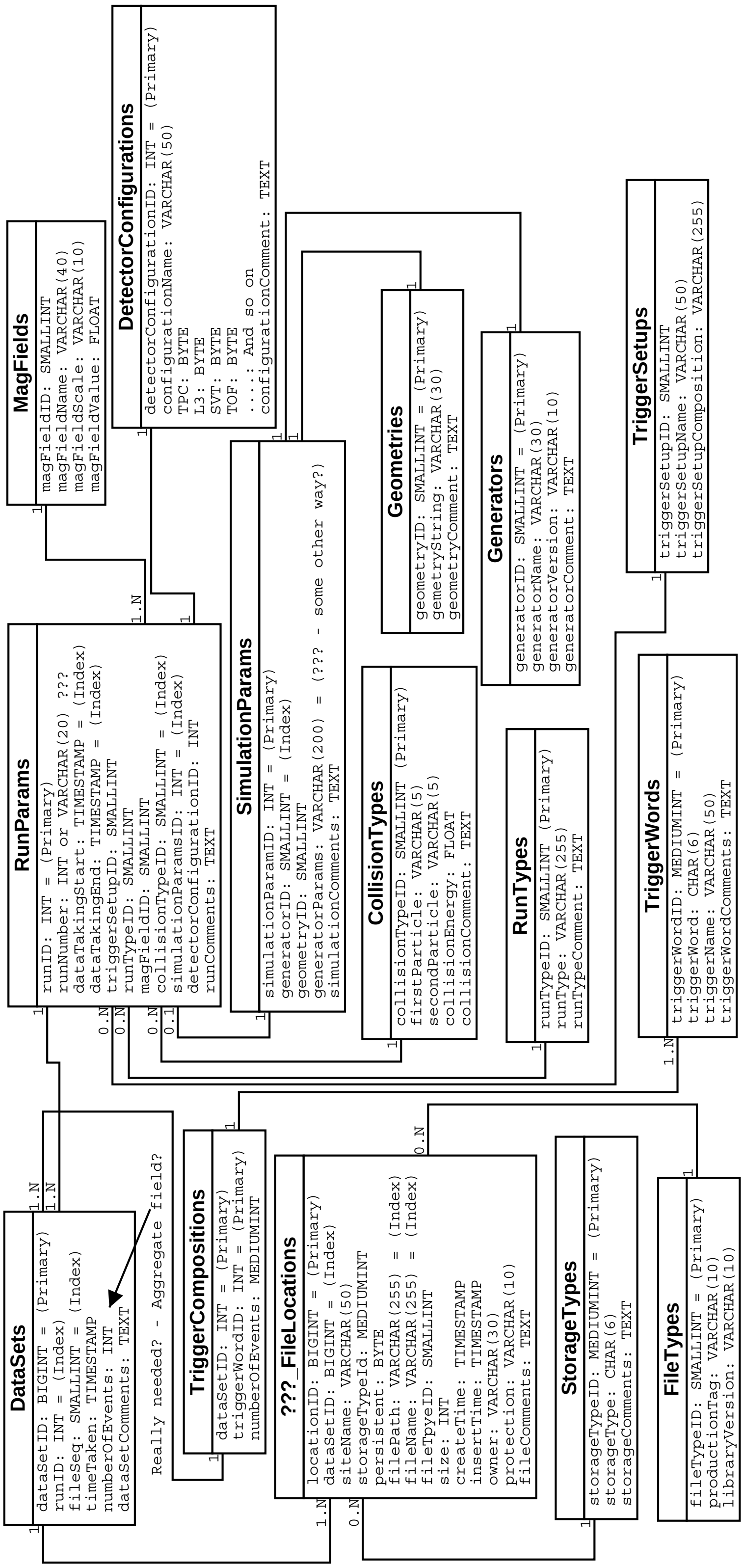

Figure C.1: The structure of the FileCatalog database

- -all: If -all is not specified only available files (with availability > 0) are returned.
- -distinct: return only distinct rows - the default setting (no repetitions)
- -keys: Specify what data You want to get from the database. A list of valid keywords, separated by colons should follow this parameter. See section C.2 for the list of all keywords. See also the description of aggregate functions below for some more sophisticated tricks.
- -cond: Specify the conditions limiting returned dataset. A list of valid expressions (consisting of a valid keyword, a valid operator and a value), separated by colons should follow this parameter. Since some of the operators are special characters, the list of expressions should always be enclosed in single quotes.
- -onefile: A special mode of operation; returns a list of files, but gives only one location (the one with highest persistence) for each file, even if the database has many.
- -start: specify the number of the record to start from. The default is to start with the first record (together with -limit can be used to get the data in chunks)
- -limit: limit the number of records returned (default 100).
- -delim: specify the characters that will separate the fields in the output (default: “::”)

C.3.1 The aggregate functions that can be used in the PERL module and the command line interface

These are special aggregate functions. They can be used in conjunction with any keyword that describes some data. Note that most of them only make sense for numerical values.

- sum: The sum of the values
- avg: The average of the values
- min: The minimum of the values
- max: The maximum of the values
- grp: Group the output - put all the records with the same value for a given keyword together.

- orda: Sort the output in ascending order by this keyword
- ordd: Sort the output in descending order by this keyword

Appendix D

Blast-wave parameterization based Monte-Carlo particle generator

The blast-wave parameterization has been introduced in section 2.4.2. It has been used in simulations presented in chapter 7. In this chapter the technical implementation of the blast-wave parameterization is described.

The blast-wave is, in essence, the analytical parameterization of the solution usually obtained in hydrodynamic models. By treating several physical variables as free parameters it is able to fit several pieces of the experimental data from RHIC - the transverse momentum spectra, the elliptic flow v_2 and the source sizes obtained from Bose-Einstein interferometry. However the analytical form of the model does not, in any way, include close-velocity two-particle correlation effects. Such effects can be simulated, on a pair-by-pair basis, by introducing pair weights - as it is done e.g. in the StHbtMaker package and CorrFit software. For this method to work, particles are needed, that can be later combined into pairs. Therefore there is a need to transform the analytic form of the "blast-wave" into particles. The proposed method is to use the Monte-Carlo numerical integration procedure as a particle generator.

In regular Monte-Carlo procedure, a numerical integral of any function can be calculated. In the case of this work function 2.13 is integrated:

$$S\left(x, K\right) \equiv \frac{d^6 N}{d^3 x d^3 p} = f_{em}^{xK}, \tag{D.1}$$

however better efficiency is obtained when one does the integration in variables that are used in the "blast-wave" parameters. It is usable to perform the substitutions: $d^3p = dyp_tdp_td\phi_p$ and $d^3x = d\eta rdrd\phi_s$. The Jacobian of the transformation needs to be added:

$$\frac{d^6N}{dydp_td\phi_pd\eta drd\phi_s} = p_trf_{em}^{xK} = f_{em}. \tag{D.2}$$

The generation process is as follows. First the range of variables is determined. In this work following values were used: $\phi_p, \phi_s \in (0, 2\pi)$, $y \in (-1, 1)$, $\eta \in (-3, 3)$. The p_t range was selected so that particle transverse velocity $\beta_t \in (0.3, 0.8)$. Radius r range is determined by R_x and R_y parameters. Then the parameters of the model are determined. Since the simulations results were used to compare to STAR results presented in chapter 6, only central collisions were needed - which gives $\rho_a = 0$ and $R_x = R_y$. The parameters for Year1 calculations were obtained from [27]. The parameters for Year2 calculations were: $T = 100\ MeV$, $\rho_0 = 1.0$, $R_x = 11.0\ fm$, $\tau_0 = 1.0\ fm/c$, $\Delta\tau = 2.0\ fm/c$, $\alpha_s = 0.0$[97]. Then a procedure is similar to Monte-Carlo integration. Values for particle momentum: y, p_t, ϕ_p are generated in a random way from a uniform distribution in the given ranges. Similarly η, r and ϕ_s. Proper emission τ time is also generated in the range $(\tau_0 - 3\Delta\tau, \tau_0 + 3\Delta\tau)$. Then emission function value is calculated according to Eq. D.2. Then a random number f_{test} is generated in range $(0, f_{em,max})$, where $f_{em,max}$ is the maximum possible value of the emission function f_{em} in the given range of variables and needs to determined earlier (by e.g. simply iterating the above procedure many times and selecting the maximum f_{em} obtained). If $f_{test} < f_{em}$ it is as if a particle with the given variables was generated. It can be stored and later used in simulations.

The above procedure was implemented in the program written in C++ language as a macro in the ROOT framework[95]. The generated particles are stored in the ROOT TTree class and saved in the ROOT file TFile. These technologies were chosen as they are the accepted standard in the STAR Collaboration. The source code of the macro integratey2.C, that was used to generate particles according to Year2 parameters, is shown below. The structure of the code is as follows: first the parameters of the BW are set, helper variables are calculated and data structures are initialized. Then helper functions, corresponding to equations 2.6, 2.5, 2.7, 2.10, 2.12 and 2.9 are defined. The proper generation code then starts. First generation parameters are set, depending on whether pions, kaons or protons are to be generated. The generation of variables from uniform distributions follows. f_{em} is calculated, f_{test} is generated and the comparison is done. If particle is accepted, its momenta and freeze-out coordinates in Cartesian reference frame are calculated and stored. The generation procedure is repeated until the desired number of particles is generated.

```
Double_t fmtogev = 0.197327;
```

```
// Model parameters
Double_t pTEMP = 0.10;
Double_t pRHOZERO = 1.0;
Double_t pRHOA = 0.0;
Double_t pRX = 11.0 / fmtogev;
Double_t pRY = 11.0 / fmtogev;
Double_t pTAU = 1.0 / fmtogev;
Double_t pDELTAT = 2.0 / fmtogev;
Double_t pALFAS = 0.0;
// Helper variables
Double_t hrxsq = pRX*pRX;
Double_t hrysq = pRY*pRY;
Double_t hrxoverrysq = hrxsq/hrysq;
Double_t htwodtsq = 2*pDELTAT*pDELTAT;
// Data structures
typedef struct {Float_t px,py,pz,e,x,y,z,t;} PARTICLE;
static PARTICLE particle;
void fbe(Double_t x)
{
  return 1.0/(TMath::Exp(x)-1);
}
// Calculate phi_b from known phi_s
Double_t getphib(Double_t aphis)
{
  Double_t tphib = TMath::ATan(hrxoverrysq*TMath::Tan(aphis));
  if ((aphis > (TMath::Pi()/2.0)) && (aphis < 3*(TMath::Pi()/2.0)))
    tphib = tphib + TMath::Pi();
  return tphib;
}
// Calculate r~ from r and phi_s
Double_t getrtilde(Double_t ar, Double_t aphis)
{
  return TMath::Hypot((ar*TMath::Cos(aphis))/pRX,(ar*TMath::Sin(aphis))/pRY);
}
// Calculate omega from r~
Double_t getomega(Double_t artilde)
{
  if (pALFAS > 0.000001)
  {
    return 1.0/(1.0+TMath::Exp((artilde-1)/pALFAS));
```

```
  }
  else
  {
    if (artilde > 1.0)
      return 0.0;
    else
      return 1.0;
  }
}
// Calculate rho from r~ and phi_b
Double_t getrho(Double_t artilde, Double_t aphib)
{
  return artilde*(pRHOZERO + pRHOA * TMath::Cos(2*aphib));
}
// Calculate k*u
Double_t getku(Double_t amt, Double_t arho, Double_t aeta, Double_t arap, Double_t ak
{
  Double_t alfa = amt*TMath::CosH(arho)*TMath::CosH(aeta-arap);
  Double_t beta = akt*TMath::SinH(arho)*TMath::Cos(aphib-aphip);
  return (alfa - beta);
}
// Calculate the emission function f_em^xK
Double_t getemfunc(Double_t apt, Double_t aphip, Double_t arap, Double_t amass,
Double_t ar, Double_t aphis, Double_t aeta, Double_t atau)
{
  Double_t tmt = TMath::Hypot(apt, amass);
  Double_t tphib = getphib(aphis);
  Double_t trtilde = getrtilde(ar, aphis);
  Double_t tomega = getomega(trtilde);
  Double_t trho = getrho(trtilde, tphib);
  Double_t tku = getku(tmt, trho, aeta, arap, apt, tphib, aphip);
  Double_t taufunc = (-TMath::Power(atau-pTAU,2.0))/htwodtsq;
  Double_t temfunc = tmt*TMath::CosH(aeta - arap)*TMath::Exp(-tku/pTEMP)*tomega*TMath
  return temfunc;
}
// Perform the particle generation
// npart - number of particles to generate
// parttype - type of the particle
// 0: pion
// 1: kaon
```

```
// 2: proton
void integratey2(int npart=100000, int parttype=0)
{
  Double_t rap, pt, phip, rad, phis, tau, eta, rx, ry;
  TRandom *rand = new TRandom(14137);
  Double_t fmax = 1.0;
  // Integral ranges
  Double_t trrange = 1.0*pRX;
  Double_t tptmin, tptmax, tmass;
  Double_t ttaurange = 6.0*pDELTAT;
  Double_t tetamax = 3.0;
  Double_t trapmax = 1.0;
  TString pname("");
  switch (parttype){
  case 0:
    tmass = 0.139;
    tptmin = 0.1;
    tptmax = 1.0;
    fmax = 1.55;
    pname = "Pi";
    break;
  case 1:
    tmass = 0.493;
    tptmin = 0.3;
    tptmax = 1.5;
    fmax = 0.23;
    pname = "K";
    break;
  case 2:
    tmass = 0.938;
    tptmin = 0.4;
    tptmax = 2.0;
    fmax = 0.008;
    pname = "P";
    break;
  }
  TFile *fout = new TFile(("tree"+pname+".root").Data(),"RECREATE");
  fout->cd();
  TTree *tree = new TTree("particles","Particle tree");
  tree->Branch("part",&particle,"px:py:pz:e:x:y:z:t");
```

```
Double_t twopi3 = TMath::Power(TMath::Pi()*2,3);
Double_t fpod, ftest;
Double_t max = 0.0;
Int_t proc = npart/100;
Int_t akc = 0;
for (int ipart=0; ipart<npart; ipart++)
{
  // Generate variables
  rap = rand->Rndm() * trapmax*2 - trapmax;
  pt = rand->Rndm() * (tptmax-tptmin) + tptmin;
  phip = rand->Rndm() * TMath::Pi()*2;
  tau = rand->Rndm() * ttaurange + pTAU;
  eta = rand->Rndm() * tetamax * 2 - tetamax;
  rad = rand->Rndm() * trrange;
  phis = rand->Rndm() * TMath::Pi()*2;
  Double_t efun = getemfunc(pt, phip, rap, tmass, rad, phis, eta, tau);

  // Calculate f_em
  fpod = pt*rad*efun;
  // Look for f_em maximum
  if (fpod>max) max = fpod;
  // Do the Monte-Carlo accept/reject test
  ftest = rand->Rndm()*fmax;
  if (ftest < fpod)
  {
    akc++;

    // Calculate particle momentum
    particle.px = pt * TMath::Cos(phip);
    particle.py = pt * TMath::Sin(phip);
    Double_t mt = TMath::Hypot(pt,tmass);
    particle.pz = mt*TMath::SinH(rap);
    particle.e = mt*TMath::CosH(rap);

    // Calculate particle freeze-out point
    particle.x = rad * TMath::Cos(phis) * fmtogev;
    particle.y = rad * TMath::Sin(phis) * fmtogev;
    particle.z = tau * TMath::SinH(eta) * fmtogev;
    particle.t = tau * TMath::CosH(eta) * fmtogev;
```

```
      // Store the particle in a TTree
      tree->Fill();
    }
    // Progress report
    if (((ipart+1) % proc) == 0)
    cout << "Done " << ((ipart+1) / proc) << " %" << endl;
  }
  cout << "Maksimum found: " << max << endl;
  cout << "Accepted " << akc << " prob " << npart << endl;
 // Store the particle tree
  tree->Write();
}
```

Appendix E

Exponential hyperbola function

The motivation for studying the exponential hyperbola function was to find a function which would be able to better fit the source distributions produced by heavy-ion collision models (see chapter 7). Such a function needs to have a simple formula with as few parameters as possible. The proposed function is an exponential hyperbola:

$$f_{EH}\left(x\right) = N \exp\left(\alpha\right) \exp\left(-\sqrt{\frac{\left(x-\mu\right)^2}{\sigma^2} + \alpha^2}\right).$$

At Fig. E.1 we show the plot of the function, compared with the normal Gaussian function. It can be seen that f_{EH} has much larger tails, which was a desired feature. It is also easily parametrized, with the σ parameter responsible for function width, and the α parameter influencing the sharpness of the peak, and to a lesser extent, it's width. The μ parameter describes the position of the peak. By changing it's value we can shift the whole distribution along the x axis. In later considerations we assume $\mu = 0$. The $\exp\left(\alpha\right)$ factor at the beginning is a normalization factor, which ensures, that

$$f_{EH}\left(0\right) = N$$

E.1 Half-width

To characterize the function we need to give it's width. The commonly used value is the value of the argument, where the function has half of the peak

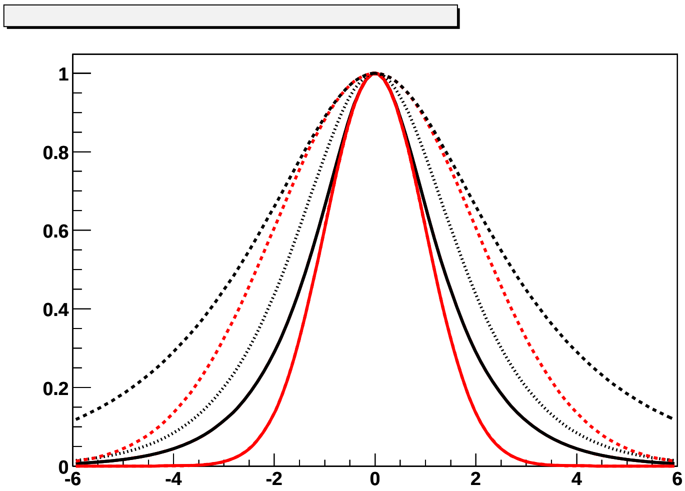

Figure E.1: An exponential hyperbola and Gaussian functions. Black lines: exponential hyperbola, red lines: Gaussian. Solid lines: $\sigma = 1, \alpha = 1$; dashed lines: $\sigma = 2, \alpha = 1$; dotted lines: $\sigma = 1, \alpha = 2$

height. For a Gaussian distribution it is simply the σ parameter. For f_{EH} we need to solve the following equation:

$$0.5 = e^{\alpha} e^{-\sqrt{\frac{x^2}{\sigma^2}+\alpha^2}}$$

which gives a half-width of:

$$x_{f_{EH}=\frac{1}{2}} = \sigma\sqrt{\left(\alpha - \log\left(0.5\right)\right)^2 - \alpha^2}$$

E.2 Function scaling

If a random variable X is described by the Gaussian probability distribution $G\left(\sigma, \mu\right)$ it is known that variable aX is described by the probability distribution $G\left(a\sigma, a\mu\right)$. It can be trivially shown that similar relation holds for exponential hyperbola: if X is described by $f_{HE}\left(\sigma, \alpha, \mu\right)$, then aX is described by $f_{HE}\left(a\sigma, \alpha, a\mu\right)$. This allows for a simple generation procedure of x: we simply generate x according to $f_{HE}\left(1, \alpha, 0\right)$ and later multiply it by σ to obtain the desired distribution.

However such scaling for the α parameter is not as straightforward. Let's assume X has a probability distribution $f_{HE}\left(\sigma, \alpha, 0\right)$; in order to find parameter b such, that bX is described by $f_{HE}\left(\sigma, a\alpha, 0\right)$ we need to solve the following equation:

$$e^{a\alpha}e^{-\sqrt{\frac{b^2x^2}{\sigma^2}+a^2\alpha^2}} = e^{\alpha}e^{-\sqrt{\frac{x^2}{\sigma^2}+\alpha^2}}$$

which gives the following formula for b:

$$b = \frac{\sigma}{x}\sqrt{\left(\alpha\left(a-1\right)+\sqrt{\frac{x^2}{\sigma^2}+\alpha^2}\right)^2 - a^2\alpha^2}.$$

It is important to note, that this formula is not independent of x, so a simple scaling similar to σ parameter is not possible.

Streszczenie

Treścią pracy jest analiza dwucząstkowych korelacji nieidentycznych mezonów. Do analizy wybrano wszystkie kombinacje par naładowanych mezonów π i K rejestrowanych w eksperymencie STAR. Praca ta jest częścią programu naukowego dotyczącego badań zderzeń ultrarelatywistycznych ciężkich jonów. Program ten realizowany jest na zderzaczu Relativistic Heavy Ion Collider (RHIC) w Brookhaven National Laboratory w USA. Jego celem jest potwierdzenie istnienia i zbadanie nowego stanu materii, który prawdopodobnie powstaje podczas takich zderzeń. Poniżej zamieszczono krótkie streszczenie pracy.

Po wstępie w rozdziale 1, w rozdziale 2 pracy zawarte jest wprowadzenie do zagadnień fizycznych dotyczących zderzeń ciężkich jonów. Przedstawiono aktualny stan poszukiwań plazmy kwarkowo-gluonowej (QGP). Szczególną uwagę zwrócono na zagadnienia przepływów kolektywnych - w szczególności przepływów eliptycznych i radialnych. Jedną z sygnatur powstawania plazmy kwarkowo-gluonowej są korelacje dwucząstkowe. Podkreślono ich związek z kolektywnym zachowaniem materii. Na zakończenie krótko scharakteryzowano modele teoretyczne, zastosowane później do analizy i interpretacji danych.

Rozdział 3 zawiera szczegółowy opis teoretyczny korelacji dwucząstkowych przy małych prędkościach względnych. Przedstawione są tam wyniki analiz dwucząstkowych korelacji cząstek identycznych oraz wnioski z nich wynikające. Opisano również podstawy teoretyczne i formalizm opisu korelacji cząstek nieidentycznych, w szczególności pomiaru asymetrii emsisji różnych typów cząstek.

W rozdziale 4 zawarto opis eksperymentu STAR jako części kompleksu badawczego zderzacza RHIC. Szczegółowo opisano detektory, które służyły do zbierania danych użytych w tej pracy, tzn. detektor STAR TPC oraz detektory wyzwalające (trigger detectors). Specjalną uwagę zwrócono na te charakterystyki detektorów, które bezpośrednio wpływały na analizę korelacji cząstek nieidentycznych oraz były źródłem błedów systematycznych. Krótko opisano metodyczną analizę danych w eksperymencie STAR, w tym bazę danych "FileCatalog" i związane z nią oprogramowanie oraz ich znaczenie dla całości działania eksperymentu.

Rozdział 5 jest poświęcony opisowi metodycznej części analizy korelacji cząstek

nieidentycznych w eksperymencie STAR. Opisano szczegółowo sposób wyboru danych do analizy oraz sposoby korekcji niepożądanych efektów. Zbadano również ich wpływ na otrzymaną eksperymentalnie funckję korelacyjną.

Rozdział 6 zawiera opis wyników fizycznych uzyskanych w tej pracy. Przedstawiono w nim funkcje korelacyjne dla wszystkich układów naładowanych pionów i kaonów przy obu dostępnych energiach zderzenia: $\sqrt{s_{NN}} = 130\ GeV$ oraz $\sqrt{s_{NN}} = 200\ GeV$. Pomiar asymetrii emisji został zaprezentowany w postaci "double-ratio", czyli stosunku dwóch funkcji korelacyjnych dla różnych znaków projekcji względnego pędu pary. Prezentowane wyniki pokazują, że po raz pierwszy w analizie zderzeń ciężkich jonów możliwe było zaobserwowanie asymetrii emisji pomiędzy różnymi typami cząstek (tu pionami i kaonami). Podano też wyniki dopasowania funkcji teoretycznych do funkcji eksperymentalnych dokonanego przy pomocy oprogramowania "CorrFit". Szczegółowo scharakteryzowano użyte modele źródła (SourceModels).

W rozdziale 7 przeprowadzono dyskusję otrzymanych wyników. Zmierzona różnica pomiędzy średnimi punktami emisji pionów i kaonów została porównana z przewidywaniami wybranych modeli teoretycznych. Różnica w przestrzennej współrzednej punktu emisji została zinterpretowana jako wynik procesu przepływu radialnego w zderzeniu ciężkich jonów i stanowi niezależne potwierdzenie istnienia korelacji przestrzeń-pęd w ewolucji takiego systemu. Zbadano również wpływ rozpadów rezonansów hadronowych na przesunięcie w średnim czasie emisji. Ostatecznie stwierdzono, że obserwowana asymetria jest superpozycją asymetrii przestrzennej i czasowej.

W załącznikach zamieszczono szczegółowy opis techniczny narzędzi stworzonych przez Autora na potrzeby tej pracy. Przedstawiono oprogramowanie eksperymetu STAR służące do analizy korelacji dwucząstkowych, w szczególności jego część służącą do obliczania postaci funkcji toretycznych. Opisano program CorrFit, niezbędny przy ilościowej analizie korelacji cząstek nieidentycznych. Przedstawiono projekt i wykonanie bazy danych FileCatalog, która służy do katalgowania informacji o plikach danych eksperymentu STAR. Na zakończenie umieszczno opis implementacji generatora cząstek opartego na parametryzacji "blast-wave", którego wyniki zostały zastosowane do porównania z danymi eksperymentalnymi.

W pracy przedstawiono po raz pierwszy funkcje korelacyjne oraz pomiar asymetrii emisji dla par pion-kaon. Jest to również jeden z pierwszych przykładów zastosowania tej techniki pomiarowej w eksperymencie. Dzięki zastosowaniu tej metody pojawiła się nowa obserwabla - asymetria emisji pomiędzy dwoma typami cząstek, która powiększa naszą wiedzę o materii produkowanej w zderzeniach ciężkich jonów i jej dynamicznej ewolucji. Jest też nowym, niezależnym testem, który musi być brany pod uwagę przy opracowywaniu modeli opisujacych dynamikę takich reakcji.

Na część techniczną tej pracy składają się dwa elementy. Pierwszym z nich było opracowanie oprogramowania potrzebnego do przeprowadzenia analizy, zarówno na etapie obróbki danych eksperymentalnych jak i w procesie modelowania korelacji cząstek nieidentycznych. Autor opracował też, jako część pracy na rzecz eksperymentu STAR, bazę danych przechowującą informacje o plikach z danymi. Drugim elementem było opracowanie i dopasowanie takich metod wyboru i obróbki danych, które pozwalały na skonstruowanie jak najmniej zniekształconych funkcji korelacyjnych. W przypadku tej analizy polegało to na opracowaniu sposobu uwzględnienia efektu "merging", czyli niemożliwości rekonstrukcji par cząstek, których tory przebiegały zbyt blisko siebie w detektorze STAR TPC oraz na eliminacji skorelowanych par elektron-pozyton powstałych poprzez konwersję kwantów γ. Innym ważnym zadaniem było dokładne ustalenie "purity", czyli tego jaką część wybranych do analizy cząstek tworzą poprawnie zidentyfikowane, pochodzące bezpośrednio z obszaru reakcji piony i kaony.

Część fizyczna pracy również składa się z dwóch elementów. W pierwszym przedstawiono otrzymane w trakcie analizy funkcje korelacyjne i "double-ratios" dla wszystkich kombinacji naładowanych pionów i kaonów produkowanych w zderzeniach *AuAu* zaobserwowanych w czasie pierwszego i drugiego roku pracy eksperymentu STAR. Pozwoliły one na szczegółową analizę źródła emitującego te cząstki, a dokładniej jego rozmiaru, dynamicznego procesu rozszerzania i kolejności emisji tych cząstek w czasie.

Drugim i końcowym krokiem było porównanie wyników eksperymentalnych z przewidywaniami modeli dynamicznych. Pierwszym z nich była parametryzacja "blast-wave", która była w stanie opisać inne, widoczne w danych eksperymentu STAR, własności systemu produkowanego w zderzeniach ciężkich jonów. Użyto również modelu RQMD, zwracając szczególną uwagę na problem średniego czasu emisji pionów i kaonów i różnicy między tymi czasami.

W wyniku tych prac wyciągnięto następujące wnioski:

- Zaobserwowano różny od jedności "double-ratio" w kierunku *out* dla wszystkich kombinacji par pion-kaon, w danych z obu lat w eksperymencie STAR. Odchylenie to pokazuje, w sposób wewnętrznie spójny, istnienie rzeczywistego efektu fizycznego, tzn. istnienie różnicy pomiędzy średnim czasowo-przestrzennym punktem emisji pionów i kaonów. Fakt ten został zaobserwowany po raz pierwszy, gdyż żadna inna metoda badawcza nie pozwala na jego wykrycie. Jakościowa analiza pokazała, że piony są emitowane średnio bliżej centrum reakcji niż kaony oraz że są one emitowane później.

- Zmierzona asymetria emisji jest zgodna z przewidywaniami parametryzacji “blast-wave”, co wskazuuje na istnienie przestrzennej różnicy w średnim punkcie emisji pionów i kaonów. Asymetria ta powstaje dzięki istnieniu korelacji “przestrzeń-pęd”, która jest istotą zjawiska zwanego “radial flow” (przepływ radialny). Technika korelacji dwucząstkowych jest najbardziej bezpośrednią metodą mierzenia korelacji “przestrzeń-pęd”, gdyż dzięki niej możliwe jest połączenie informacji o przestrznnej częsci przestrzeni fazowej z informacją o części pędowej. Inne sposoby badania przepływu radialnego bazują jedynie na części pędowej. Istnienie przestrzennej asymetrii może być wytłumaczone jedynie poprzez wzajemne zależności pomiędzy przepływem kolektywnym, a ruchami termicznymi w gorącej i gęstej materii.

- Dzięki modelowi RQMD, który chrakteryzuje się tym, że w możliwie kompletny sposób opisuje zachowanie się cząstek-rezonansów hadronowych, można było zbadać efekty różnicy w czasie emisji pionów i kaonów. Model przewiduje istnienie takiej właśnie różnicy, która powinna być widoczna w obserwowanej asymetrii emisji. Jednak aby uzyskać ilościową zgodność rozmiaru tej asymetrii z wynikami eksperymentalnymi, asymetria musi pochodzić z dwóch źródeł - asymetrii przestrzennej i czasowej. Można więc wyciągnąć wniosek, że eksperymentalnie obserwowana asymetria jest kombinacją tych dwóch składników.

- Oprócz analizy asymetrii emisji dokonano również porównania ilościowego rozmiarów źródła otrzymywanych w eksperymencie i w obliczeniach teoretycznych. Zaobserwowano niezgodność pomiędzy nimi. Pozostaje ona nie wyjaśniona, jej przyczyny będą przedmiotem dalszych badań. W trakcie porównań odkryto również, że przewidywana przez modele teoretyczne przestrzenna postać źródła nie jest symetryczną gaussowską kulą.

- Ogólna procedura dopasowywania dwucząstkowych funkcji korelacyjnych, która została rozwinięta (i zaimplementowana w postaci kodu komputerowego) w tej pracy pozwala na testowanie nowych, niekoniecznie symetrycznych, czy gaussowskich parametryzacji źródła. Może to pomóc w wytłumaczeniu obserwowanych niezgodności. Autor zaproponował i przetestował jedną z możliwych odmiennych parametryzacji, otrzymując zgodność lepszą, niż dla tradycyjnej parametryzacji gaussowskiej.

Zaprezentowane wyniki i technika analizy pokazują, że eksperyment STAR jest idelanie przystosowany do analizy korelacji cząstek nieidentycznych. Wykonane prace i stworzone w jej trakcie narzędzia otwierają nowe możliwości badania korelacji cząstek w eskperymencie STAR i w innych eksperymentach fizycznych.

Przedstawione analizy mogą być kontynuowane i rozszerzone w przyszłości. Badanie asymetrii emisji w funkcji centralności zderzenia może służyć znalezieniu warunków, przy których zaczyna tworzyć się przepływ radialny. Można studiować korelacji innych rodzajów cząstek: analizy korelacji pion-proton i kaon-proton pomogą stowrzyć pełen obraz emisji lekkich cząstek w obszarze małych pędów poprzecznych, zaś korelacje pion-Ξ mogą udzielić odpowiedzi na pytanie, czy bariony zawierające kwarki dziwne również uczestniczą w kolektywnej ekspansji. Nowe poddetektory eksperymentu STAR (w szczególności detektor czasu przelotu TOF) pozwolą na badanie korelacji cząstek nieidentycznych w funkcji prędkości pary, co pomoże w badaniu profilu przepływu. Można też analizować nowe partie danych - w szczególności korelacje w zderzeniach proton-proton i deuteron-jądro, co pozwoli na badanie struktury dżetów i odpowie na pytanie, czy przepływ radialny istnieje nawet w tak podstawowych procesach.

Bibliography

[1] F. Karsh; "*Lattice results on QCD Thermodynamics*", Nucl. Phys. **A698**, (2002) p 199-208

[2] Animations from webpage: `http://www.th.physik.uni-frankfurt.de/~weber/CERNmovies/index.html`

[3] G.E. Bruno; "*New Results From NA57 Experiment*", **nucl-ex**/0403036, Proceedings of the **Quark Matter 2004** conference

[4] R.A. Fini; "*Results From CERN WA97 / NA57 Experiments on Strange Baryon Production in Pb Pb Collisions*", Proceedings of "**Gargnano 2002, Quark confinement and the hadron spectrum**", p 436-438

[5] D. Varga (for the NA49 Collaboration); "*Recent results on strangeness production from CERN experiment NA49*", **hep-ex**/0105035

[6] P. Bordalo et al. (NA50 Collaboration); "*Recent results on J/ from experiment NA50*", Nucl. Phys. **A698**, p 127-134

[7] A.P. Kostyuk, M.I. Gorenstein, H. Stocker, W. Greiner; "*Statistical Coalescence Model Aanalysis of J/PSI Production in Pb + Pb Collisions at 158-A-GeV*", Phys. Lett. **B531** (2002) p 195-202; **hep-ph**/0110269

[8] A. Capella, D. Sousa; "*New J/PSI Suppression Data and The Comovers Interaction Model*", **nucl-th**/0303055

[9] G.E. Brown, C.H. Lee, M. Rho, E. Shuryak; "*The Instanton Molecule Liquid and 'Sticky Molasses' Above T(C)*", **hep-ph**/0402068

[10] J.P. Wessels et al. (CERES/NA45 Collaboration); "*Latest Results From CERES / NA45*", Proceedings of "**16th International Conference on Ultrarelativistic Nucleus-Nucleus Collisions: Quark Matter 2002 (QM 2002)**" Nucl. Phys. **A715** (2003) p 262-271; **nucl-ex**/0212015

[11] J.D. Bjorken; Phys. Rev. **D27** (1983) p 140

[12] H. Satz; "*Limits of Confinement: The First 15 Years of Ultrarelativistic Heavy Ion Studies*", Proceedings of "**16th International Conference on Ultrarelativistic Nucleus-Nucleus Collisions: Quark Matter 2002 (QM 2002)**", Nucl. Phys. **A715** (2003) p 3-19; **hep-ph**/0209181

[13] W.A. Zajc et al. (PHENIX Collaboration); "*Overview of PHENIX Results From The First RHIC Run*", Proceedings of "**15th International Conference on Ultrarelativistic Nucleus-Nucleus Collisions (QM2001)**", Nucl. Phys. **A698** (2002) p 39-53; **nucl-ex**/0106001

[14] E.V. Shuryak; "*What RHIC Eexperiments and Theory Tell Us About Properties of Quark-Gluon Plasma?*", **hep-ph**/0405066

[15] M. Gyulassy, L McLerran; "*New Forms of QCD Matter Discovered at RHIC*", **nucl-th**/0405013

[16] C. Alt et al. (NA49 Collaboration); "*Directed And Elliptic Flow of Charged Pions and Protons in Pb + Pb Collisions at 40-A-GeV and 158-A-GeV*", Phys. Rev. **C68** (2003) 034903; **nucl-ex**/0303001

[17] K.H. Ackermann et al. (STAR Collaboration); "*Elliptic Flow in Au+Au Collisions at sqrt(snn) = 130 GeV*", Phys. Rev. Lett. **86** (2001) 402

[18] C. Adler et al. (STAR Collaboration); "*Identified Particle Elliptic Flow in Au+Au Collisions at sqrt(snn) = 130 GeV*", Phys. Rev. Lett. **87** (2001) 182301

[19] C. Adler et al. (STAR Collaboration); "*Azimuthal anisotropy of K0s and Lambda + Lambdabar production at mid-rapidity from Au+Au collisions at sqrt(snn) = 130 GeV*", Phys. Rev. Lett. **89** (2002) 132301

[20] J. Adams et al. (STAR Collaboration); "*Particle-type dependence of azimuthal anisotropy and nuclear modification of particle production in Au+Au collisions at sqrt(snn) = 200 GeV*", Phys. Rev. Lett. **92** (2004) 052302

[21] F. Retiere; "Collective flow", Talk given at "**17th International Conference on Ultrarelativistic Nucleus-Nucleus Collisions: Quark Matter 2004 (QM 2004)**", 15 Jan 2004, available at: `http://www.lbl.gov/nsd/qm2004/program.html`

[22] J. Adams et al. (STAR Collaboration); "*Identified particle distributions in pp and Au+Au collisions at sqrt{snn}=200 GeV*", Phys. Rev. Lett. **92** (2004) 112301

[23] H. Sorge; "*Flavor Production in Pb (160-A/GeV) on Pb Collisions: Effect of Color Ropes and Hadronic Rescattering*", Phys. Rev. **C52** (1995) p 3291-3314; **nucl-th**/9509007

[24] S. Soff, S. Bass, D. Hardtke, S. Panitkin; Nucl. Phys. **A715** (2003) p 801

[25] U. Heinz, P.F. Kolb; Nucl. Phys. **A702** (2002) p 269; **hep-ph**/0111075

[26] B. Tomasik, U.A. Wiedemann, U. Heinz; Heavy Ion Phys. **17** (2003) p 105-143

[27] F. Retiere, M.A. Lisa; "*Observable implications of geometrical and dynamical aspects of freeze-out in heavy ion collisions*"; **nucl-th**/0312024

[28] U.A. Wiedemann, P. Scotto, U. Heinz; Phys. Rev. **C53** (1996) p 918

[29] R. Hanbury-Brown, R.Q.Twiss; *"A new type of interferometer for use in radio-astronomy*", Phil. Mag. **45** (1954) p 663-682

[30] R. Hanbury-Brown; "*Photons, Waves and Stars, Measuring the size of things in the Universe: HBT interferometry and heavy-ion physics"*, Proceedings of **"CRIS '98** 2^{nd} **Catania Relativistic Ion Studies**", Acicastello, Italy, June 8-12, (1998) World Scientific p 1-10

[31] Goldhaber et al.; PR **120** (1960) p 300

[32] Kopylov, Podgoretsky; Sov. J. Part. Nucl. **20** (1969) p 266

[33] G. I. Kopylov, V. L. Lyuboshits and M. I. Podgoretsky, *"Correlations Between The Particles Which Have Small Relative Momenta"* JINR-P2-8069; http://www.slac.stanford.edu/spires/find/hep/www?r=jinr-p2-8069

[34] G. I. Kopylov and M. I. Podgoretsky, *"Interference Of Two-Particle States In Elementary-Particle Physics And Astronomy"* Zh. Eksp. Teor. Fiz. **69** (1975) 414.

[35] R. Lednický ; "*Space-Time Picture of the Heavy-Ion Collision*", Heavy-Ion Reactions Group Seminar, 1999

[36] R. Lednický; "*Exotic correlation effects*", Talk presented at **"Particle Correlations - from STAR to ALICE via Warsaw**", Warsaw, 8-11 May 2002; `http://hirg.if.pw.edu.pl/en/meeting/may2002/talks/lednicky/1/main.htm`

[37] R. Lednický; "*Correlation Femtoscopy*", Talk presented at **"Second Warsaw Meeting on Particle Correlations and Resonances in Heavy-Ion Collisions**", Warsaw, 15-18 Oct 2003; `http://hirg.if.pw.edu.pl/en/meeting/oct2003/talks/lednicky/lednicky_warsaw03.ppt`

[38] G. Baym; *"The Physiscs of Hanbury Brown-Twiss Interferometry: Form Stars to Nuclear Collisions to Atomic and Condensed Matter Systems"*, Measuring the size of things in the Universe: HBT interferometry and heavy ion physics, Proceedings of **"CRIS '98 2^{nd} Catania Relativistic Ion Studies"**, Acicastello, Italy, June 8-12, 1998, World Scientific, 11-27

[39] U. Heinz; *"Handbury Brown - Twiss interferometry in high energy nuclear and particle physics"*, **hep-ph**/9806512

[40] G. Bertsh; Nucl. Phys. **A498** (1989) 173c; S. Pratt; Phys. Rev. **D33** (1986) p 1314

[41] M. I. Podgoretsky, *"On The Comparison Of Identical Pion Correlations In Different Reference Frames"* Sov. J. Nucl. Phys. **37**, 272 (1983) [Yad. Fiz. **37**, 455 (1983)].

[42] M.A. Lisa et al. (E895 Collaboration); "*Azimuthal Dependence of Pion Interferometry at the AGS*", Phys. Lett. **B496** (2000) p 1-8; e-Print Archive: **nucl-ex**/0007022

[43] H. Appelshauser et al. (NA49 Collaboration); Eur. Phys. J **C2** (1998) p 661

[44] I.G. Bearden et al. (NA44 Collaboration); Eur. Phys. J **C18** (2000) p 317

[45] M.M. Aggerwal et al. (WA98 Collaboration); Eur. Phys. J **C16** (2000) p 445

[46] F. Antinori et al. (WA97 Collaboration); J. Phys. **G27** (2001) p 2325

[47] S.V. Afanasiev et al. (NA49 Collaboration); "*Bose-Einstein correlations of charged kaons in central Pb + Pb collisions at E(beam) = 158-A-GeV*", Phys. Lett. **B557** (2003) p 157-166

[48] S.S. Adler et al. (PHENIX Collaboration); "*Bose-Einstein Correlations of Charged Pion Pairs in Au+Au Collisions at sqrt(s_NN)=200_ GeV*", **nucl-ex**/0401003

[49] C. Adler et al. (STAR Collaboration); Phys. Rev. Lett. **87**, 082301 (2001)

[50] Mercedes Lopez Noriega (for the STAR Collaboration); "*Identical Particle Interferometry at STAR*", Contribution to **Quark Matter 2002**, Nantes, France, July 2002, Nucl. Phys. **A715** (2003) p 623-626

[51] D. Teaney, J. Lauret, E.V. Shuryak; "*A Hydrodynamic Description of Heavy Ion Collisions at the SPS and RHIC*", **nucl-th**/0110037

[52] S.V. Akkelin, Yu.M. Sinyukov; Phys. Lett. **B356** (1995) p 525

[53] Yu.M. Sinyukov, S.V. Akkelin, A.Yu.Tolstykh; "*Interferometry radii for expanding hadron resonance gas*", Nucl. Phys. **A610** (1996) p 278c-285c

[54] U. Heinz, B.V. Jacak; Ann. Rev. Nucl. Part. Sci. **49** (1999) p 529; U.A. Wiedemann, U. Heinz; Phys. Rept. **319** (1999) p 145

[55] G. I. Kopylov and M. I. Podgoretsky, *"Multiple Production And Interference Of Particles Emitted By Moving Sources"*, Sov. J. Nucl. Phys. **18** (1974) 336 [Yad. Fiz. **18** (1973) 656].

[56] P. Grassberger; "*Interference effects from inclusive resonance production*", Nucl. Phys. **B120**, 14 March 1977, p 231-252

[57] R. Lednicky and M. I. Podgoretsky, *"On Correlations Of Identical Particles In The 'Resonance Particle' System"*, JINR-P2-12302 (1979)

[58] M. G. Bowler, *"Bose-Einstein Correlations In Quark Initiated Jets"*, Part. World **2**, 1 (1991).

[59] A.N. Makhlin, Yu.M. Sinyukov; Z. Physics **C39** (1988) 69

[60] M.G. Bowler; Phys. Lett. **B270** (1991) p 69

[61] Yu.M. Sinyukov et al.; Phys. Lett. **B432** (1998) p 249

[62] R. Lednický, V.I. Lyuboshitz, B. Erazmus, D. Nouais; Phys. Lett. **B373** (1996) p 30.

[63] R.Lednický, V.L.Lyuboshitz 1982 *Sov. J. Nucl. Phys.* **35** p 770; *Proc. CORINNE 90, Nantes, France*, 1990 (ed. D.Ardouin, World Scientific, 1990) p 42; 1996 *Heavy Ion Physisc* **3** 93

[64] S. Voloshin, R. Lednický, S. Panitkin, N. Xu; Phys. Rev. Lett. **79** (1997) p 30

[65] R.Lednický 2003 **nucl-th**/0305027

[66] R. Lednicky and V. L. Lyuboshits, *"Final State Interaction Effect On Pairing Correlations Between Particles With Small Relative Momenta"*, Sov. J. Nucl. Phys. **35** (1982) 770 [Yad. Fiz. **35** (1981) 1316].

[67] R. Lednicky, S. Panitkin and N. Xu; *"Search for delays between unlike particle emissions in relativistic heavy-ion collisions"*, **nucl-th**/0304062.

[68] R. Lednický ; "*Finite-size effects on two-particle production in continuous and discrete spectrum*", DIRAC Note, to be published.

[69] R. Lednický ; "*Recent NA49 results on Unlike Particle Correlations in Central Pb+Pb Collisions at 158 AGeV*"; Talk presented at **CERN Heavy-Ion Forum**, 14 Nov 2000

[70] D. Miskowiec; "*Separation between sources of pions and protons in central Au + Au collisions at the AGS (E877)*", **nucl-ex**/9808003

[71] A.S. Dawydow, "*Mechanika Kwantowa*", Panstwowe Wydawnictwo Naukowe, Warszawa 1969

[72] C. Adler et al. (PHENIX Collaboration); Phys. Rev. Lett. **88** (2002) 0122301

[73] C. Adler et al. (STAR Collaboration); Phys. Rev. Lett. **89** (2002) 202301

[74] J. Adams et al. (STAR Collaboration); Phys. Rev. Lett. **91** (2003) 172302

[75] C. Adler et al. (STAR Collaboration); Phys. Rev. Lett. **90** (2003) 082302

[76] J. Adams et al. (STAR Collaboration); Phys. Rev. Lett. **91** (2003) 072304

[77] C. Adler et al. (STAR Collaboration); Phys. Rev. Lett. **90** (2003) 032301

[78] J. Letessier, J. Rafelski; *"Hadrons and Quark-Gluon Plasma*", Cambridge University Press, Cambridge, UK, first edition, 2002.

[79] T. Roser; *"RHIC Status and Plans*", Talk presented at **RHIC Retreat 2000**, `http://www.agsrhichome.bnl.gov/AP/RHIC2000/Retreat/submissions/retreat00-setting-the-stage.ppt`

[80] M. Adamczyk et al.; Nucl. Instr. and Meth. **A 499** (2003) p~437-468

[81] B.B. Back et al.; Nucl. Instr. and Meth. **A 499** (2003) p~603-623

[82] K. Adcox et al.; Nucl. Instr. and Meth. **A 499** (2003) p~469-479

[83] K.H. Ackermann; Nucl. Instr. and Meth. **A 499** (2003) p~624-632

[84] F. Bergsma; Nucl. Instr. and Meth. **A 499** (2003) p~633-639

[85] M. Anderson; Nucl. Instr. and Meth. **A 499** (2003) p~659-678

[86] F.S. Bieser; Nucl. Instr. and Meth. **A 499** (2003) p~766-777

[87] A. Tang; *"Elliptic flow in Au+Au collisions at sqrt(NN) 130 GeV*", PhD Thesis, Kent State University 2002.

[88] B.G.Gibbard, T.G. Throwe, Nucl. Instr. and Meth. **A 499** (2003) p~814-818

[89] A.Kisiel, J.Lauret, *“FileCatalog user manual”*, `http://www.star.bnl.gov/STAR/comp/sofi/FileCatalog/user.html`

[90] C. Adler et al.; Phys. Rev. Lett. **8**9, 092301 (2002)

[91] J. Adams et al. (STAR collaboration); Phys. Lett. **B567**, p 167-274 (2003)

[92] J. Adams et al. (STAR collaboration); to be published in Phys. Rev. Lett., **nucl-ex**/0307024

[93] J. Adams, A. Kisiel et al. (STAR collaboration); Phys. Rev. Lett. **91**, 262302 (2003)

[94] C. Adler et al. (STAR Collaboration); “*Identified particle distributions in pp and Au+Au collisions at sqrt{snn}=200 GeV*”, Phys. Rev. Lett. **92** (2004) 112301; **nucl-ex**/0310004

[95] ROOT package homepage; `http://root.cern.ch`

[96] STAR Off-line Software homepage; `http://www.star.bnl.gov/STAR/comp/ofl/`

[97] F. Retiere; private communication